Aus dem
Institut für Physiologische Chemie
der
Philipps-Universität Marburg
Geschäftsführender Direktor: Prof. Dr. Andrej Hasilik

Arbeitgruppe Molekulare Enzymologie
Leiter: Prof. Dr. Klaus-Heinrich Röhm

Systematic site-directed mutagenesis to characterize subunit interactions in *E. coli* asparaginase II, an enzyme used in leukemia treatment

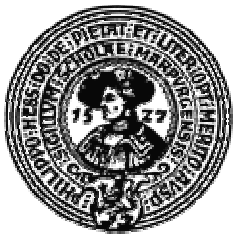

INAUGRAL-DISSERTATION
Zur Erlangung des Doktorgrades der Humanbiologie
(Dr. rer. physiol.)

dem Fachbereich Humanmedizin
der Philipps-Universität Marburg
vorgelegt

von

Shikha Verma
Aus Meerut, Indien

Marburg 2005

Dedicated to my lovingly Parents

Angenommen vom Fachbereich Humanmedizin der Philipps-Universität Marburg
am

Dekan: Prof. Dr. B. Maisch
Referent: Prof. Dr. K. H. Röhm

Contents

1. Introduction

1.1 Historical development

L-asparaginases (EC 3.5.1.1) catalyze the hydrolysis of L-asparagine to L-aspartic acid and ammonia. Both the substrates and the product of this enzymatic reaction play important roles in a number of metabolic processes in all organisms, from bacteria to mammals. The interest in asparaginases was greatly enhanced by the fact that some of these enzymes exhibit anti-tumor activity. In 1922, Clementi tested mammalian sera for asparaginase activity and found significant activity only in guinea pig serum (Clementi, 1922). In 1953, John Kidd in New York observed that guinea pig serum inhibits tumor growth in rats and mice and suggested that the active material was a protein (Kidd, 1953). Ten years later Broome showed that it was not the complement in the serum which provoked the tumor regression as first assumed, but rather the enzyme L-asparaginase (Broome, 1963). He confirmed the results of Clementi's work from the early 1920s and showed that a correlation existed between his results and those of Kidd. Soon after Broome's finding, an asparaginase was isolated from *Escherichia coli* B that was much more efficient in to inducing remissions in children with acute lymphoblastic leukemia (Mashburn & Wriston, 1964; Hill *et al.,* 1967; Oettgen *et al.,* 1967). The *E. coli* enzyme and several others were purified and studied by a number of researchers leading to the explosive growth of this area of research.

1.2 Bacterial amidohydrolases

On the basis of their substrate specificity, bacterial L-amidohydrolases can be assigned to two major classes. Enzymes of the first class are true **asparaginases** (EC 3.5.1.1) which primarily utilize L-asparagine as a substrate. The enzymes belonging to the second class, also referred to as **glutaminase-asparaginase** (EC 3.1.5.38)**,** catalyze the hydrolysis of both L-asparagine and L-glutamine with comparable efficiency.

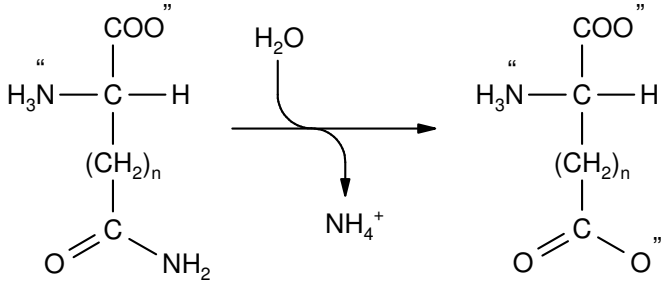

Figure 1.1 Reactions catalyzed by bacterial amidohydrolases. The substrates asparagine (n=1) or glutamine (n=2) are hydrolyzed to the corresponsing dicarboxylates, aspartate and glutamate.

Another distinction refers to the subcellular localization of these enzymes. Type I amidohydrolases are low-affinity cytosolic enzymes, while type II asparaginases are located in the periplasm of Gram-negative bacteria and have a much higher affinity for their substrates. Both amidohydrolase types are found in many bacterial species, but only type II enzymes from *Escherichia coli* (*E. coli* asparaginase II) and a related enzyme from *Erwinia chrysanthemi* are being used for leukemia treatment. In 1969, EcA2 was obtained in a crystalline form for the first time (Ho *et al.,* 1969) and its crystal structure was solved in 1992 (Swain *et al.,* 1993). Today the structures of five type II amidohydrolases are known (enzymes from *E. coli*, *Erwinia*, *Acinetobacter*, *Wolinella succinogenes* and *Pseudomonas* spec.)

1.3 Mechanism of action of asparaginase as a drug

It is now well established that the antineoplastic activity of asparaginases is mainly due to the depletion of asparagine in the blood serum. Certain lymphosarcomas and the leukocytes transformed in acute lymphatic leukemia (ALL), unlike normal cells, cannot compensate for the lack of asparagine, because they show a diminished expression of asparagine synthetase (Haskell and Canellos, 1969). Therefore, these cells depend on an extracellular supply of L-asparagine which they obtain from the circulating pools (Rogers, 1989). Intravenous treatment with asparaginase leads to depletion of the supply of asparagine and can thus be cytotoxic for the neoplastic cells (Bauer, 1969).

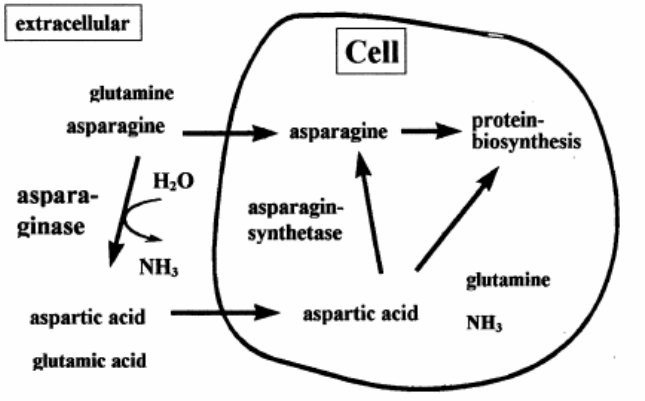

Fig 1.2 Mechanism of the anti-tumor activity of L-asparaginase.

The inclusion of asparaginase in the combination chemotherapy of ALL leads to markedly longer period of sustained remission and fewer relapses (Clavell *et al.,* 1986; Nesbit *et al.,* 1981). L-asparaginase in combination with methotrexate and other drugs is highly effective in the therapy of both primary and acute lymphoblastic leukemia of children and adults (Capizzi, 1981, 1983). At a later stage, the continued application of asparaginase helps to prevent further outbreaks (Mueller & Boos, 1998).

Unfortunately, the therapy with asparaginases may have serious side effects on pancreas, liver, blood coagulation and the CNS (Haskell *et al.,* 1969; Whitecar *et al.,* 1970, Gralnick and Henry, 1969). In addition, the L-asparaginase enzyme is not very stable in blood plasma, which limits its use in treatment of leukaemia.

Two factors important for the antineoplastic activity of asparaginases are the K_m values for asparagine and the rate of clearance from circulation. The more rapidly an enzyme is removed from circulation, the lower its antineoplastic activity. The half-life for clearance of guinea pig L-asparaginase from the serum of patients is about 8 h (Boyse *et al.,* 1967) and that of *E. coli* L-asparaginase has been shown to vary between 8 to 24 h (Tomao *et al.,* 1969).

1.4 *Escherichia coli* asparaginases

Escherichia coli contain two L-asparaginase isozymes that can be separated by standard protein fractionation techniques (Schwartz *et al.,* 1966; Campbell *et al.,* 1967). These enzymes have been designated EC1 and EC2 in *E. coli* B (Campbell *et al.,* 1967), or EcA1 and EcA2 in *E. coli* K-12 (Cedar and Schwartz 1967). The amino acid sequences of EcA1 and EcA2 are rather dissimilar except for a few regions of significant homology (Maita and Matsuda *et al.,* 1986, Jerlstörm *et al.,* 1989, cf. Figure 1.3). In this work we use the abbreviations EcA1 and EcA2, respectively for *E. coli* asparaginase isozymes 1 or 2.

1.4.1 Properties

Cedar and Schwartz (1967) first showed that EcA2, but not EcA1, is secreted into the surrounding medium, both during the formation of spheroplast by treatment with lysozyme and EDTA, and after osmotic shock. It was concluded that EcA2 is located in the periplasmic space, between the bacterial plasma membrane and the outer membrane, while EcA1 is cytoplasmic.

EcA2 is regulated by the oxygen level in the medium, with the high level of induction under anaerobic conditions (Cedar and Schwartz, 1967, 1968). In contrast, no definite form of regulation has been reported for EcA1, which is considered a constitutive enzyme (Jerlström, 1989).

Apart from their differing cellular location and regulation, the *E .coli* enzymes differ with respect to their catalytic properties. EcA1 and EcA2 have K_m values for asparagine of 3.5 mM and 11.5 μM, respectively (Ho and Milikin, 1970). The active form of EcA1 was reported to be a dimer with a subunit mass of 35.4 kDa (Jerlstroem, 1989), although recent results suggest a tetrameric structure. The active form of EcA2 is a homotetramer with a mass of 4 x 34.6 kDa (Maita and Matsuda, 1980).

The amino acid sequence of EcA2 has been determined by protein sequencing in the seventies (Maita *et al.,* 1974). In 1990 the nucleotides sequence of the *ansB* gene was reported by Beacham and coworkers (Figure 1.3). The EcA2 precursor has a 22-residue N-terminal signal peptide which is cleaved between residues 22 and 23 to yield the mature protein with N-terminal leucine residues. The mature enzyme consists of 326 amino acids with a calculated molecular weight of 34594. The primary structure as deducted from the nucleotide sequence is also shown in figure 1.3. The other type II asparaginases are highly homologous to EcA2. A sequence alignment of several high-affinity asparaginases is shown in figure 1.4.

The production of *E. coli* L-asparaginase is regulated by two pleitropic regulatory proteins i.e. the FNR protein (Jelström *et al.,* 1987) which activates a number of genes during anaerobiosis (Unden and Guest, 1984; Jayaram *et al.,* 1987; Spiro and Guest, 1987) and the cyclic AMP receptor protein CRP (Chesney, 1983; Russell and Yamazaki, 1978) which controls the initiation of transcription of genes in various catabolic pathways (De Crombrugghe *et al.,* 1984; Ebright and Beckwith, 1985; Harms *et al.,* 1991).

```
                      Met GLu Phe Phe Lys Lys Thr Ala Leu Ala Ala Leu Val Met Gly
  GTAACTGGAGGAATGAA ATG GAG TTT TTC AAA AAG ACG GCA CTT GCC GCA CTG GTT ATG GGT
                            ↓
Phe Ser Gly Ala Ala Leu Ala Leu Pro Asn Ile Thr Ile Leu Ala Thr Gly Gly Thr Ile
TTT AGT GGT GCA GCA TTC GCA TTA CCC AAT ATC ACC ATT TTA GCA ACC GGC GGG ACC ATT
                         20                                  30
Ala Gly Gly Gly Asp Ser Ala Thr Lys Ser Asn Tyr Thr Val Gly Lys Val Gly Val Glu
GCC GGT GGT GGT GAC TCC GCA ACC AAA TCT AAC TAC ACA GTG GGT AAA GTT GGC GTA GAA
                         40                                  50
Asn Leu Val Asn Ala Val Pro Gln Leu Lys Asp Ile A1a Asn Val Lys Gly Glu Gln Val
AAT CTG GTT AAT GCG GTG CCG CAA CTA AAA GAC ATT GCG AAC GTT AAA GGC GAG CAG GTA
                         60                                  70
Val Asn Ile Gly Ser Gln Asp Met Asn Asp Asn Val Trp Leu Thr Leu Ala Lys Lys Ile
GTG AAT ATC GGC TCC CAG GAC ATG AAC GAT AAT GTC TGG CTG ACA CTG GCG AAA AAA ATT
                         80                                  90
Asn Thr Asp Cys Asp Lys Thr Asp Gly Phe Val Ile Thr His Gly Thr Asp Thr Met Glu
AAC ACC GAC TGC GAT AAG ACC GAC GGC TTC GTC ATT ACC CAC GGT ACC GAC ACC ATG GAA
                        100                                 110
Glu Thr Ala Tyr Phe Leu Asp Leu Thr Val Lys Cys Asp Lys Pro Val Val Met Val Gly
GAA ACT GCT TAC TTC CTC GAC CTG ACC GTG AAA TGC GAC AAA CCG GTG GTG ATG GTC GGC
                        120                                 130
Ala Met Arg Pro Ser Thr Ser Met Ser Ala Asp Gly Pro Phe Asn Leu Tyr Asn Ala Val
GCA ATG CGT CCG TCC ACG TCT ATG AGC GCA GAC GGT CCA TTC AAC CTG TAT AAC GCG GTA
                        140                                 150
Val Thr Ala Ala Asp Lys Ala Ser Ala Asn Arg Gly Val Leu Val Val Met Asn Asp Thr
GTG ACC GCA GCT GAT AAA GCC TCC GCC AAC CGT GGC GTG CTG GTA GTG ATG AAT GAC ACC
                        160                                 170
Val Leu Asp Gly Arg Asp Val Thr Lys Thr Asn Thr Thr Asp Val Ala Thr Phe Lys Ser
GTG CTT GAT GGC CGT GAC GTC ACC AAA ACC AAC ACC ACC GAC GTA GCG ACC TTC AAG TCT
                        180                                 190
Val Asn Tyr Gly Pro Leu Gly Tyr Ile His Asn Gly Lys Ile Asp Tyr Gln Arg Thr Pro
GTT AAC TAC GGT CCT CTG GGT TAC ATT CAC AAC GGT AAG ATT GAC TAC CAG CGT ACC CCG
                        200                                 210
Ala Arg Lys His Thr Ser Asp Thr Pro Phe Asp Val Ser Lys Leu Asn Glu Leu Pro Lys
GCA CGT AAG CAT ACC AGC GAC ACG CCA TTC GAT GTC TCT AAG CTG AAT GAA CTG CCG AAA
                        220                                 230
Val Gly Ile Val Tyr Asn Tyr Ala Asn Ala Ser Asp Leu Pro Ala Lys Ala Leu Val Asp
GTC GGC ATT GTT TAT AAC TAC GCT AAC GCA TCC GAT CTT CCG GCT AAA GCA CTG GTA GAT
                        240                                 250
Ala Gly Tyr Asp Gly Ile Val Ser Ala Gly Val Gly Asn Gly Asn Leu Tyr Lys Ser Val
GCG GGC TAT GAT GGC ATC GTT AGC GCT GGT GTG GGT AAC GGC AAC CTG TAT AAA TCT GTG
                        260                                 270
Phe Asp Thr Leu Ala Thr Ala A1a Lys Thr Gly Thr A1a Val Val Arg Ser Ser Arg Val
TTC GAC ACG CTG GCG ACC GCC GCG AAA ACC GGT ACT GCA GTC GTG CGT TCT TCC CGC GTA
                        280                                 290
Pro Thr Gly Ala Thr Thr Gln Asp Ala Glu Val Asp Asp Ala Lys Tyr Gly Phe Val Ala
CCG ACG GGC GCT ACC ACT CAG GAT GCC GAA GTG GAT GAT GCG AAA TAC GGC TTC GTC GCC
                        300                                 310
Ser Gly Thr Leu Asn Pro Gln Lys Ala Arg Val Leu Leu Gln Leu Ala Leu Thr Gln Thr
TCT GGC ACG CTG AAC CCG CAA AAA GCG CGC GTT CTG CTG CAA CTG GCT CTG ACG CAA ACC
                        320
Lys Asp Pro Gln Gln Ile Gln Gln Ile Phe Asn Gln Tyr  *
AAA GAT CCG CAG CAG ATC CAG CAG ATC TTC AAT CAG TAC TAA TCGCCTCGCCCCGGTATCGTGC
```

Figure 1.3 Nucleotide and predicted sequence of *the ansB* gene (Jennings and Beacham, 1990).

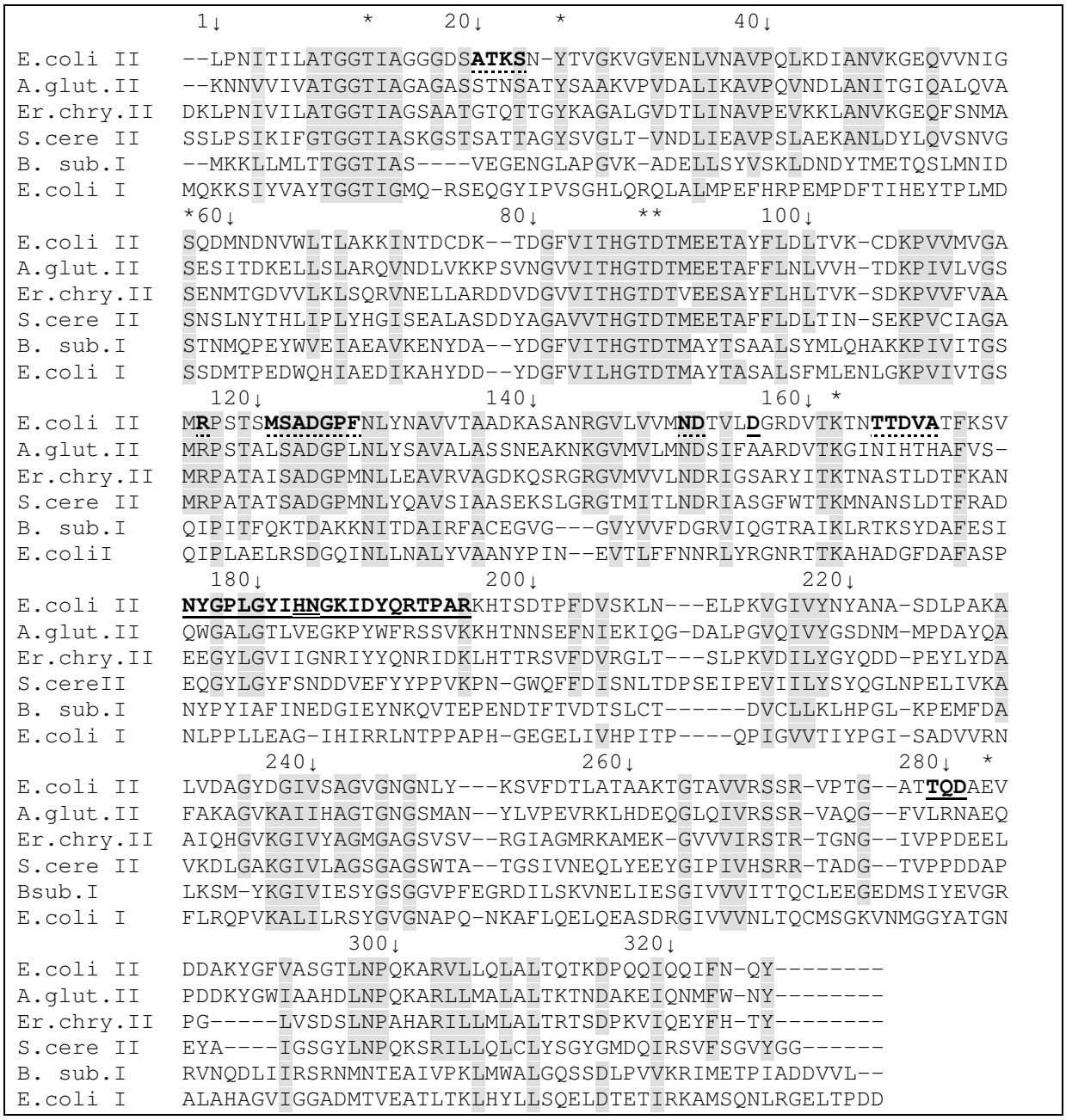

Figure 1.4 Sequence alignment of different asparaginases. Highly conserved sequences are shown in shaded print. The amino acids taking part in the formation of the tetramer in *E. coli* asparaginase II are printed in bold. Amino acids present at the B/C or A/D interfaces are underlined. The amino acids present at the B/A or D/C interfaces are underlined by a dotted line. Amino acids present on all interfaces are double underlined. Stars (*) indicate catalytically important residues.

The sequences shown are: *E. coli* II – Asparaginase II from *Escherichia coli* [Jennings and Beacham, 1990], A. glutam II - Glutaminase-Asparaginase (Typ II) from *Acinetobacter glutaminasificans* [Harrison *et al.,* 1987], Er. chry. II Asparaginase (Typ II) from *Erwinia chrysanthemi* [Minton *et al.,* 1986], S. cere II Asparaginase (Typ II) from *Saccharomyces cerevisea* [Kim *et al.,* 1988], B. sub. I Asparaginase (Typ I) from *Bacillus subtilis* [Sun und Setlow, 1991], and *E. coli* I Asparaginase (Typ I) from *Escherichia coli* [Jerlström *et al.,* 1989]

1.4.2 Structure of *E. coli* asparaginase II

The crystal structure of the *E. coli* asparaginase II (EcA2) has been determined to 2.3 Å resolution by A. Woldawer and his colleagues (Swain *et al.,* 1993). During the last years, the structures of several other asparaginases have been solved [Swain *et al.,* 1993; Lubkowski *et al.,* 1996; Rao *et al.,* 1996]

1.4.2.1 Tertiary and quaternary structure

The asparaginase subunit (Figure 1.5) consists of two α/β domains that are connected by a linking sequence involving residues 191-222 (blue). The N-terminal domain (top) contains an eight-stranded mixed β-sheet and four α–helices. A disulfide bridge is located between the residues Cys77 and Cys105 of N-terminal domain (Greenquist and Wriston, 1972). The smaller C-terminal domain (bottom, residues 213-326) consists of a four stranded parellel β–sheet and four β-helices.

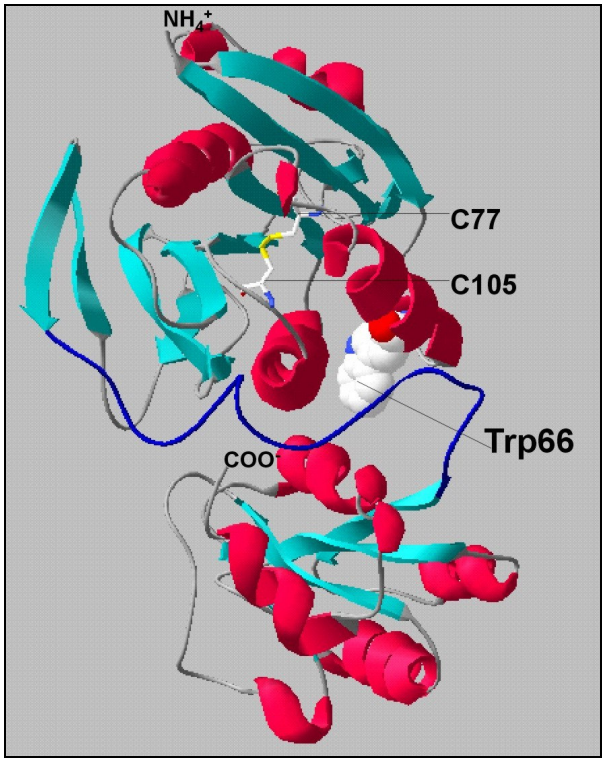

Figure 1.5 Schematic representation of the EcA2 monomer. Secondary structure elements in both the N-terminal (top) and C-terminal domain are shown in different colours. (Palm *et al.,* 1997)

The native tetrameric form of EcA2 is composed of four identical subunits, A, B, C, and D, with 222 symmetry (Figure 1.6). There are six pairwise interactions among the

subunits. The interactions between subunit A and C and between B and D, respectively, form two 'intimate' pair of subunits. Therefore, the tetramer is best described as a dimer of identical dimers.

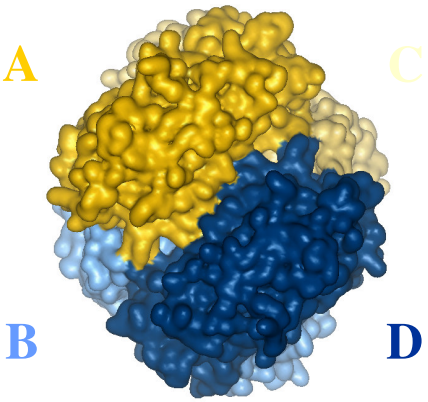

Figure 1.6 Quaternary Structure of EcA2. Subunits A (yellow) and C (light yellow), or B (light blue) and D (blue), respectively, form structurally equivalent dimers. (a) Each monomer contains one active site indicated by bound aspartate (red). W66 buried in the interior of subunit (pink). Residues Y176 and Y181 at the A/D and B/C interfaces are represented by the green surface (b) Model rotated by 90°.

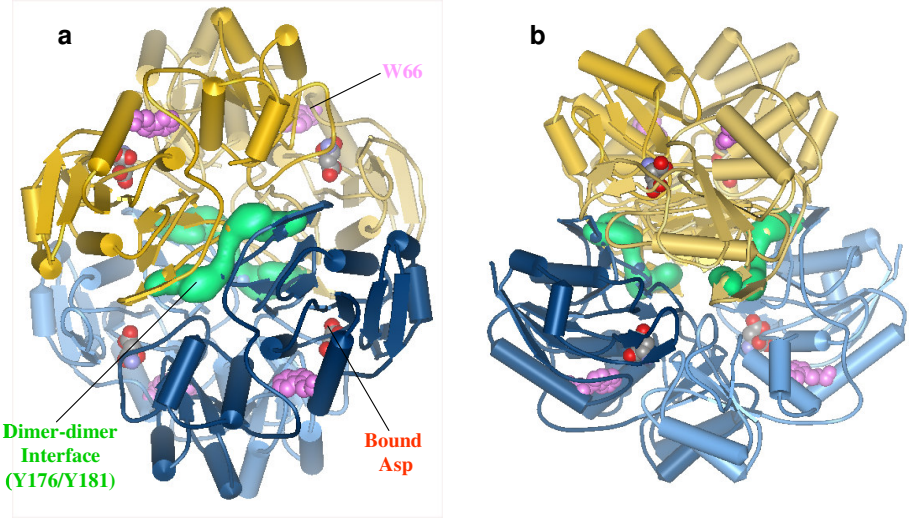

The asparaginase tetramer has four active sites. Their location has been identified by the presence of the bound aspartate, which is clearly visible in the electron density map. The active sites are located between subunits in the intimate dimers, so that each dimer has two active sites. Each of the four active sites of L-asparaginase is located between the N- and C-terminal domains of two adjacent monomers.

1.4.2.2 Dimer-dimer interfaces

Each EcA2 subunit has two areas of contact with either subunit of other "intimate dimer". In Figure 1.7 this is illustrated for subunit A which forms interfaces with subunits B and D, respectively (B-A and D-A). Corresponding interfaces exist for the other subunits as well. Some prominent residues at each interface are indicated in Figure 1.7. These are S122 and D124 for the B-A contact and the tyrosines Y176 and Y181 at the D-A contact site.

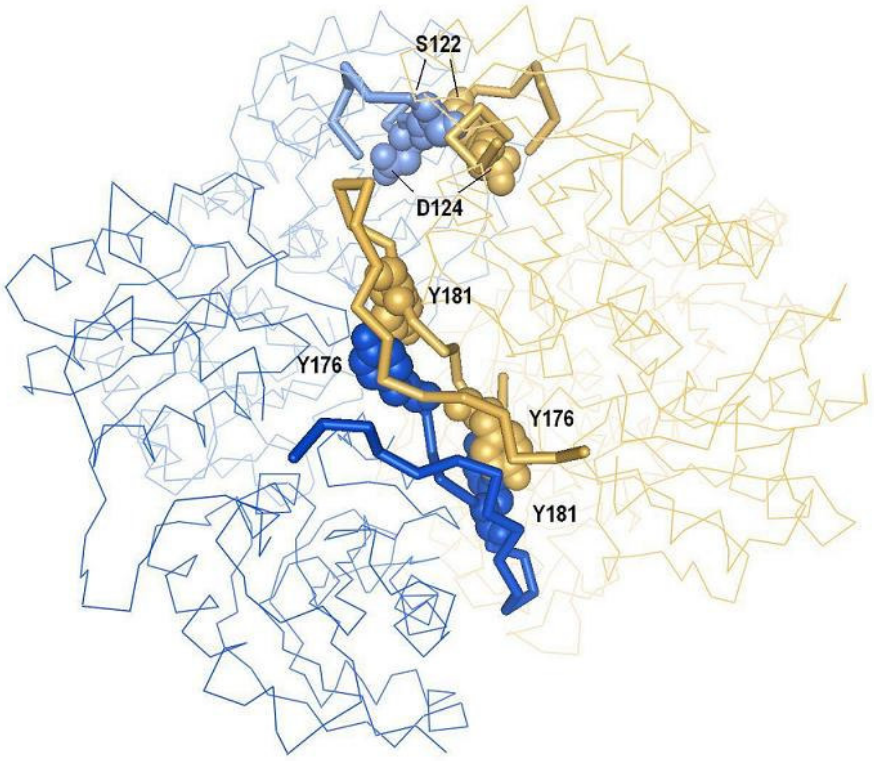

Figure 1.7 Important residues at the AB and AD interfaces of wild-type EcA2.

Previous experiments from our group have shown that a S122A mutant exhibited little change in its kinetic properties and showed normal stability in urea solutions (Derst *et al.,* 1992). The stability of a D124A mutant, on the other hand, was strongly impaired stability even in the absence of denaturants (Schubert *et al.,* 1996).

The local structure at the A/D interface is shown in more detail in Figure 1.8. Hydrogen bonds (green) connect the phenolic OH-groups of Y176 and Y181 with the backbone carbonyl oxygens of residues D188 and N175 in the opposing subunit. Salt bridges

(red) connect the carboxylate groups of D188 and D156 with the guanido groups of R195 and R191 in the opposing subunit.

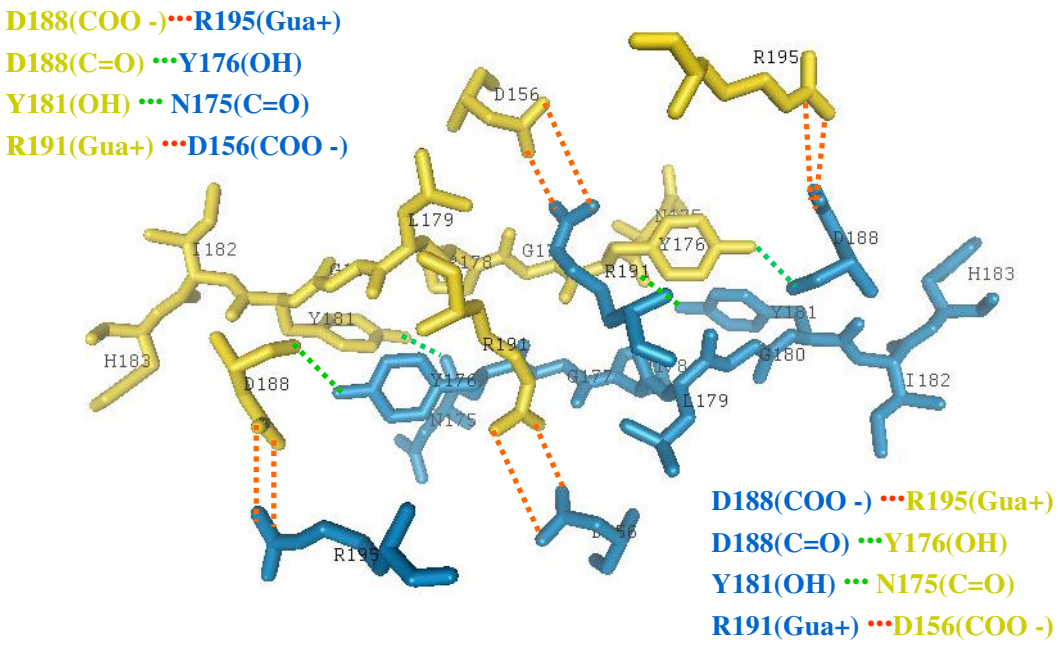

Figure 1.8 Hydrophobic and electrostatic interactions at the dimer-dimer (A/D) interface of EcA2 (PDB entry 3eca). Hydrogen bonds are shown in green dashed lines and salt bridges are shown as red dashed lines. The figure was created with WebLab Viewer.

One of the residues at the A/D interface, Y181, has been included in a mutagenesis study before. A Y181S mutant showed a complex denaturation profile in guanidine hydrochloride with the significant appearance of a folding intermediate (Wehner 1992; Derst 1994).

1.5 Active center and mechanism of catalysis

An extensive-site directed mutagenesis study of *Escherichia coli* asparaginase II (Wehner *et al.,* 1994; Aung, H.P, 1997) together with the information from X-ray crystallography (Palm *et al.,* 1996) revealed a number of amino acid residues that are important for catalysis and substrate binding. Among them Tyr 25, Thr 12, Thr 89 and Lys 162 play a catalytic role, while Asp 90, Ser 58, Asn 248 and Glu 283 assist substrate binding

(Wehner *et al.,* 1994). The structural data show that all these essential residues are located in the active sites (Palm *et al.,* 1996).

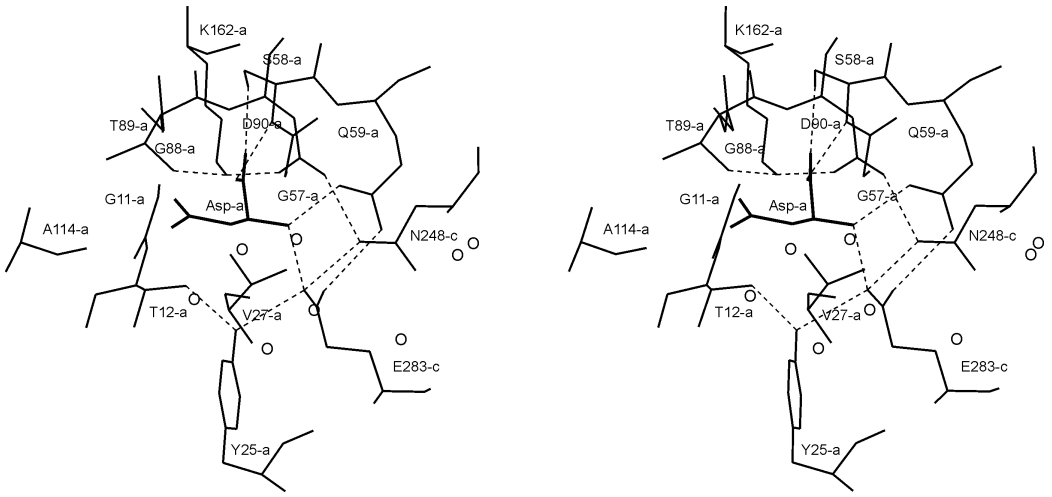

Figure 1.9 Stereo view of the EcA2 active site (from Derst *et al.,* 2000). Open circles indicate conserved water molecules.

Ser 58, Ala 114, Asp 90 and Glu 283 mediate substrate binding by direct hydrogen bonding interactions with the substrate. The residues important for catalysis include Lys 162, Thr 89, Tyr 25, and Thr 12. They directly interact with the substrate through Asp 90 and Glu 283 by hydrogen bonding (Derst *et al.,* 2000). One half of the active sites is covered by a flexible loop containing Thr 12 and Tyr 25 (Aung *et al.,* 2000).

The hydoxyl group of Thr 12 and Thr 89 are closest to the side chain carboxylate of bound aspartate and thus the most likely candidate for the catalytic nucleophile. In fact, the activity of mutant Thr89Val is decreased by factor of 25,000 (Palm *et al.,* 1996) while the activity of mutant enzyme Thr12Ala is only 0.02% of that of wild type (Harms *et al.,* 1991). This means that both hydroxyl groups in position 89 and in position 12 are absolutely required for catalysis. In agreement with this assumption, the activity of mutant enzyme Thr89Ser reaches 20% of that of the wild type and mutant Thr12Ser is also quite active (Palm *et al.,* 1996).

In the active center of *E. coli* asparaginase II, there are two groups of three amino acids each (‘triads’). One of the putative triads contains Thr 89, Lys 162, and Asp 90, while

the other one is formed by Thr 12, Tyr 25 and Glu 283 (Derst *et al.* 2000). The residues in the triad are also connected through hydrogen bonds. These structures resemble the catalytic triad of the serine proteinase which is made up by an aspartate, a histidine, and a serine residues.

Normally ionization of the serine side chain is insignificant because of its high pK_a = 14. In serine proteinases and other enzymes with similar mechanism the partial negative charge on the oxygen atom is due to activation by a nearby histidine, which accepts a proton and thus increases the nucleophilicity of the serine side chain (Blow *et al.,* 1969; Bachovchin and Roberts, 1978). However, it is not clear whether, in the bacterial asparaginases, Lys 162 can play the same role as histidine in the serine proteinase, since its pK_a should be too high to allow a function as a base down to pH 5.

A series of further amino acid residues line the active site without being essential for catalysis. These residues were replaced with other amino acids of different and polarity by using systematic site-directed mutagenesis (Derst *et al*. 2000). Theses residues include Gly 11 and Gly 88, both of which are immediately adjacent to the catalytic threonine. Gly 57 and Gln 59 are located on either side of Ser 58, a residue important for substrate binding: Val 27, which lines the active lines at the left and Asn 248 of another subunit comes in the active site from the right. Asn 248 is engaged in hydrogen bonds with residues Asp90 and Glu283. Mutants of Gly11, Gly88, Gly57 and Gln 59 showed reduced glutaminase activity. From the kinetics and stability data, it became clear that in EcA2, residues Gln 59 and Asn 248 both modulate substrate specificity in a selective manner.

1.6 Expressions system (Harms *et al.,* 1991)

Harms *et al*. have described the construction of expression vector pTWE1 for *E. coli* asparaginase II, a derivative of pT7-7 (Tabor and Richardson, 1985). The expression plasmid pTWE1 is shown in figure 1.5. From this plasmid the *ans*B gene will be transcribed from the bacteriophage T7 promoter Φ10 when transformed in the *E .coli* strain BL21Ω (CU1783). The gene for the β-lactamase causes the Ampicillin-resistance.

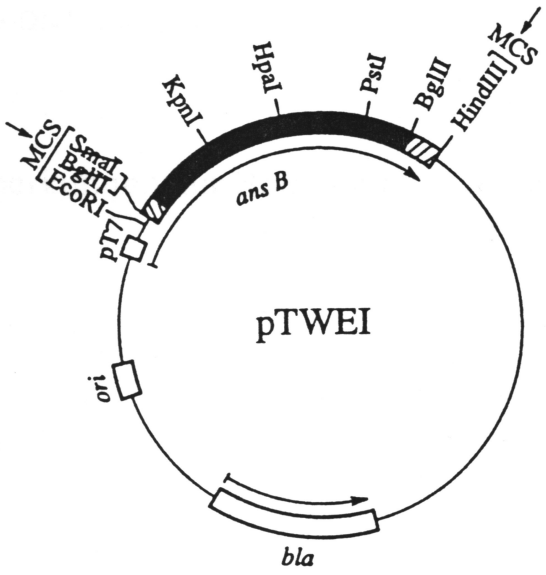

Figure 1.5 Expression plasmid pTWE1.
MCS: remnants of *multiple cloning site*
pT7: Promotor for T7-RNA-Polymerase
ori: ColEI *origin of replication*
bla: Gene for β-Lactamase
(Harms *et al.,* 1991)

EcA2 mutants are denoted by AS1nnnAS2 where n specifies the sequence position, while AS1 correspond to wild-type amino acid and AS2 the mutant residue. e.g. Y176S means that the original tyrosine residue at position 176 is replaced with serine.
The following nomenclature is used for expression plasmids:

1) pT7-7	Plasmid without the asparaginase (ansB) gene
2) pTWE 1	Plasmid with wild-type ansB
3) pTWE*	Plasmid with mutant ansB*
4) pTWE/Y176S	Plasmid with ansB/Y176S
5) CU1783/ pTWE/Tyr176Ser	Bacterial host cell containing pTWE/Tyr176Ser

1.7 Aims and outlines of the studies

There is a direct relationship between the stability and the therapeutic activity of any protein. A key factor for the stability of oligomeric protein is the interactions between its subunits. Very limited information is available on the interactions that stabilize the native oligomeric state of large proteins.

EcA2 is as an excellent model to study the interactions that stabilize the native oligomeric state of large proteins:

- High-resolution crystal structures are available (Swain *et al.,* 1993).

- The protein unfolds and refolds reversibly in chemical denaturation, and it is readily amenable to site-directed mutagenesis.
- There is only one tryptophan residue (W66) per subunit, localized in an unpolar environment in the native enzyme (Homer, 1972) which simplifies spectroscopic analysis of folding/ unfolding and dissociation/association phenomenon.

Using equilibrium and kinetic methods we analyzed such processes with wild-type EcA2 and a number of variants with amino acid replacements in the interior of the subunits or at interfaces between monomers. The results of these studies may help to construct EcA2 variants with improved stability for applications in leukemia treatment

The aim of the present study is to understand the molecular basis of the interactions between the subunits of EcA2. Moreover, we are interested in constructing EcA2 mutants with improved stability for possible application in leukemia treatment. To this end, site-directed mutagenesis reaction was used to create many single mutants namely EcA2 (Y176F), EcA2 (Y176S), EcA2 (D188N), and, EcA2 (D156N) at the dimer-dimer interface. On the basis of EcA2 (W66Y) (Derst *et al.,* 1994), we have created two double mutants EcA2 (W66Y/Y176W), and EcA2 (W66Y/Y181W) on the dimer-dimer interface. To monitor the stability of EcA2 (WT) and its mutants we used guanidine hydrochloride (Gu.HCl) equilibrium denaturation, enzymatic activity assay, fluorescence and circular dichroism (CD) spectroscopy. Thermal unfolding of EcA2 and its mutants was examined by differential scanning calorimetry (DSC), CD, light scattering, and activity assays. For EcA2 (WT) several basic parameters like pH-dependence and protein concentration dependence of denaturation, have been investigated, leading to a strong basis for the design of EcA2 mutants with improved protein stability in the future.

2. Materials

2.1 Apparatus

Analytical balance	Mettler Toledo, Gießen
Autoclave	Tuttnauer (Systec), Wettenberg
CD spectrometer, AVIV 62-DS	Aviv Associates, Lakewood, NJ
Centrifuge, Suprafuge 22	Heraeus, Osterode
Centrifuge, Minifuge	Heraeus, Osterode
Differential scanning microcalorimeter	Microcal, Amherst, MA
DNA thermocycler	Biometra, Goettingen
FPLC, Advanced Protein Purification 650E	Waters, Milford, USA
FPLC, Variable wavelength Monitor	Knauer, Berlin
Fraction collector, Frac-100	Amersham Pharmacia, Freiburg
Heat bath, F3	Haake, Karlsruhe
Heat incubation cupboard	Heraeus, Osterode
Incubation shaker, Model G25	New Brunswick, Edison, USA
Micropipettes	Gilson, France
Millex GS; (0.25 μm)	Millipore, Bedford, USA
Millex GS; (0.45 μm)	Millipore, Bedford, USA
Nitrocellulose filter (0.2 and 0.45 μm)	Schleichernd Schuell, Dassel
PD-10 desalting column	Amersham Pharmacia, Freiburg
pH-meter, Toledo 340	Mettler, Gießen
Refractometer	Carl-Zeiss, Jena
Servapor 21mm, Dialysis membrane	Serva, Heidelberg
Spectrofluorimeter, SFM 25	Kontron-instrument, Zeurich
Spectrophotometer 551S	Perkin-Elmer, Langen
Spectrophotometer, Ultrospec 3000	Amersham Pharmacia, Freiburg
Speed-Vac concentrator	Savant, Martinsried, Germany
Superdex 200 HR 10/30	Amersham Pharmacia, Freiburg

2.2 Chemicals

Standard laboratory chemicals (usually of analytical grade) were supplied by Merck, Sigma, Serva, Roth, and used without further purification.

8-Hydroxyquinoline	Sigma-Aldrich, Steinheim
Acrylamide/Bisacrylamide (30%,0.8%)	Roth , Karlsruhe
Agar-Agar	Fluka, Buchs
Agarose	Sigma-Aldrich, Steinheim
Ammoniumperoxodisulfate	Roth , Karlsruhe
Ampicillin	Roth , Karlsruhe
Bromophenol blue	Roth , Karlsruhe
Calcium chloride	Fluka, Buchs
Coomassie Brillant Blue	Serva, Heidelberg
EDTA	Fluka, Buchs
Ethanol p.A.	Sigma-Aldrich, Seelze
Ethidium bromide	Roth, Karlsruhe
Glycerol, 87%	Sigma-Aldrich, Seelze
Glycine	Roth , Karlsruhe
Guanidine hydrochloride	Fluka, Buchs
HEPES	Sigma-Aldrich, Steinheim
L-aspartic acid β-hydroxymate	Sigma-Aldrich, Steinheim
Luria-Broth (LB) medium	Gibco, Karlsruhe
MES	Sigma-Aldrich, Steinheim
MOPS	Sigma-Aldrich, Steinheim
N,N,N',N'-Tetramethylenediamine	Serva, Heidelberg
Piperazine	Fluka, Buchs
Polybuffer 74	Amersham Pharmacia, Freiburg
Polybuffer exchanger (PBE-94)	Amersham Pharmacia, Freiburg
Sucrose	Roth, Karsruhe
Serva Blue G	Serva, Heidelberg
Sodium dodecylsulphate	Sigma-Aldrich, Seelze
Trichloroacetic acid	Fluka, Buchs

Tris	Roth, Karlsruhe
Xylenecyanol FF	Sigma-Aldrich, Steinheim
β-Mercaptoethanol	Roth, Karlsruhe

2.3 Kits, Enzymes, and Markers

2.3.1 Kits

QIAprep-spin, Plasmid Mini-Kit	Qiagen, Hilden
QUIAEX Gel extraction kit	Qiagen, Hilden

2.3.2 Enzymes

*Eco*RI, Restriction endonuclease (10 U/µl)	Boehringer, Mannheim
*Hind*III, Restriction endonuclease (10 U/µl)	Boehringer, Mannheim
*Dpn*I, Restriction endonuclease (10 U/µl)	Stratagen, Heidelberg
PfuTurbo™, DNA-Polymerase	Stratagen, Heidelberg

2.3.3 Markers for Gel electrophoresis and Gel filtration:

Dalton Marker VII for SDS Gel electrophoresis	Sigma, Deisenhofen
peqGold 1 kb DNA-Ladder	Peqlab, Erlangen
peqGold 100 bp DNA-Ladder	Peqlab, Erlangen

2.4 Oligonucleotides and Plasmids

All synthetic nucleotides were synthesized by MWG Biotech (Ebersberg).

2.4.1 Oligonucleotide primers for mutagenesis

The following synthetic oligonucleotide primers were employed (mutagenic base changes are shown in underlined boldface):

Mutation *ansB*/Y176→F

MUTansB Y176F F:	5`-TCTGTTAACT**T**CGGTCCTCTG-3`
MUTansB Y176F B:	3`-AGACAATTGA**A**GCCAGGAGAC-5`

Mutation *ansB*/Y176→S

MUTansB Y176S F:	5'-TCTGTTAACT**C**CGGTCCTCTG-3'
MUTansB Y176S B:	3'-AGACAATTGA**G**GCCAGGAGAC-5'

Mutation *ansB*/Y176→W #1

MUTansB Y176W F:	5`-TCTGTTAACT**GG**GGTCCTCTGG-3`
MUTansB Y176W B:	3`-AGACAATTGA**CC**CCAGGAGACC-5`

Mutation *ansB*/Y176→W #2

MUT Y176W F:	5`-ACCTTCAAGTCTGTTAAGT**GG**GGTTCCTCTGGGTTACATTC-3`
MUT Y176W B:	3`-TGGAAGTTCAGACAATTCA**CC**CCAAGGAGACCCAATGTAAG-5`

Mutation *ansB*/Y181→W

MUTansB Y181W F:	5`-CCTCTGGGTT**GG**ATTCACAACG-3`
MUTansB Y181W B:	3`-GGAGAACCAA**CC**TAAGTGTTGC-5`

Mutation *ansB*/D188→N

MUTansB D188N F:	5`-CATTCACAACGGTAAGATT**A**ACTACCAGCGTACCCCGGC-3`
MUTansB D188N B:	3`-GCCGGGGTACGCTGGTAGT**T**AATCTTACCGTTGTGAATG-5`

Mutation *ansB*/D156→N

MUTansB D156N F:	5`-TGAATGACACCGTGCTT**A**ATGGCCGTGACGTCACC-3`
MUTansB D156N B:	3`-GGTGACGTCACGGCCAT**T**AAGCACGGTGTCATTCA-5`

2.4.2 Oligonucleotides primers for sequencing

ansB SEQ F1:	5`-AAC GCG GTA GTG ACC GCA GC-3`

T7-Seq:	5'-TAA TAC GAC TCA CTA TAG GG-3'

2.4.3 Plasmids for EcA2 expression

pTWE1	Laboratory
pTWE/W66→Y	Laboratory

2.5 Microorganisms

Microorganism	Genotype	Reference
E. coli XL-1 blue	recA1 endA1 gyrA96 thi-1 hsdR17 supE44 relA1 lac[F' proAB $lacI^q$ ZΔM15 $Tn10(Tet^R)$]	Stratagen, Heidelberg
E. coli BL21Ω (CU11783)	F^- gal met r^- m^- hsdS $ansB^-$ k lys placUV5-T7-Gen1 $plac^q$-lacI	Harms et al., 1991

Stocks of all microorganisms were prepared in sterile 87% glycerol and kept at -80 ^oC.

2.6 Computer programs and Internet links

Biotools	http://www.mbshortcuts.com/biotools
Crystal structure	http://www.rcsb.org
PicoLog for Windows	Pico Technology, UK
PowerPoint	Microsoft
Sigmaplot	Jandel Scientific
SPDB-Viewer	http://www.expasy.ch/spdbv
WebLab Viewer pro	Accelrys Inc.
Windows	Microsoft
Word	Microsoft

3. Methods

3.1 General precautions

All potentially harmful operation were carried out in restricted areas. Media, solutions, and instruments required for molecular biology were autoclaved to sterilize them. Temperature-sensitive solutions were sterilized by means of sterile filtration through 0.45 μM filters. All bacterial waste was decontaminated by autoclaving for a minimum of 30 min at 121 ^{o}C or higher before disposal. Waste containing ethidium bromide was disposed of separately. All dangerous chemicals were handled using safety glasses and gloves.

3.2 Bacterial growth

3.2.1 Medium

LB-medium	LB Medium 25 g/l composed of: Tryptone 10 g/l Yeast extract 5 g/l NaCl 10g/l pH 7.5

10 g tryptone, 5 g yeast extract, and 10 g NaCl were dissolved in 800 ml dH_2O. pH was adjust to 7.0 with 1 N NaOH and the volume was adjusted to 1 liter with dH_2O. This medium was sterilized by autoclaving.

LBAmp-Plates	LB medium 25g/l Agar 15 g/l pH 7.5 Ampicillin 100 mg/l

To 1 liter LB medium 1.5 % agar was added. After autoclaving, the medium was cooled in a 55 °C water bath. Before plating out, 100 mg/ml ampicillin was added. Per small agar plate (9 cm diameter) ca. 25 ml medium was poured and allowed to cool. LBAmp plates

were kept at room temperature overnight and stored at 4 °C.

3.2.2 Storage and revival of bacterial cultures

10 µl of frozen cells from a 87% glycerol stock was inoculated into 5 ml of LB medium. *E. coli* cultures were grown overnight with shaking at 37 °C. A loopful of culture was streaked on LB plates and the plates were incubated overnight at 37 °C. The colonies formed could be used up to 1 month when kept at 4 °C. For longer storage, a fresh culture of exponentially growing cells was mixed with sterile 87% glycerol in an 1:1 ratio (v/v) and stored at -80 °C.

3.3 Preparation of competent cells

Transformation buffer TFB-1	100 mM RbCl 50 mM $MnCl_2$ 30 mM CH_3COOK 10 mM $CaCl_2$ 15 % Glycerol Adjust to pH = 5.8 with 0.2 M CH_3COOH Sterilised by filtration
Transformation buffer TFB-2	10 mM MOPS 10 mM RbCl 75 mM $CaCl_2$ Adjust to pH = 7.0 with NaOH Sterilised by filtration

100 ml of LB medium was inoculated with 1 ml of a fresh overnight culture of *E. coli* XL-1 blue or BL21Ω, and growth continued with shaking at 37°C to an OD_{550} nm of 0.4-0.5. Bacterial cells were transferred to a sterile, ice-cold 50-ml polypropylene tube and the cells were recovered by centrifugation at 5000 x g for 10 min at 4 °C. The medium was decanted and the cell pellet was resuspended by swirling in 15 ml sterile TFB-1 and incubated in ice for 15 min at 4 °C. After incubation, cells were spun down at 5000 x g for 5 min at 4 °C. The

pellet was resuspended in 2 ml of TFB-2. Aliquotes of this cell suspension were kept at -80 ^{o}C up to one year. [Dager and Ehrlich, 1979; Hanahan und Meselson 1983]

3.4 Preparation of Plasmid-DNA

The QIAprep-spin plasmid kit (250) from QIAGEN was used for the preparation of double-stranded DNA. 3 ml of LBA medium was inoculated with 10 µl glycerol stock of transformed *E. coli* cells with shaking for overnight at 37°C. This culture was centrifuged at 4°C for 10 min at 14,000 x g to isolate the cell pellet.

Reagents	
P1	Cell resuspension buffer
P2	Cell lysis buffer
N3	Neutralization buffer
PB	Wash buffer
PE	Wash buffer
EB (Elution buffer)	10 mM Tris/HCl, pH=8.5

The pelleted bacterial cells were resuspended in 250 µl of buffer P1. After that, 250 µl of SDS-containing lysis buffer P2 was added and mixed with the cell pellets by inverting 4-6 times. 350 µl of chilled neutralization buffer N3 was added to the lysate and mixed by gentle inversion to precipitate the cell components. The precipitate was removed by centrifugation at 4°C for 10 min at 14,000 x g and the supernatant was discarded. A QIAprep-spin column was placed in a micro centrifuge tube and the supernatant was applied to the column. After centrifugation for 1 min, the fluid in the spin column was drained into the micro centrifuge tube, while the plasmid DNA from the supernatant was bound to the column material. The column was then washed by adding 500 µl of PB buffer and again centrifuged for 1 min. The flow-through was discarded. The column was washed another time with 750 µl of PE buffer as above. Finally, the bound DNA was eluted with 100 µl of TE buffer by centrifugation.

3.5 Determination of DNA concentration

The concentration of DNA was estimated according to the following equation:

μg DNA = A_{260} * 50 * volume of total solution (ml) * dilution ratio

3.6 DNA Sequencing

For sequencing, template DNA was diluted to concentrations of 100-200 ng/µl and dried in the Speed-Vac for 1 h. Plasmid DNA was sent to MWG Biotech (Ebersberg) for primer synthesis and sequencing.

3.7 Mutagenesis [Stratagene, 1992]

The QuikChange site-directed mutagenesis kit is used to create point mutations, switch amino acids, and delete or insert single or multiple amino acids. The QuikChange site-directed mutagenesis method uses *PfuTurbo*® DNA polymerase and a temperature cycler. *PfuTurbo* DNA polymerase replicates both plasmid strands with high fidelity and without displacing the mutant oligonucleotide primers. The basic procedure utilizes a supercoiled double-stranded DNA (dsDNA) vector with an insert of interest and two synthetic oligonucleotide primers containing the desired mutation. The oligonucleotide primers, each complementary to opposite strands of the vector, are extended during temperature cycling by *PfuTurbo* DNA polymerase. Incorporation of the oligonucleotide primers generates a mutated plasmid containing staggered nicks. Following temperature cycling, the product is treated with *Dpn* I. The *Dpn* I endonuclease is specific for methylated and hemi-methylated DNA and is used to digest the parental DNA template and to select for mutation-containing synthesized DNA (Nelson *et al.,* 1992). DNA isolated from almost all *E. coli* strains is methylated and therefore susceptible to *Dpn* I digestion. The nicked vector DNA containing the desired mutations is then transformed into XL1-Blue supercompetent cells.

3.7.1 Mutagenesis-PCR

PfuTurbo™ DNA-Polymerase	2.5 U/µl
Polymerase-Buffer 10 x	
Template DNA	Miniprep 1:20
Primer A	10 pmol/µl
Primer B	10 pmol/µl
DNTP-Mix	dATP, dGTP, dTTP, dCTP) each 10 mM
DMSO-Solution	50 % DMSO

Sample reactions were prepared in 50 µl volumes as indicated below :

5 µl 10 x Polymerase-Buffer

1 µl Template DNA (ca. 5 – 50 ng)

1.25 µl Primer A (125 ng)

1.25 µl Primer B (125 ng)

1 µl dNTP-Mix 10 mM each dNTP

2 µl DMSO

38.5 µl H_2O

Before starting the PCR, 1 µl PfuTurbo™ was added in the reaction mixture. Cycling Parameters for the QuikChange Site-Directed Mutagenesis Method were as listed below:

Steps			
1	30 Sec	95 °C	1 x
2	30 Sec	95 °C	15 x
3	1 min	55 °C	
4	12 min	68 °C	
5	∞	4 °C	

3.7.2 *Dpn*I Digestion of the Amplification Products

DpnI	10 U/µl

1 µl of the *Dpn*I restriction enzyme (10 U/µl) was directly added to each amplification reaction and incubated at 37 °C for 1 h. *Dpn*I-treated DNA was transformed in *E. coli* XL-1 blue competent cells.

3.7.3 Transformation of supercompetent *E. coli* XL-1 blue cells

5-10 µl of the *Dpn*I-treated DNA was mixed with 100 µl of competent *E. coli* XL-1 blue cells and incubated in ice for 15 min. The cells were then heated in a water bath (42 °C) for 60 s and immediately cooled down in ice for 5 min. 800 µl of LB-medium was added to the competent cells. The cells were incubated at 37 °C for 30-45 min. After incubation, the cells suspension was spread on LBA plates with a sterile glass spreader. After drying up excess liquid, the plates were incubated at 37°C for overnight. 5 ml of LBA medium was inoculated with a single clone on agar plates and incubated overnight at 37 °C with shaking. Plasmid DNA was prepared from overnight culture and checked for sequencing as in section 3.4.

3.8 Analytical DNA digestion by restriction endonucleases

Buffer B	10 mM Tris/HCl, pH 8.0 100 mM NaCl 5 mM $MgCl_2$ 1 mM 2-mercaptoethanol
*Eco*RI	10 U/µl
*Hin*dIII	10 U/µl

5 – 10 µl Mini-Plasmid-Preparation was added with

2.0 µl Buffer B

0.7 µl *Eco*RI

0.7 µl *Hin*dIII

and incubated for 2 h at 37 °C. DNA fragment digested with *EcoRI/HindIII* can be identified by agarose gel electrophoresis (section 3.9). Insert DNA was detected as 1.4 kb fragments and plasmid DNA (pT7-7) was detected at 2.5 kb fragment.

3.9 Agarose gel electrophoresis (Maniatis *et al.*, 1982)

In agarose gels, DNA fragments can be separated from each other according to their size. The electrophoretic mobility of DNA fragments is inversely related to their length, as each nucleotide in a nucleic acid molecule carries a single negative charge.

Electrode buffer, 1 x TAE	1 mM EDTA 20 mM Tris/HAc; pH 8.0
Gel-Solution	1 % (w/v) agarose 10^{-4} % ethidium bromide in 1 x TAE-Buffer
Gel loading dye solution 10 x	25 mg bromophenol blue 25 mg xylenecyanol 5 ml 85 % glycerol 2 ml 50 x TAE 3 ml dd H_2O

DNA bands can be detected by staining with ethidium bromide. The dye ethidium bromide fluoresces under ultravoilet light when bound to DNA.

The gel matrix was prepared as follows: 0.4 g of agarose was dissolved in 40 ml of 1xTAE buffer by boiling. 5 µl of ethidium bromide was added to this gel solution and poured into the corresponding gel apparatus. After solidification of the gel, 800 ml electrode buffer was poured into the apparatus to cover the gel surface. 20 µl of DNA solution was mixed with 3 µl of dye solution and placed in the wells of the gel. After that, the DNA was separated for 45 min at the voltage of 100 V. The DNA bands in the gel were then visualized on a transilluminator using UV light (365 nm).

3.10 Transformation of supercompetent *E. coli* BL21Ω

5-10 µl of the BL21Ω/pTWE* was mixed with 100 µl of competent *E. coli* BL21Ω cells and incubated in ice for 15 min. The cells were then heated in a water bath (42 °C) for 60 s and immediately cooled down in ice for 5 min. 800 µl of LB-medium was added to the

competent cells. The cells were incubated at 37 °C for 30-45 min. After incubation, the cells suspension was spread on LBA plates with a sterile glass spreader. After drying up excess liquid, the plates were incubated at 37 °C overnight. 5 ml of LBA medium was inoculated with a single clone on agar plates and incubated overnight at 37 °C with shaking. Plasmid DNA was prepared from overnight culture and checked for sequencing as in section 3.4.

3.11 Determination of protein concentration

3.11.1 UV Spectroscopy (Homer and Allsopp, 1976)

Asparaginase concentrations were determined from UV spectra by assuming an absorption of $A(1\%)_{280} = 7.7$ (i. e., a 10 mg/ml solution has an A_{280}=7.7).

3.11.2 Bradford method (Bradford, 1976)

Bradford-Reagent	10 % (w/v) Serva Blue G 10 % (v/v) 85 % phosphoric acid 5 % (v/v) 95 % ethanol
BSA-Standards	25/50/100/200/400 µg/ml BSA in ddH_2O.

For quantitative protein determination, 1 ml of 1 M NaOH was added to 20 ml of Bradford-Reagent. 100 µl of protein solution was mixed with 1 ml Bradford reagent and incubated at room temperature for 20 min. Absorption was measured at 595 nm against a blank (100 µl H_2O, 5 ml Bradford reagent). For the standard curve, 10 sample solutions of diluted ovalbumin were measured in the same way.

3.12 Expression of EcA2 (Harms *et al.,* 1991; Wehner, 1993)

3.12.1 Bacterial cultures

100 ml of LBA medium was inoculated with 10 µl of a BL21Ω/pTWE* glycerol culture and incubated overnight at 37 °C with shaking. After that, the culture was transferred to 1 liter of LBA medium and cells were grown for further 6 h.

3.12.2 Osmotic shock

Spheroblast buffer	100 mM Tris/HCl; pH 8.5 0.5 M Sucrose 0.5 mM EDTA

The bacterial cells from 2 l culture were collected by centrifugation at 1,800 x g for 15 min at 4 °C. The cells pellet was suspended in 200 ml of spheroblast buffer by vortexing. These resuspended cells were incubated in ice for 10 min. After that, the suspension was centrifuged at 4 °C for 20 min at 6,000 x g. The supernatant was discarded and the pellet retained.

This pellet was resuspended in 50 ml of ice-cold water using a vortex and then incubated in ice for 15-20 min. The periplasmic proteins were separated from the cells by centrifugation at 10,000 x g for 30 min at 4 °C. The enzyme-containing supernatant was collected, taking care to avoid contamination with bacterial cells.

3.12.3 Precipitation with ammonium sulphate

The supernatant was first brought to 50% ammonium sulphate (29.5 g/100 ml) saturation within 1 h at 4 °C. The precipitation was collected by centrifugation at 15,000 x g for 15 min at 4 °C. After that, the supernatant was brought to 95% saturation by further addition of ammonium sulphate (27.2 g/100ml) and kept at 4 °C before chromatofocusing.

3.12.4 Chromatofocusing (Sluyterman and Elgersma, 1978, Sluyterman and Wijdenes, 1978)

Column material	PBE^{TM}94 Polybuffer exchanger
Starting buffer	25 mM piperazine/HCl; pH 5.5
Elution buffer	0.1 x Polybuffer® 75/HCl; pH 4.0

The ammonium sulphate precipitate was centrifuged at 15,000 x g, 4 °C for 15 min. The pellet was dissolved in the minimum volume of starting buffer and dialysed against 2x

500 ml of the same buffer to remove ammonium sulphate. The resulting solution was centrifuged to remove impurities before loading to the column.

The chromatofocusing column (250 x 10 mm) containing polybuffer exchanger was equilibrated with 250 ml of starting buffer. Before loading the sample, the column was eluted with 2 ml of polybuffer. After loading the protein solution, the flow of elution buffer was adjusted to a velocity of 20-30 ml/h. 90 fractions of 1.5-2.5 ml were collected. After each run, the column was washed with 1.0 M NaCl.

All fractions were analyzed for protein concentration (section 3.11.1), pH values and asparaginase activity (section 3.16.3). In addition, protein purification was checked by SDS-PAGE (section 3.14). The fractions of interest were collected according to the elution profiles and the protein was precipitated by adding ammonium sulphate to 95% saturation to remove the polybuffer. The precipitates could be stored at 4 °C for prolonged times before use.

3.13 Preparative Gel Filtration

The aim of gel filtration was to completely separate protein from remaining polybuffer. Gel filtration separates protein molecules according to their size. Large molecules are unable to penetrate the pores of the cross-linked polymer and are eluted from a Sephacryl column ahead of small molecules. The molecular weight of asparaginases is 144,000, so gel filtration is the most suitable method to remove polybuffer.

Gel matrix	Sephacryl® S-300
Starting and elution buffer	100 mM Tris/HCl; pH 7.0

Enzyme solutions in 95% ammonium sulphate were centrifuged to get a pellet which was dissolved in the minimum volume (ca. 1 ml) of starting buffer and dialyzed against the same buffer (2x 500 ml). The protein solution was filtered through a 0.45 µm nitrocellulose membrane and degassed by sonication. The column (450 mm x 20 mm) was equilibrated with starting buffer. After dialysis, the enzyme sample was loaded on the column. The elution of the sample was carried out at a velocity of 12 ml/h. After determination of protein

concentration (section 3.11.1) and asparaginase activity (Section 3.16.3), the fractions of interest were collected for protein precipitation with ammonium sulphate (32.5 g/50 ml) and stored at 4 ^{o}C.

3.14 SDS polyacrylamide gel electrophoresis (SDS-PAGE) (Laemmli, 1978, Biorad Instruction Manual, 1987)

Proteins can be separated on the basis of their mass by SDS polyacrylamide gel electrophoresis under denaturing conditions. Sodium dodecyl sulphate (SDS), an anionic detergent disrupts nearly all noncovalent interactions in native proteins. Mercaptoethanol reduces the disulphide bonds of the protein.

Acrylamide solution	30 % acrylamide 0,8 % bisacrylamide
Separating gel buffer	1.5 M Tris/HCl; pH 8,8
Stacking gel buffer	0.5 M Tris/HCl; pH6,8
Sample loading buffer	0.1 M Tris/HCl; pH 6,8 2 % SDS 3 % mercaptoethanol 10 % glycerol 0.01 % (w/v) bromophenol blue
10 x running buffer	250 mM Tris 1.9 M glycine 35 mM SDS

Composition of the gel solution

Gel solution:		
Separating gel: (15 % Acrylamide)	Stacking gel : (4.5 % Acrylamide)	
4.000 µl	650 µl	acrylamide solution

2.500 µl	-----	separating gel buffer
-----	1.250 µl	stacking gel buffer
100 µl	50 µl	10 % SDS
3.350 µl	3.000 µl	dd H_2O
50 µl	25 µl	10 % APS
10 µl	5 µl	TEMED

On the average one SDS molecule binds for every two amino acids. Therefore, the complexes of SDS with the denatured protein carry a large net negative charge and migrate towards the anode. The velocity of migration of SDS-protein complexes is approximately inversely proportional to the mass of the protein.

The protein solution was mixed with sample loading buffer in (1:1) ratio (v/v) and placed in boiling water for 3 min for denaturation. 3.5 ml of separating gel solution was added to the spaces between two glass plates in the gel apparatus. Stacking gel solution was added immediately to the top of the separating gel solution layer and the comb was placed in the stacking gel solution. About 1 h later the gel had polymerized. Before sample loading into the wells, running buffer was filled up to cover the gel. The comb was removed carefully and the wells were cleaned up with running buffer to remove the gel pieces. The samples were then loaded into the wells under the running buffer with an Eppendorf pipette. Separation of the proteins was carried out at the voltage of 80 V for 15 min. Once protein entered into the separation gel the current was set at 200 V and allow to run for an additional 45 min. Finally, the proteins in the gel were visualized by staining with coomassie blue.

3.15 Coomassie staining

Staining solution	45 % methanol 10 % acetic acid 0.1 % (w/v) Coomassie Brillant Blue

De-staining solution	45 % methanol 10 % acetic acid

After electrophoresis, the separating gel was immersed in the staining solution for 15 min at 50 °C. The gel was then rinsed with water. After that, it was de-stained at 50 °C for 1-2 h. The de-staining solution has to be changed more than 2 times during the process. Before drying the gel it was washed again with water then dried at 70 °C for 90 min under vacuum.

3.16 Asparaginase assays

Asparaginase activity towards L-asparagine can be measured by monitoring the decrease of the amide band absorption at 225 nm. This method, although convenient, is rather insensitive and subject to systematic error. Therefore, in this work discontinous assays were used for kinetic studies.

3.16.1 Assay of NH_3 with Nessler's reagent

The hydrolysis of L-asparagine was examined by ammonia determination with Nessler's reagent. Immediately after addition of the reagent, the absorption was measured at 480 nm. The absorption coefficient of the product is A_{480}=1130$\pm$50 $M^{-1}cm^{-1}$.

3.16.2 Principle of the AHA assay (Frear and Burrel, 1955, Derst *et al.,* 1994)

The Nessler method is not sensitive enough to accurately determine K_m values below 1 mM. Therefore the discontinous AHA assay was used for kinetic studies. EcA2 has comparable activities towards its natural substrate, L-asparagine and L-aspartic acid β-hydroxamate (AHA). The assay is based on the reaction of hydroxylamine liberated from AHA with 8-hydroxyquinoline (oxin) at high pH. The resulting green oxindol dye has an absorption coefficient of about 1.75x 10^4 $M^{-1}cm^{-1}$ at 705 nm and is thus detectable with high sensitivity.

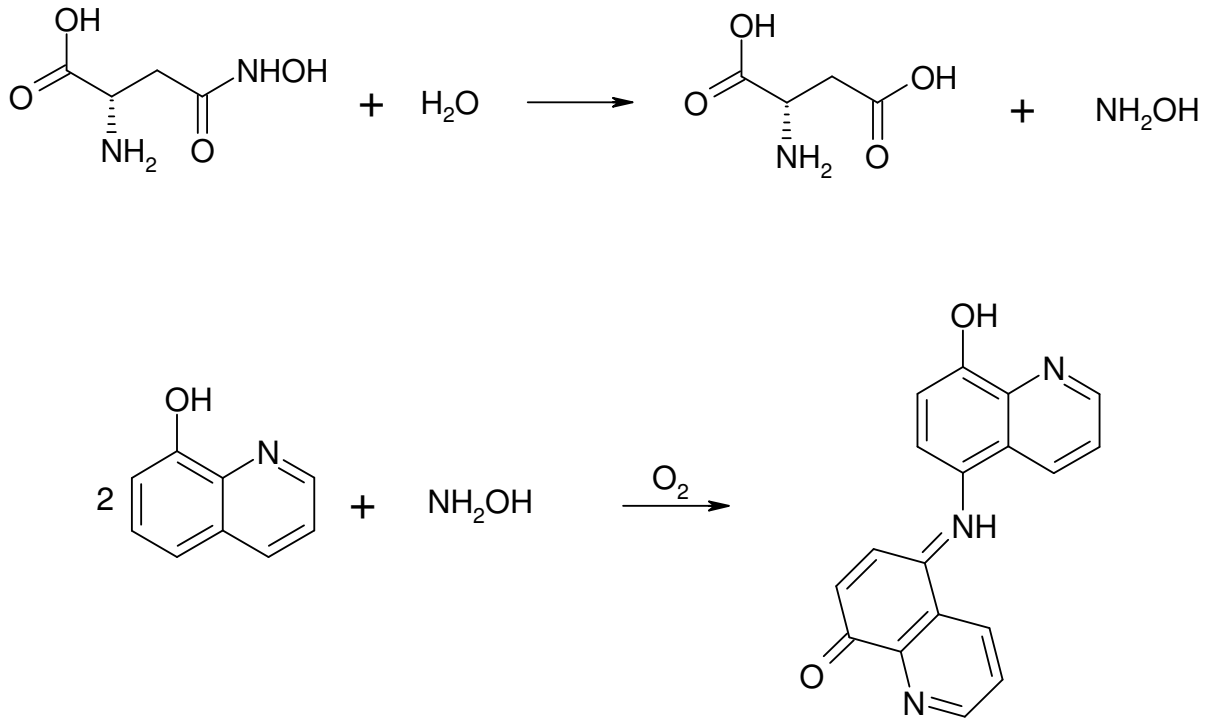

In this work, L-AHA was used as the substrate for activity profile and kinetic studies. For activity profiles, relative activities of the enzyme (mU) and for enzyme kinetics, specific activities (mU/mg) were calculated. 1 unit (U) of asparaginase activity is the amount of enzyme that catalyze the hydrolysis of 1 µmol substrate in 1 min at 25 °C.

3.16.3 Activity profile after chromatofocusing

Reaction buffer	50 mM MES; pH 5,0
Substrate solution	20 mM AHA in 50 mM MES, pH 5.0
Oxin solution	25 % (v/v) 2 % 8-hydroxyquinoline in ethanol 75 % 1 M Na_2CO_3
Stop solution	12 % TCA

10 µl of enzyme solution from each fraction after chromatofocusing was added to 180 µl of reaction buffer. 10 µl of AHA solution was added to start the reaction and incubated for 1 min at room temperature. 50 µl of 12% (w/v) TCA solution was added to stop the reaction.

After addition of 1000 µl of oxin/Na_2CO_3, the samples were heated in water bath (100 °C) for 1 min to complete the reaction. The samples were measured against the blank without enzyme solution at 705 nm after cooling the samples to room temperature.

3.16.4 Kinetic Characterization

Oxin solution	25 % (v/v) 2 % 8- hydroxyquinoline in ethanol 75 % 1 M Na_2CO_3
Stop solution	12 % TCA
Reaction buffer	50 mM Tris/HCl, pH 8.0

1 ml enzyme suspension in 95% ammonium sulphate was centrifuged for 10 min at 4 °C. The enzyme pellet was dissolved in 1 ml of 50 mM Tris/HCl (pH=7.0) and dialysed against the same buffer for 5 h. The resulting solution was centrifuged for 10 min to remove impurities. The protein concentration was determined by UV spectroscopy, and the protein concentration adjusted to 0.30 mg/ml or less.

Depending on the enzyme concentration and activity, 20-100 µl of enzyme was added to 1 ml of a substrate solution (25 µM-1.5 mM AHA in 50 mM Tris/HCl; pH 8.0). The assays were incubated for 1-30 min at 25 °C, depending on activity. At regular intervals (at least 5 times), 100 µl-aliquots were removed and added to microcentrifuge tubes containing 25 µl 12 % (w/v) TCA to stop the reaction. 1 ml of colour reagent (oxin/Na_2CO_3) was added to each tube. All microcentrifuge tubes were closed tightly and heated in boiling water bath for 1 min to develop the color. After allowing to cool for 10 min, the absorption was read at 705 nm.

Initial rates of AHA hydrolysis were calculated from parabolic fits to plots of A_{705} vs. time. The kinetic parameters V_{max} and K_m were calculated from non-linear fits of the Michaelis-Menten equation to the data using SigmaPlot.

$$V = \frac{V_{max} \cdot [S]}{Km + [S]}$$

V_{max} is the maximum velocity and K_m is the Michaelis-Menten constant. V_{max} is given as units/mg. One asparaginase unit will liberate 1.0 µmol of NH_3 or NH_2OH (from L-

asparaginase or L-asparagine ß-hydroxymate) per min at a given pH at 25 °C. K_m is the substrate concentration at half-maximal velocity. In the simplest case, it corresponds to the dissociation constant of the ES complex.

3.17 Determination of conformational stability

3.17.1 Chemical denaturation (Pace *et al.,* 1989: Shirley, 1992)

The stability of the active asparaginase tetramer was monitored by measurements of its tryptophan fluorescence at various concentrations of guanidine/HCl. In a hydrophobic environment, such as in the interior of a folded protein, tryptophan fluorescence emission occurs at shorter wavelength of 320-330 nm. During denaturation e.g. by guanidine/HCl, a strong decrease in tryptophan fluorescence is produced by the transfer of a residue (tryptophan) from the protein interior (hydrophobic environment) to aqueous environment with a concomitant red shift of the emission maximum to about 350 nm (Schmid, 1989).

Buffer	50 mM Tris/HCl; pH 8,0
Denaturant stock solution	3 M Gu/HCl

Enzyme suspension in 95% ammonium sulphate solution were centrifuged for 10 min and the pellet dissolved in 1 ml 50 mM Tris/HCl (pH=8.0). The resulting enzyme solution was dialysed against 50 mM Tris/HCl (pH=8.0) overnight to remove residual ammonium sulphate and bound aspartate. After that, the enzyme solution was centrifuged for 10 min to remove impurities and diluted to about 1 mg/ml (A_{280}=0.77).

The denaturant solution, double-distilled water, the buffer and the enzyme solution were filtered through 1.2 µm nitrocellulose filters to remove small particles which disturb the fluorescence measurements by light scattering.

Samples containing different concentration of the denaturant guanidine/HCl were prepared by mixing 50 µl enzyme solution with appropriate volumes of 3 M guanidine/HCl, 1 M Hepes stock solution (pH=8.0) and water. The resulting sample had a buffer concentration of 50 mM and a volume of 1 ml. 30 such samples were prepared. The first sample solution contained no denaturant, while the last one contained 1.5-2.0 M guanidine/HCl.

The mixture was incubated at 25 °C for 3 h to allow for equilibration. During the incubation period, the refractive index of each sample was measured with a refractometer to determine the exact guanidine/HCl concentration. Then fluorescence emission spectra were recorded in a SFM 25 spectrofluorimeter (Biotek). All samples were excited at 285 nm and their emission was measured between 300 to 400 nm.

3.17.1.1 Evaluation of denaturation experiments (Pace *et al.*, 1989)

The actual denaturant concentration of each sample was calculated from its refractive index n according to Nozaki (Nozaki, 1972).

III.1 $\Delta n = n(\text{guanidine/HCl}) - n(H_2O)$

III.2 $[\text{guanidine/HCl}] = 57.147\,(\Delta n) + 38.68\,(\Delta n)^2 - 91.6\,(\Delta n)^3$

The fraction of unfolded protein (f_d) as a function of Gu.HCl was calculated as described below. From these data the conformational stability in water, $\Delta G(H_2O)$ and a measure of the dependence of ΔG on denaturant concentration (m) were estimated.

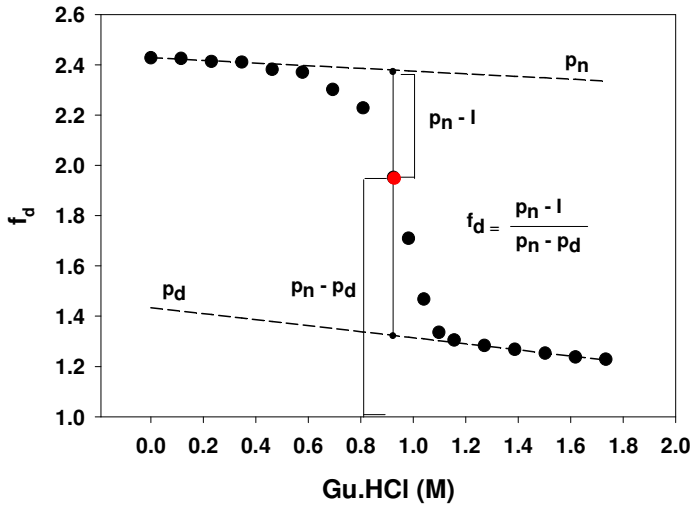

Figure 3.1 Sketch of a protein unfolding transition, as measured by fluorescence spectroscopy, p_n and p_d are the values of folded and unfolded forms, respectively, which both depend upon the concentration of denaturatnt (Gu.HCl). The fluorescence intensity is shown as a function of denaturant concentration.

For some EcA2 variants, the denaturation curves (fluorescence versus denaturant concentration) obeyed a simple two state model (Pace, 1989; see figure 3.1)

By assuming a two state mechanism, only the folded and unfolded forms of the protein are presented at significant concentrations and

$$fn + fd = 1 \qquad (1)$$

Where *fn* and *fd* represents the fractions of total protein in the folded and unfolded conformations, respectively. The value at any point on the transition curve is given by

$$I = pn \cdot fn + pd \cdot fd \qquad (2)$$

Where I is any observable parameters chosen to follow unfolding, and p_n and p_d represents the values of I characteristic of the folded and unfolded protein. The values of p_n and p_d for any point in the transition region are obtained by extrapolation of the pre- and post-transition baselines, which is generally achieved by a least-square analysis (Pace *et al.,* 1989). Combining Eqs. 1 and 2 yields:

$$pn = mn \cdot In + bn \qquad \text{(native fraction)} \qquad (3)$$

$$pd = md \cdot Id + bd \qquad \text{(denatured fraction)} \qquad (4)$$

The equilibrium constant can be calculated by using following equation:

$$K_D = \frac{fd}{fn} \qquad (5)$$

Combining Eqs. 1, 2, and 5 yields apparent fraction of denatured protein:

$$fd = \frac{K_D}{1 + K_D} = \frac{pn - I}{pn - pd} \qquad (6)$$

$$K_D = \frac{fd}{fn} = \frac{pn - I}{I - pd} \qquad (7)$$

The free energy change in the absence of denaturant ΔG_{H2O} for the folding-unfolding reaction can be calculated using:

$$\Delta G = -RT \cdot \ln K_D, \tag{8}$$

$$\Delta G_D = \Delta G_{H2O} - m \cdot [D] \tag{9}$$

Where ΔG_D is the free energy change at the denaturant concentration [D], R is the gas constantn and T is the absolute temperature (^oK). Combining Eqs. 8 and 9 yields:

$$K_D = e^{-\left(\frac{m[D]+\Delta G_{H2O}}{RT}\right)} \tag{10}$$

$$I = gn - \frac{K_D \cdot (gn - gd)}{1 + K_D} \tag{11}$$

Equation 9 was fit to I vs. [D] data to estimate values of ΔG_{H2O} and m. The parameter m is a measure of the dependence of ΔG on denaturant concentration.

For 3-state model

$$fn + fi + fu = 1 \tag{12}$$

Where f_i is the fractions of total protein in intermediate form. The observed value at any point on the transitions curve is given by

$$I([D]) = p_n \cdot f_n + p_i \cdot f_i + p_d \cdot f_d \tag{13}$$

Where I[D] is the fluorescence intensity chosen to follow unfolding at particular denaturant concentration. p_n , p_d and p_i represents the values of I[D] characteristic of the native, dissociated and completely dissociated protein. The relative concentrations are calculated as:

$$fn = \frac{1}{1 + \frac{1}{K_{D1}} + \frac{1}{K_{D1} \cdot K_{D2}}} \tag{14}$$

$$fi = \frac{fn}{K_{D1}} \tag{15}$$

$$fd = \frac{1}{K_{D2}} \tag{16}$$

K_{D1} and K_{D2} are the equilibrium constants for the first and second dissociation equilibrium. They can be calculated from the equations:

$$K_{D1} = e^{s1\cdot[D]+o1} \quad (17)$$

$$K_{D2} = e^{s1\cdot[D]+o2} \quad (18)$$

s1 and o1 as well as s2 and o2 are for the range of the transition phase.

$$\Delta G_{H2O}x = -R \cdot T \cdot ox \quad (19)$$

$$mx = RT \cdot sx \quad (20)$$

Where ΔG_{H2O}x is the dissociation enthalpies in respective phase in the absence of denaturant and m is a measure of the dependence of ΔG on denaturant concentration in respective phase.

In the 3-state model we can use the Eqs. 14 to 18 to calculate the value of ΔG_{H2O} x and m values. Half denaturation point $[D]_{1/2}$, i.e. the Denaturant concentration, at which both phases are present at same portions can be calculated by using following equation:

$$[D]_{1/2} = -\frac{\Delta G_{H2O}}{m} \quad (21)$$

3.17.2 Thermal denaturation

To understand the effects of temperature on the protein stability, thermal denaturation studies were carried out with the wild type and mutant EcA2. The residual activity of enzyme after heat treatment was estimated according to the previously described method (Derst, C., Thesis, 1995).

Reagents	
Buffer	50 mM Hepes (pH = 8.0)
Substrates	1 mM AHA (pH = 5.0) in the above buffer
TCA solution	12% (w/v) trichloroacetic acid in water
Oxin/Na_2CO_3 (1:3) (v/v)	2% (w/v) 8-hydroxyquinoline in ethanol and 1 M Na_2CO_3
Mineral oil	

An enyzme suspension in ammonium sulphate was centrifuged for 10 min and the enzyme pellet was dissolved in 50 mM Hepes (pH=8.0). The solution was first dialyzed against 50 mM Hepes (pH=8.0) overnight to remove residual ammonium sulphate and bound aspartate. After that, the enzyme solution was centrifuged for 10 min to remove impurities. The enzyme concentration was determined by UV spectroscopy. Concentration of 0.25-0.30 mg/ml were suitable for thermal denaturation.

100 µl of the above enzyme solution was placed into each one of the three reaction cups, and 2 drops of mineral oil were added. The layer of oil protects the enzyme solution from quick evaporation. The reaction cups with enzyme solution were placed at the thermocycler and the temperature gradient was programmed as follows:

First cycle	25 °C	1 min
Second cycle	25 °C - 80 °C	45.8 min

The enzyme solution was first pre-warmed for 1 min at 25 °C and then slowly heated to 85 °C with a change of temperature of 1.2 °C/min. 10 µl of enzyme solution was removed every minute and immediately mixed with 200 µl of 1 mM AHA substrate solution (working pH was same as that of the dialysis buffer). After incubation of solution for 1 min, 50 µl of 12% (w/v) TCA was added to stop the reaction. 500 µl of oxin/ Na_2CO_3 solution was added to each cups and heated in boiling water bath (100 °C) for 1 min to develop the colour. After cooling down for 10 min, the absorption was measured at 705 nm. From these data, relative activities (in mU) were calculated and activity was plotted vs. temperature (°C).

3.17.3 Renaturation after thermal unfolding

First cycle	25 °C	1 min
Second cycle	60 °C	30 min
Third cycle	25 °C	29.2 min

The enzyme solution was first pre-warmed for 1 min at 25 °C and then heated to 60 °C for 30 min for denaturation of enzyme. The enzyme solution was then slowly cooled to

25 °C with a change of temperature of 1.2 °C/min. 10 µl of enzyme solution was removed every minute and immediately mixed with 200 µl of 1 mM AHA substrate solution. All samples were analysed for asparaginase activity as described in section 3.16.3.

3.18 Analytical Gel filtration

Column	Superdex 200 10/30
Starting and Elution buffer	50 mM Hepes/HCl; pH 8.0 X M Gu/HCl
Gu.HCl-Buffer	3.0 M Gu/HCl 50 mM Hepes/HCl; pH 8.0
Marker proteins: Cytochrome c (horse heart) Carbonic Anhydrase (bovine blood) Albumin (bovine serum) Alcohol-Dehydrogenase (yeast) β-Amylase (sweet potato) Dextrane Blue	 12,4 kDa 29 kDa 66 kDa 150 kDa 200 kDa 2.000 kDa

The column was connected to an Äkta Explorer 100 FPLC system (Amersham Pharmacia Biotech). It was pre-equilibrated with different concentration of GuCl in 50 mM Hepes buffer of pH 8.0 at a flow rate of 0.5 ml/min. Protein samples (1 mg/ml) were incubated for 3 h with different concentrations of Gu/HCl at room temperature and centrifuged at 15000 x g for 10 min to remove insoluble material and loaded on the column through a 100 µl loop. Elution at a flow rate of 0.5 ml/min was monitored by absorbance at 280 nm.

3.19 Sedimentation equilibrium centrifugation

Sedimentation equilibrium ultracentrifugation was performed in a high-speed air-turbine centrifuge (Airfuge, Beckman; cf. Bothwell *et al.,* 1978). Carbonic anhydrase (29 kDa), Ovaalbumin (45 kDa), Bovine serum albumin (66 kDa), Phosphorylase B (95 kDa)

were employed as molecular weight standards. The final solutions in 300 µl volume were prepared by mixing 300 µg protein and different concentration of Gu.HCl (0 M-1.5 M) with 270 µl of a 5 mg/ml Dextran-100 solution, each dissolved in 50 mM Hepes pH 8.0 (dextran is routinely included to stabilize the equilibrium distribution of the protein during deceleration of the rotor, Bothwell *et al.,* 1978). 200 µl samples in 300-µl centrifuge tubes were spun in the "Airfuge" at room emperature for 16 hr at 60,000 rpm, whereas the 100 µl of control solutions were kept outside the centrifuge. After centrifugation, the upper 20 µl of samples and controls were carefully withdrawn and assayed for protein concentration by using Bradford assay (Section 3.11.2).

From the analytical data, the protein fraction depletion F ($F = A/A_o$) was calculated, where A is protein concentration in the sample and A_o is the corresponding value in the control. Calibration curves (log F of standard proteins versus their molecular mass were used to estimate the average mass of the catalytically active forms of EcA2 at different Gu.HCl concentrations.

3.20 Circular Dichroism (CD) Spectroscopy and Light Scattering

A plane-polarized light beam can be represented as a sum of right- and left- circularly polarized beams of equal intensity. When plane-polarized light passes through a chiral medium, differential absorption of the two circular components converts the plane polarized light into elliptically polarized light. The ellipticity is the angle Θ, the tangent of which is the ratio of the minor to the major axis of the ellipse. The ellipticity is directly proportional to the differential absorption. Thus CD spectra are often reported in terms of ellipticity (Fasman 1996).

Most biological molecules are chiral and therefore give rise to a CD signal. Since the CD signal is sensitive to protein conformation, CD is a method for monitoring secondary structure. All major protein secondary structure have their characteristic CD spectra. All-α proteins show a strong double minimum at 222 and 208 nm and a stronger maximum at 191-193 nm, which are characteristic of a α-helix. All ß-proteins usually have a single negative and a single positive CD band. They usually show a single minimum between 210-225 nm and a stronger positive maximum between 190-200 nm.

Mainly aromatic side chains contribute to the protein near-UV CD spectrum. Since aromatic residues are planar (and thus non-chiral), they have very small intrinsic ellipticity in the near-UV range. However, if aromatic groups are located in an asymmetric environment (such as that resulting from tertiary or quaternary packing), they acquire an induced near-UV CD signal. Therefore, near-UV CD spectra of proteins can be used to qualitatively characterize tertiary and/or quaternary protein structures. Even though the spectral amplitude and sign may vary among different proteins, the wavelengths of the bands corresponding to various aromatic groups are relatively well-defined. The strongest contribution to near-UV CD usually comes from Trp that has a major peak centered near 295 nm, with a shoulder at about 285 nm. Tyr gives a weaker signal centered around 285 nm. Phe has a complex near - UV CD that may contain multiple bands in the wavelength range from 250-270 (Strickland 1974).

The CD technique is nondestructive to biological samples, requires only a small amount of sample, and can be applied to molecules in solution. The limit is that it can only give information on secondary structure content, not on detailed molecular structure.

3.20.1. CD experiments

CD data were recorded using an upgraded AVIV 62-DS spectropolarimeter equipped with a Peltier temperature control. Far-UV CD data (185-250 nm) were collected with enzyme solutions (~0.1 mg/ml) in 20 mM PBS, placed in 2 mm cells. Near-UV CD data (250-320nm) were measured with similar solutions at 3.2 - 3.5 mg/ml protein placed in 5 mm cells. The spectra were recorded with a bandwidth of 1 nm, a step size of 1 nm, and an accumulation time per data point of 15 s over two or three scans. The melting curves were recorded at 222 and 285 nm during sample heating and consecutive cooling from 25 to 80 ^{o}C, with a 1 ^{o}C increment and an accumulation time per data point of 30 s or 300 s, which corresponds to the heating and cooling rates of 80 ^{o}C /h or 11 ^{o}C /h, respectively. In far-UV CD, the signal $\Theta_{222}(T)$ at 222 nm (that is proportional to the protein α-helical content) was used to monitor thermal unfolding of the EcA2 (WT) and mutants protein. In near-UV CD, the largest heat-induced changes in EcA2 (WT) and mutants were observed at 270-280 nm; the CD signal at 280 nm, $\Theta_{280}(T)$, was used to monitor these changes, which optimized the signal-to-noise ratio. The buffer baselines were subtracted from the data that were

normalized to the protein concentration and were expressed as molar residue ellipticity, in far-UV CD, and as molar ellipticity in near-UV CD. ORIGIN software was used for the data analysis and display. All CD experiments were repeated 2-3 times to ensure reproducibility.

Heat-induced changes in turbidity were monitored by the dynode voltage $V(T)$ that was recorded simultaneously with the CD melting data $\Theta(T)$,. The dynode voltage, which is high voltage applied to the photomultiplier of the UV detector, is proportional to the reduction in the light intensity due to the combined effects of light absorption and scattering. Although $V(T)$ does not significantly change during thermal unfolding of non-aggregating proteins, our studies of EcA2(WT) and mutants revealed that it increases substantially with the heat-induced increase in the particle size, reflecting increased light scattering of these particles. Therefore, measuring the $V(T)$ function in CD experiments is useful for monitoring the heat-induced changes in the size and/or morphology of EcA2(WT) and mutants. The resulting light scattering melting curves are correlated with the DSC data recorded in similar heating experiments.

3.20.2 Analysis of CD data

At 222 nm, the CD spectra of EcA2 were dominated by the contributions from α-helices. The α-helical content of the protein was roughly proportional to the CD signal $[\Theta]_{222}$, and were estimated from the measured ellipticity at 222 nm as:

$$\% \text{ α-helix} = (-[\Theta_{222}] + 3.000)/ 39.000$$

The raw data (in mdeg) was converted to mean residue ellipticity [Θ] by the following equation:

$$[\Theta]= \Theta*MRW/(10*l*c)$$

where, Θ = CD signal in mdeg, MRW = Mean residue weight of the protein, l= Path length of the cell in cm, and c = Protein concentration in mg/ml

3.21 Differential Scanning Calorimetry

The heat capacity $C_p(T)$ of protein samples was recorded at concentrations of 0.4-1.2 mg/mL in 20 mM PB buffer (pH 8.0) using a model MC-2 differential scanning microcalorimeter (Microcal, Amherst, MA), which contained matched Tantalum sample and reference cells (volume = 1.2343 ml). The calorimeter was interfaced to an IBM PC via a DT-2801 A/D conversion board (Analog Devices, Marlboro, MA) which allows automated data collection and analysis. Samples were exhaustively dialyzed at 4 ^{o}C against the appropriate buffer. Prior to introduction into the calorimeter cells, both dialysate and protein were thoroughly degassed under vacuum (without stirring for protein-containing samples) at room temperature. The reference solution (dialysate), protein sample, and calorimeter cells were at room temperature at the time of sample introduction, and subsequently cooled. Degassed protein solution and buffer solutions were subjected to a nitrogen pressure of 20 psi. The $C_p(T)$ data were recorded during heating at a rate of 90 ^{o}C/h (1.5 ^{o}C/min) from 10 ^{o}C to the maximal temperature of 100 ^{o}C, followed by cooling and incubation at 5 ^{o}C for 1-2 hours before the next scan was recorded. Following the buffer baselines subtraction, the data were normalized to protein concentration. Analysis and evaluation of data for calorimetric enthalpy (ΔH) values from the heat capacity versus temperature curves and van't Hoff enthalpy (ΔH_{VH}) values were performed using the software provided with the MC-2. This analysis uses the methodology and theoretical framework described by Freire and Biltonen and Rigell, de Saussure, and Freire. The T, for a given transition was taken to be the point of maximum excess heat capacity. The ΔH was calculated from the area under each calorimetric peak. Numerical integration of peak areas and resolution of overlapping peaks were performed using curve-fitting procedures utilizing either linear baselines (Krishnan *et al.,* 1978) or sigmoidal ("spline") baselines (Fukada *et al.,* 1983) when a change in heat capacity of the sample accompanied the thermal transitions. The ratio of the calorimetric to van't Hoff enthalpy ($\Delta H/\Delta H_{VH}$) was calculated according to the formula (Biltonen *et al.,* 1978),

$$\Delta H/ \Delta H_{VH} = \Delta H^2/C_{P',max}4RT_m^2$$

where, ΔH is the calorimetric enthalpy, $C_{P',max}$, is the maximum in the heat capacity function, R is the gas constant, and T, is the transition temperature. This ratio is 1 if the transition is

from one state to another (two-state type), greater than 1 if more than two states are involved, and may be less than 1 in certain cases if the process is irreversible (Biltonen *et al.,* 1978; Privalov *et al.,* 1974; Privalov *et al.,* 1986).

The molecular weight of asnase II used for calculation of molar quantities was M_R 138,000. This value reflects the molecular weight contribution from the 1304 amino acid residues. The EcA2 protein unfolding and the irreversible character of the thermal transitions, precluded the quantitative thermodynamic analysis of the calorimetric data. All DSC experiments were repeated 2-3 times to ensure reproducibility.

4. Results

4.1 Overview

The construction and characterization of EcA2 mutants is explained in the following schematic flow chart (Figure 4.1).

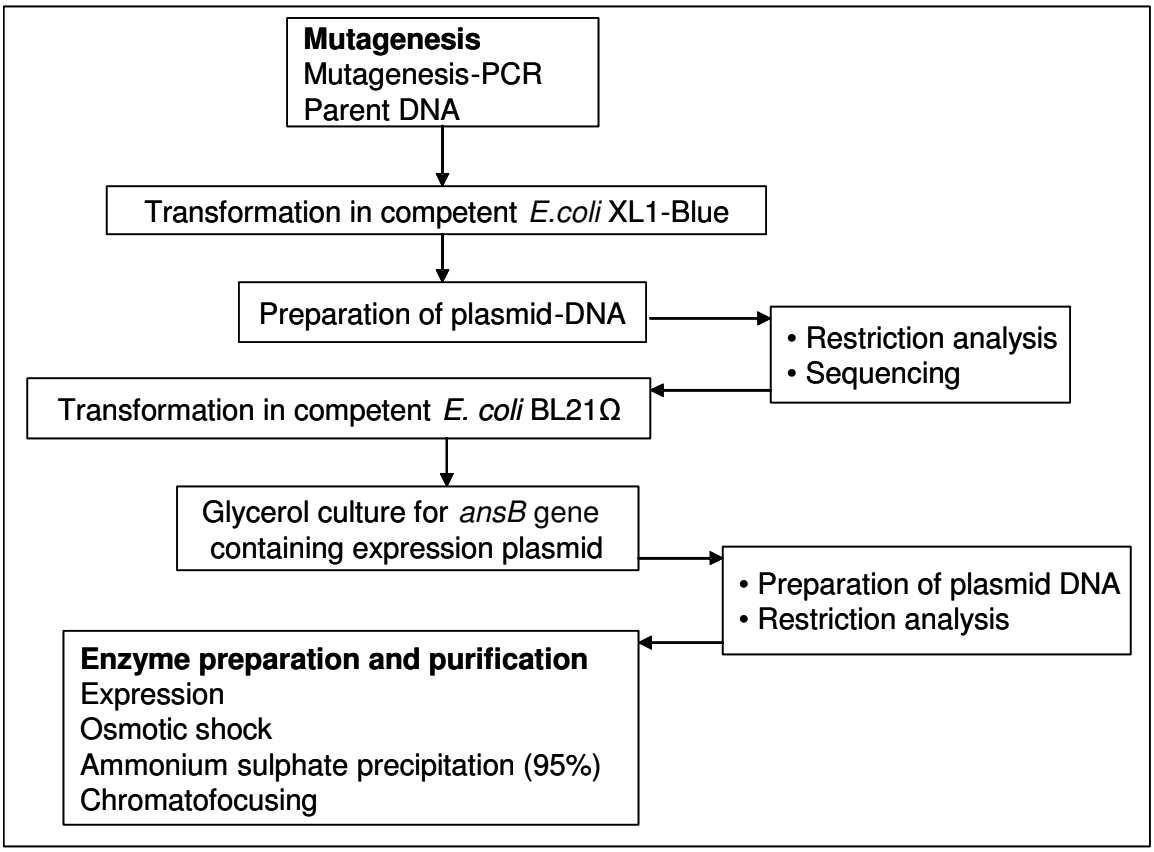

Figure 4.1 Schematic flow chart explaining EcA2 expression and purification.

4.2 Selection of residues for site-directed mutagenesis

In the context of the present study, we were mainly interested in the function of residues at the dimer-dimer interface of the EcA2 protein. Residues to be replaced by site-directed mutagenesis were selected according to their location in the protein, or due to their evolutionary conservation (See Introduction, Figure 1.4) within the class II amidohydrolase family. The location of these residues at the dimer-dimer interface and their relationship with other residue is shown in Figure 1.8 (see Introduction).

Following this, site-directed mutagenesis was used as a tool to create many single mutants at the dimer-dimer interface namely EcA2(Y176F), EcA2(Y176S), EcA2(D188N), and, EcA2(D156N). On the basis of a mutant constructed earlier in our laboratory i.e. EcA2(W66Y) (Derst *et al.,* 1994), we created two more double mutants EcA2(W66Y/Y176W), and EcA2(W66Y/Y181W) on the dimer-dimer interface.

4.3 Expression and purification of mutant enzymes

All enzyme species were readily expressed and purified as previously described for EcA2(WT) (Harms *et al.,* 1991). The purification procedure involves only two steps. In the first one, the protein is precipitated from the crude periplasmic fluid with ammonium sulphate (50-90% saturation). In the second step almost homogenous enzyme is obtained by chromatofocusing in the pH range 6.2 to 4.5.

In chromatofocusing, a pH gradient is formed by equilibrating the column with starting buffer and eluting with polybuffer of a lower pH. The choice of the pH range depends on the isoelectric point of the protein. The wild type enzyme and most of the other engineered mutants had comparable isoelectric points between 4.8–5.0. In the double mutant EcA2(W66Y/Y181W), the isoelectric point was about 4.4. All samples were first dialysed against 25 mM Piperazine/HCl (pH=5.5, starting buffer) and eluted with 1:10 diluted polybuffer (pH=4.0). Some of the mutants showed a second small activity peak in addition to the main enzyme fraction. These preparations needed re-chromatofocusing to remove the contaminating activity from the main protein peak. Gel filtration was carried out only when very high quality purification was required. Samples of elution profiles are shown in figure 4.2, 4.3, and 4.4. The protein concentration of each fraction was determined by UV spectroscopy at 280 nm and enzyme activity was assayed with AHA. In addition, the pH value of each fraction was determined. Fractions, the protein concentration of which matched asparaginase activity were collected and the enzyme precipitated with ammonium sulphate at 95 % saturation. The resulting preparations were examined by SDS/PAGE and were at least 95% pure. Yields varied between 5 and 20 mg of purified enzyme per liter of *E. coli* culture, depending on the stability of the respective protein. By gel filtration, on a calibrated Superdex 200 column it was ascertained that the mutants had the native tetrameric structure.

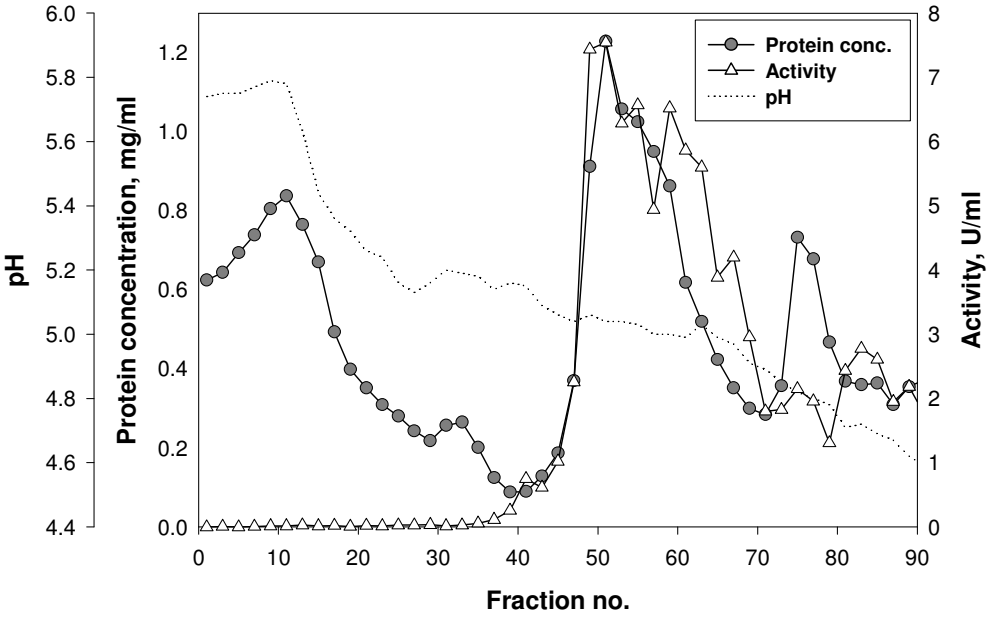

Figure 4.2 Purification of EcA2(WT) by chromatofocusing. The elution diagram shown was obtained as described in section 3.14. Activity towards 1 mM AHA at pH = 7.0 (mU/ml) and protein concentration (mg/ml) are plotted versus fraction number. Elution was by a pH gradient from 6.2-4.5. Collected fractions: 40-70

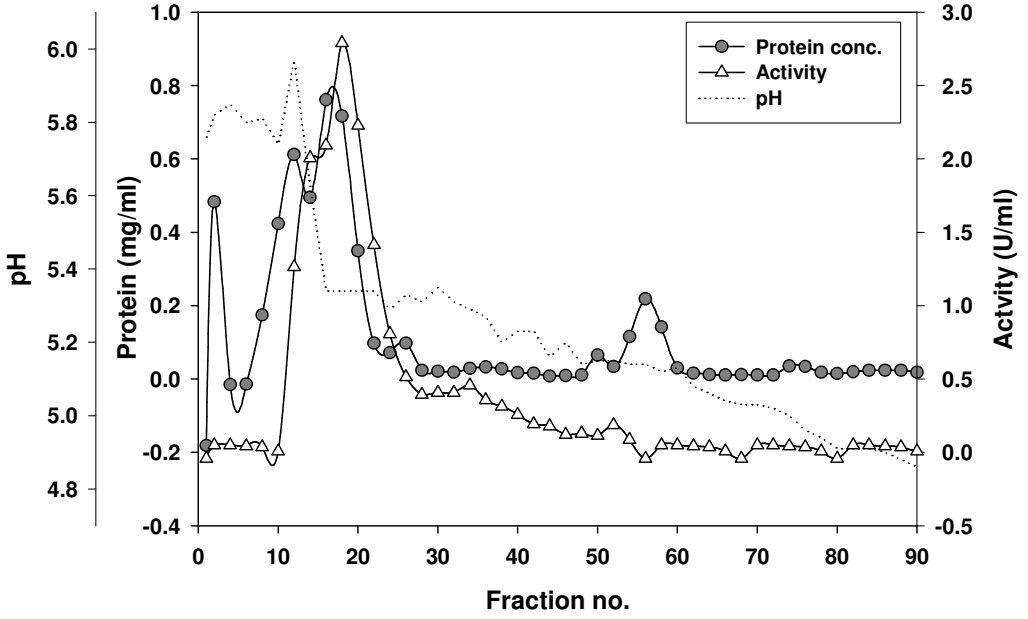

Figure 4.3 Purification of mutant EcA2(D188N) by chromatofocusing. The elution diagram shown was obtained as described in section 3.14. Activity towards 1 mM AHA at pH = 7.0 (mU/ml) and protein concentration (mg/ml) are plotted versus fraction number. Elution was by a pH gradient from 6.2-4.5. Collected fractions: 13-25.

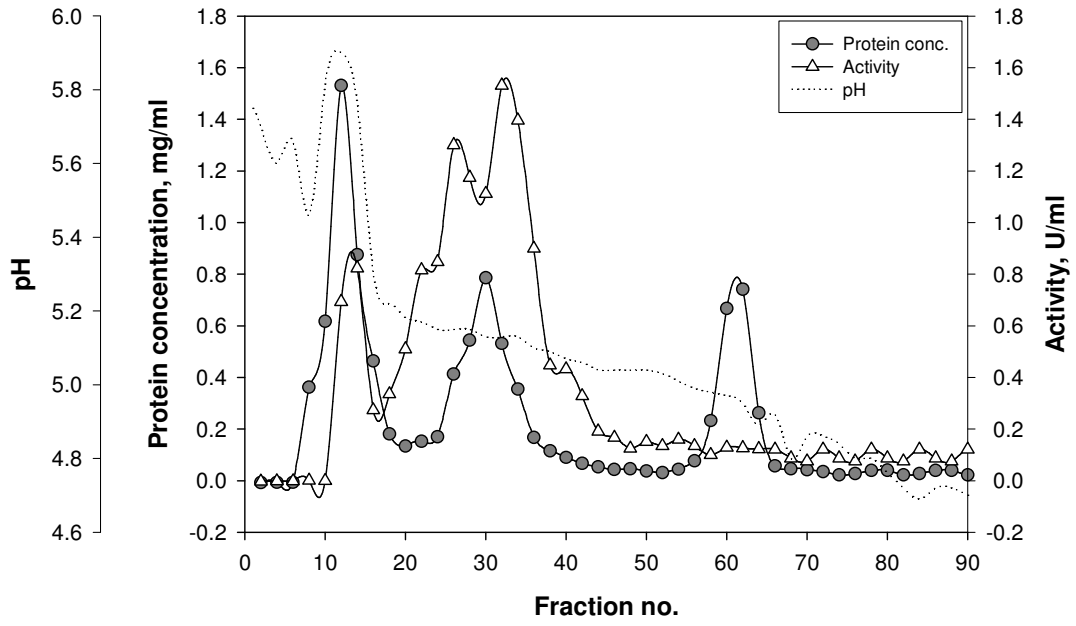

Figure 4.4 Purification of mutant EcA2(D156N) by chromatofocusing. The elution diagram shown was obtained as described in section 3.14. Activity towards 1 mM AHA at pH = 7.0 (mU/ml) and protein concentration (mg/ml) are plotted versus fraction number. Elution was by a pH gradient from 6.2-4.5. Collected fractions: 20-36.

4.4 Conformation and stability of EcA2 II

Denaturation studies are quite useful in establishing the stability of a protein and some aspects of its structure in the solution (Pace, 1990). Three independent methods were used to estimate the effects of the mutations on the stability of EcA2(WT) and its mutant i.e.

- equilibrium denaturation in Gu.HCl (monitored by the fluorescence of the only tryptophan residue of EcA2, W66)
- gel filtration to detect changes in tertiary and quatenary structure
- thermal denaturation (monitored by activity measurement, circular dichroism (CD), differential scanning calorimetry (DSC), and light scattering).

The $\Delta G(H_2O)$ values derived from chemical denaturation experiments are true thermodynamic constants, while in thermal denaturation T_m values are purely empirical "melting temperatures," i.e., the temperature where half of the activity was lost under the conditions of the experiments. Due to the different probes used, equilibrium denaturation only detected gross changes of conformation (W66 is at a distance of 14 Å from the active

site aspartate), while the loss of activity upon thermal denaturation may also reflect small local changes in the active sites.

4.4.1 Chemical denaturation studies

The native conformation of protein is mainly stabilized by non-covalent interactions. Therefore, extreme pH values, high temperatures, and chemical substances (denaturants) lead to the denaturation of the native conformation. In simple cases, denaturation by chemical substance is a reversible two-state process.

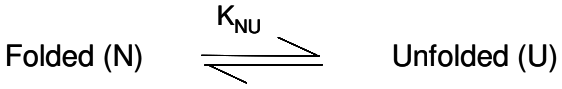

Also EcA2 is tetramer, this simple relationship can be applied to some of the EcA2(WT) mutants. The conformational stability of EcA2(WT) and its mutants was examined as described in the literature (Derst *et al.,* 1994) by denaturation experiment in guanidine hydrochloride solutions. It was reported earlier that the emission maximum of asparaginase at 327 to 320 nm is contributed in large part by the tryptophan residues that are located in a very hydrophobic environment (Shifrin *et al.,* 1971).

EcA2(WT)

Fluorescence spectra of EcA2(WT) in several different concentrations of Gu.HCl were obtained after excitation at 285 nm, with the result shown in figure 4.5 (A). The completely dissociated enzyme in 1.5 M Gu.HCl shows the loss of the 319 nm emission maximum and its replacement by a peak at 348 nm, which is characteristics of free tryptophan in aqueous solutions (Teale *et al.,* 1957). Indeed, the isoemissive point at 362 nm suggests that each spectrum is a combination of not more than two contributing components - one being the native and the other the dissociated protein.

Figure 4.5 B shows the plots of the fluorescence intensity (blue), activity (red), far-UV CD (green), and emission maximum (magenta) as a function of the molar concentration of the Gu.HCl.

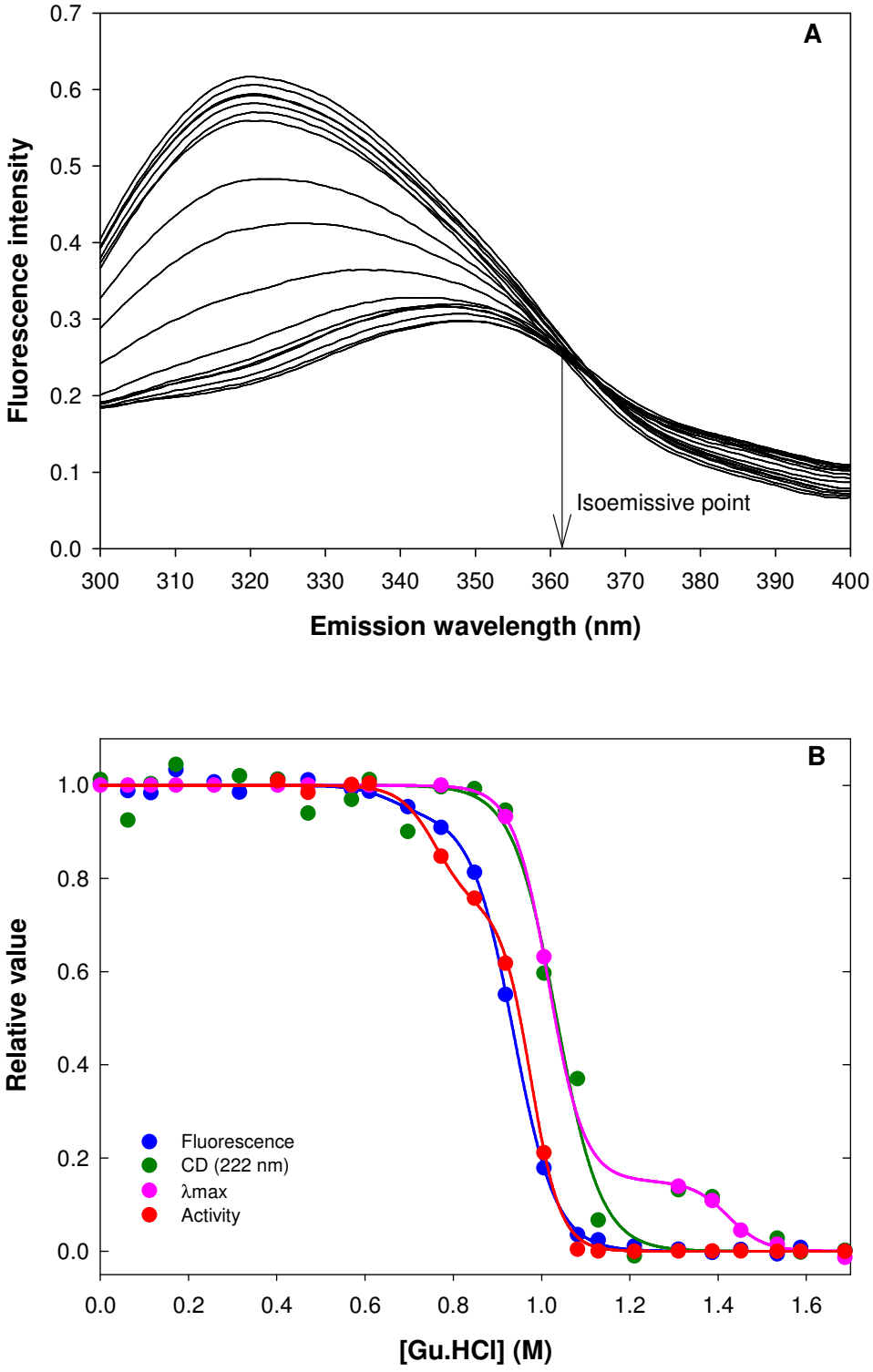

Figure 4.5 (A) Fluorescence spectra of EcA2(WT) at different concentrations of Gu.HCl**.** (B) Gu.HCl-induced denaturation curves of EcA2(WT). The appropriate fraction of denatured protein (F_{app}) was plotted versus denaturant concentration (Gu.HCl). The data was measured at pH 8.0 and 25 ^{o}C. The curves represent fits of the 2-state (CD) or 3-state model to the data (Section 3.17.2).

.

Parameters	Fluorescence	CD	Activity	λ(max)
ΔG_{H2O} (1) (kJ/mol)	38	51	46	62.9
m (1) (kJ/mol/M)	-48.7	-49	-72	-86.6
ΔG_{H2O} (2) (kJ/mol)	57.6	--	61	61.9
m (2) (kJ/mol/M)	-52	--	-74	-60.8
X_n	0	0	0	0
X_i	0.06	--	0.26	0.85
X_u	0.9	1.0	1.0	1.0

Table 4.1 Parameters calculated from the denaturation curves shown in Figure 4.5 B for EcA2(WT) in Gu.HCl at pH 8.0, 25 °C.

Unfolding of EcA2(WT) monitored by fluorescence and activity revealed that the protein is completely unfolded beyond 1.1 M Gu.HCl. The Gu.HCl-induced unfolding process probed by the ellipticity changes at 222 nm (a composite CD signal contributed by the secondary structural elements and optically active aromatic groups in the protein) and the fluorescence emission maximum shows that EcA2(WT) indicates complete unfolding only beyond 1.3 M Gu.HCl.

The emission maximum is the another fluorescence signal used to monitor protein unfolding which usually results in a red shift in the emission of its tryptophan residues, and this observation can give a qualitative indication of a significant conformational transition. The fact is that the state (native or unfolded) with the larger quantum yield dominates the emission maximum, so that the emission maximum (or the center of gravity of the emission maximum) will be skewed toward the state with larger quantum yield. Here, in case of the emission maximum the apparent transition is shifted to higher denaturant concentration (apparent mid-point of 1.1 M and much higher values of $\Delta G(H_2O)$ and m values, as compared to that for the fluorescence data), since the native state has a larger quantum yield than the denatured state of the protein (Eftink, 1998). The denaturation parameters estimated from the data are summarized in table 4.1.

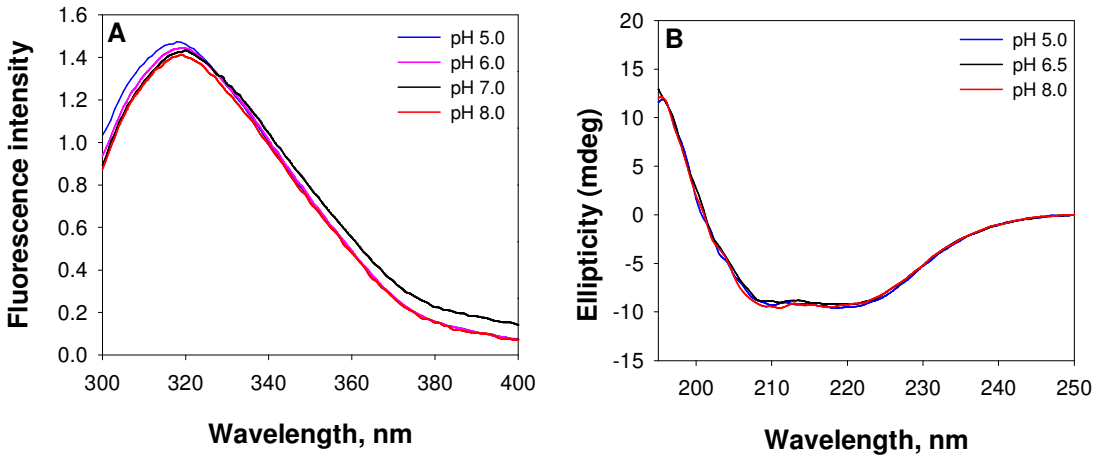

Figure 4.6 (A) Fluorescence spectra, and (B) far-UV CD spectra of EcA2(WT) recorded at different pH 5.0-8.0 at 25 °C.

The fluorescence and far-UV CD spectra of EcA2(WT) at pH values ranging from 5.0 to 8.0 were monitored at room temperature to investigate the pH-dependence of stability. It was found that both the fluorescence emission and the CD spectra showed little change at pH 5.0 (Figsure 4.6 A and 4.6 B). These results suggests that EcA2(WT) does not lose its native structure within the pH range 5.0-8.0.

In order to study the conformation stability of EcA2(WT) under different pH range 5.0-8.0, we used emission maximum, fluorescence intensity, far-UV CD, and activity as a function of the molar concentration of the Gu.HCl (Figure 4.7). There was a slight shift of the profiles to lower Gu.HCl concentrations at pH-values below 7. However, the calculated stabilities expressed as $\Delta G(H_2O)$ were 46-50 kJ/mol for all pH-values between 5.0 and 8.0.

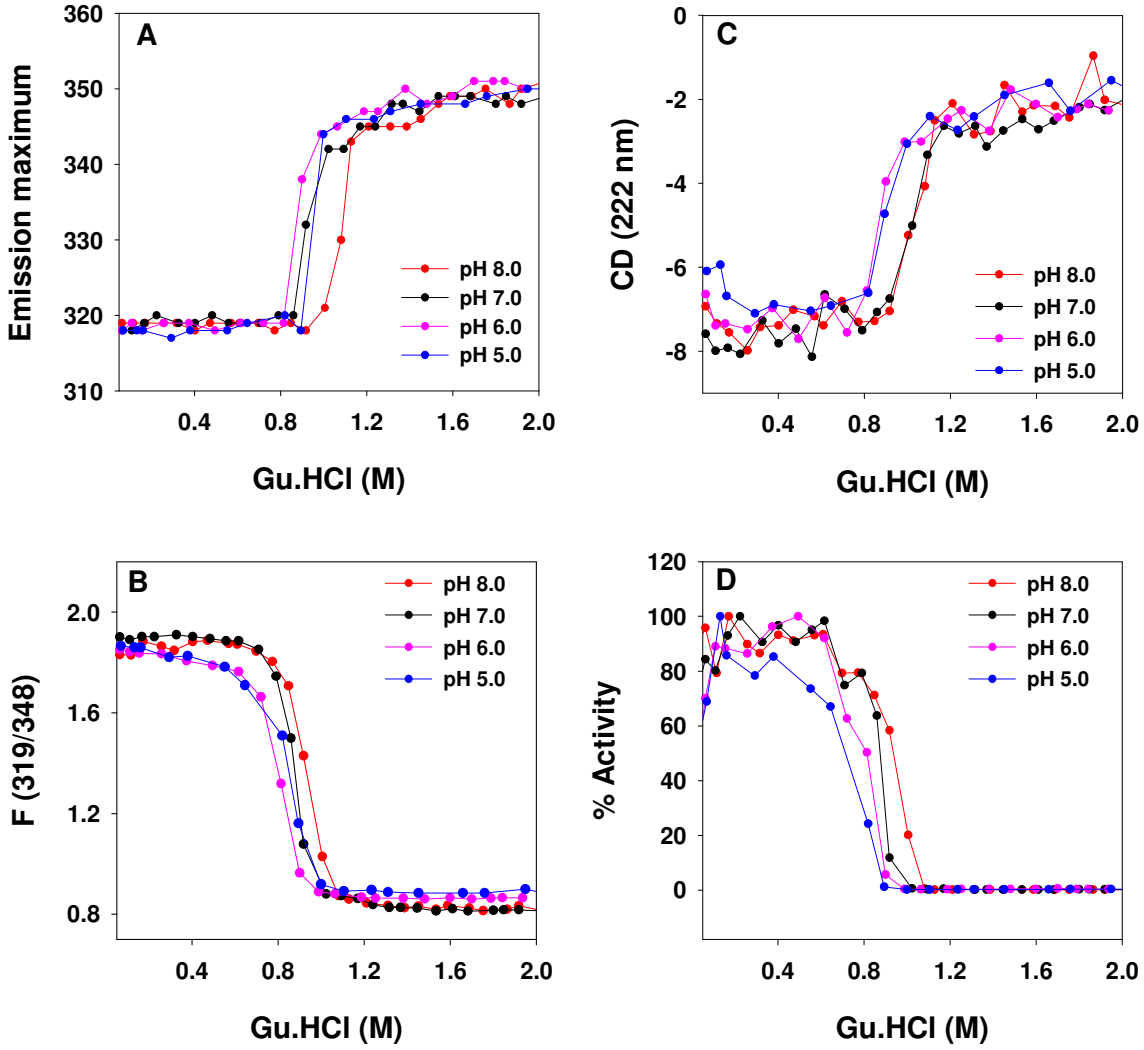

Figure 4.7 Gu.HCl induced unfolding of EcA2(WT) at 25 °C at different pH 5.0-8.0. (A) shift in the emission max (B), ratio F (319/348) (C), ellipticity at 222 nm and (D), activity of the Gu.HCl treated protein.

As native asparaginase II is tetrameric, the unfolding profiles may show a dependency on protein concentration. However, as shown by figure 4.8 and table 4.2, the denaturation parameters for 2 protein concentrations were in fact independent of protein concentration, at least in the range tested (100 - 1000 µg/ml).

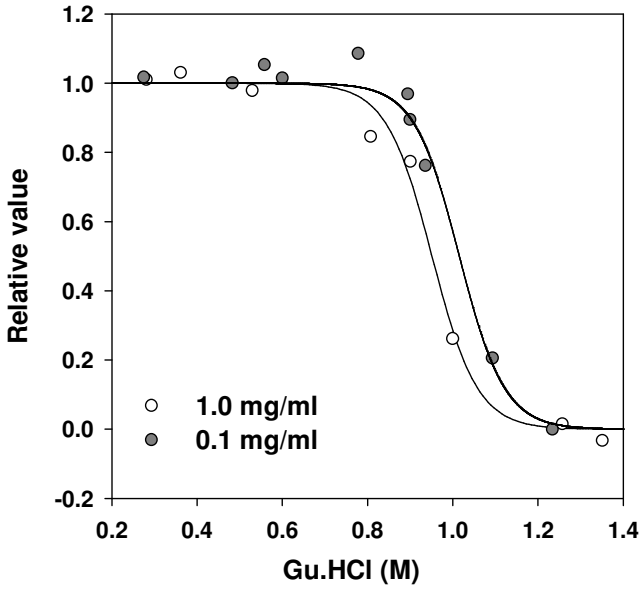

Figure 4.8 EcA2(WT) at different protein conc. in Gu.HCl at pH 8.0, 25 °C.

Protein conc. (µg/ml)	ΔG_{H2O}, kJ/mol	m, kJ/mol/M
1000	44.0 +/-8.0	-46.0 +/-5.0
100	48.0 +/-5.0	-47.0 +/-5.0

Table 4.2 Result of denaturation curves (Figure 4.8) analysis for EcA2(WT) in Gu.HCl at pH 8.0, 25 °C.

Sedimentation equilibrium studies with EcA2(WT)

In order to analyze whether one of the transitions observed by spectroscopic techniques is accompanied by a dissociation of tetramers or dimers, we used sedimentation equilibrium ultracentrifugation in a high-speed air-turbine centrifuge (Airfuge, Beckman; cf. Bothwell *et al.,* 1978). The change of EcA2 quaternary structure with Gu.HCl (0 M-1.5 M) was monitored by sedimentation equilibrium (Bothwell *et al.,* 1978).

Figure 4.9 summarizes the apparent molecular mass of EcA2(WT) as a function of different Gu.HCl concentrations (shown on a logarithmatic scale). A typical curve of log F versus mass is given as inset. At low Gu.HCl ~0.65 M concentrations, the observed masses suggest that tetramers (138 kDa) are in equilibrium with dimers (66 kDa). Between 0.7 and 0.8 M Gu.HCl, the apparent mass decreases to reach a plateau value of ~36 kDa at

concentrations above 0.9 M Gu.HCl. This indicated that at higher concentration monomers are formed.

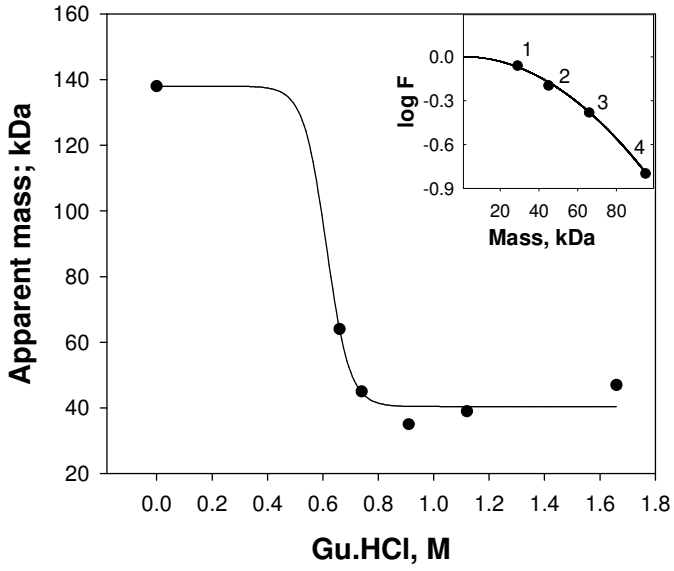

Figure 4.9 The apparent molecular weight of the EcA2(WT) in 50 mM Hepes pH 8.0 determined by high-speed air centrifuge equilibrium sedimentation, as a function of different Gu.HCl concentration.

Inset: Calibration curve for ultra-centrifugation experiments: dependence of the logarithm of fractional protein depletion (log F) on protein concentration. Molecular weight standards used: (1) Carbonic anhydrase (29 kDa), (2) Ovaalbumin (45 kDa), (3) Bovine serum albumin (66 kDa), (4) Phosphorylase B (95 kDa)

These ultracentrifugation results of EcA2(WT) confirmed that at Gu.HCl concentrations between 0.5 and 0.8 M the apparent molecular mass indeed decreases from that of the tetramer to the expected mass for a monomer.

EcA2(Y176F)

Denaturation of EcA2(Y176F) with Gu.HCl resulted in a simple one-step unfolding profile without any detectable intermediate. The fluorescence spectra of EcA2(Y176F) were similar to those of wild-type EcA2 (Figure 4.10 A). The native protein exhibited a emission maximum around 319 nm, which shifted to 355 nm at denaturant concentrations $\geq$ 1.2 M as a result of denaturation. All methods applied (ellipticity at 222 nm, and the fluorescence intensity at 323 nm) gave nearly indistinguishable denaturation profiles, with a half denaturation point $(D)_{50\%}$ at 1.29 M Gu.HCl (Figure 4.10 B). In comparison with wild type enzyme, the mutant EcA2(Y176F) is significantly more stable with a $\Delta G(H_2O)$ of ~63.7 kJ/mol. The denaturation parameters are summarized in table 4.3. As with wild-type enzyme, experiments at pH 7 and 8 did not show significant difference in any of denaturation profiles (Figure 4.11).

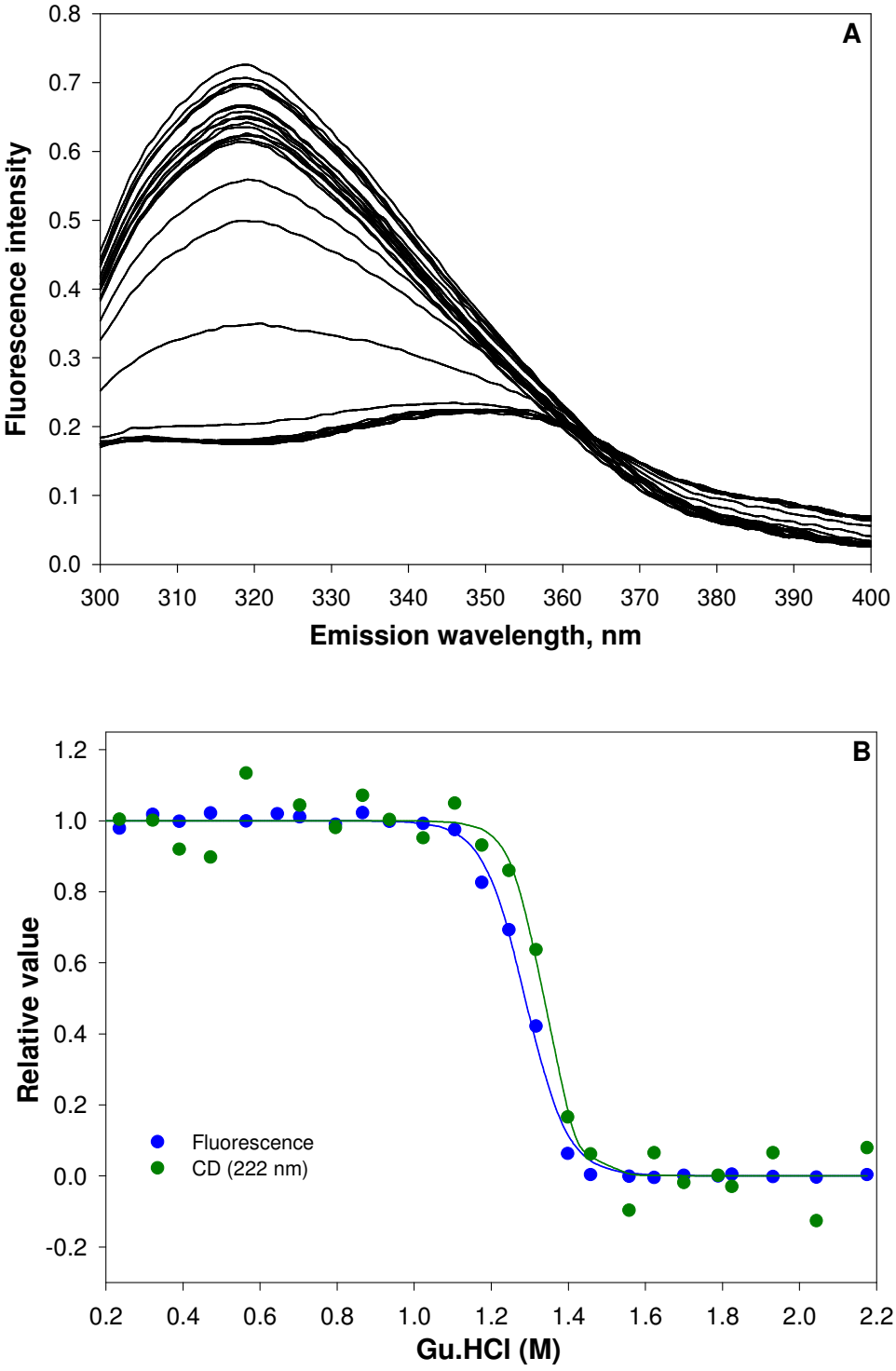

Figure 4.10 (A) Fluorescence spectra of EcA2(Y176F) at different concentrations of Gu.HCl. (B) Gu.HCl-induced denaturation curves of EcA2(Y176F). The appropriate fraction of denature protein (Fapp) was plotted versus denaturant concentration (Gu.HCl). The data was measured at pH 8.0 and 25 ^{o}C. The curves correspond to two-state of denaturation

Parameters	Fluorescence	CD
ΔG_{H2O} (kJ/mol)	63.7	36.5
m (kJ/mol/M)	-56.0	-32.4

Table 4.3 Evaluation of denaturation analysis for EcA2(Y176F) in Gu.HCl at pH 8.0, 25 °C (Figure 4.10 B).

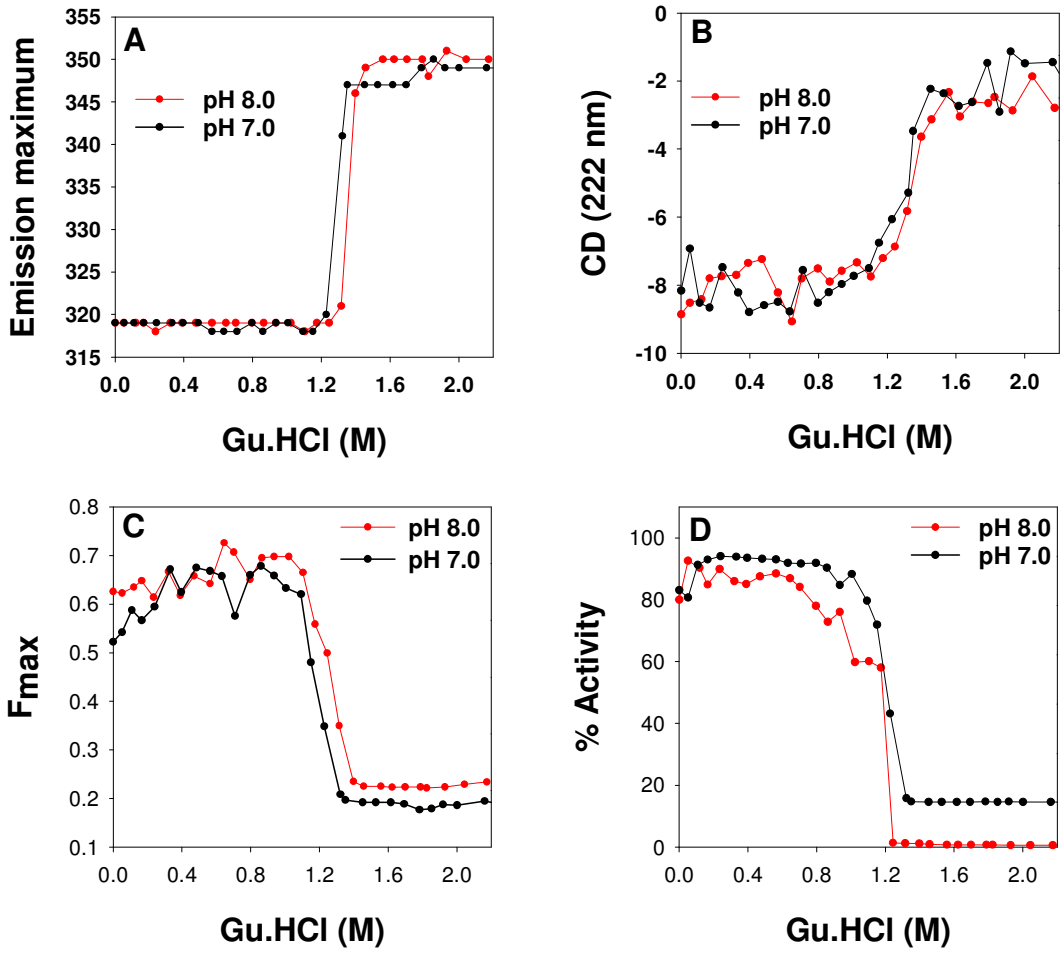

Figure 4.11 Gu.HCl induced unfolding of EcA2(Y176F) at different pH. (A), shift in the emission max (B), ratio F (319/348) (C), ellipticity at 222 nm and (D) activity of the Gu.HCl treated protein.

EcA2(W66Y)

The removal of W66, the fluorescent main probe in wild type EcA2, leaves only the 11 tyrosine residues of the protein as fluorescent entities. The W66Y variant therefore shows an emission spectrum with maximum emission occurring at 310 nm instead of 323 nm (Figure 4.12 A) due to the accumulated fluorescence of the tyrosine residues. As shown in figure 4.12 B fluorescence measurement gave nearly indistinguishable denaturation profiles, with a half denaturation point (D) 50% at 0.69 M Gu.HCl. In comparison with the wild type enzyme, the mutant EcA2(W66Y) is slightly less stable with a $\Delta G(H_2O)$, of 37 to 39 kJ/mol at pH 8.0 (Figure 4.12 B). The denaturation parameters are summarized in Table 4.5. Similar to EcA2(WT), fluorescence emission and ellipticity of mutant EcA2(W66Y) was proportional to protein concentration (Figure 4.13).

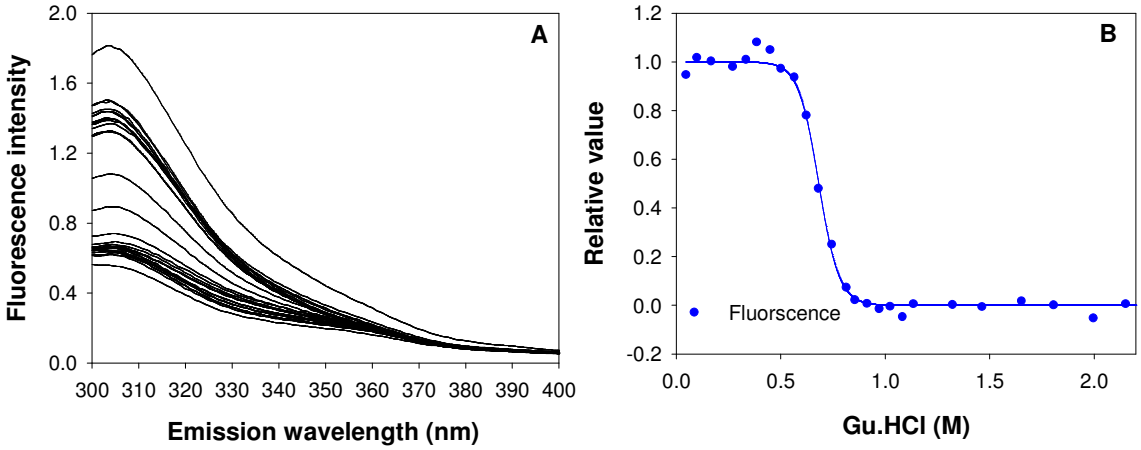

Figure 4.12 (A) Fluorescence spectra of EcA2(W66Y) at different concentrations of Gu.HCl. (B) Gu.HCl-induced denaturation curve of EcA2(W66Y). The appropriate fraction of denature protein (Fapp) was plotted versus denaturant concentration (Gu.HCl). The data was measured at pH 8.0 and 25 °C. The curve corresponds to two-state of denaturation.

Mutant	ΔG_{H2O} **kJ/mol**	**m kJ/mol/M**
EcA2(W66Y)	36.6 +/-1.9	-50.87 +/-2.7

Table 4.4 Result of denaturation curves (Figure 4.12 B) analysis for EcA2(W66Y) in Gu.HCl at pH 8.0, 25 °C.

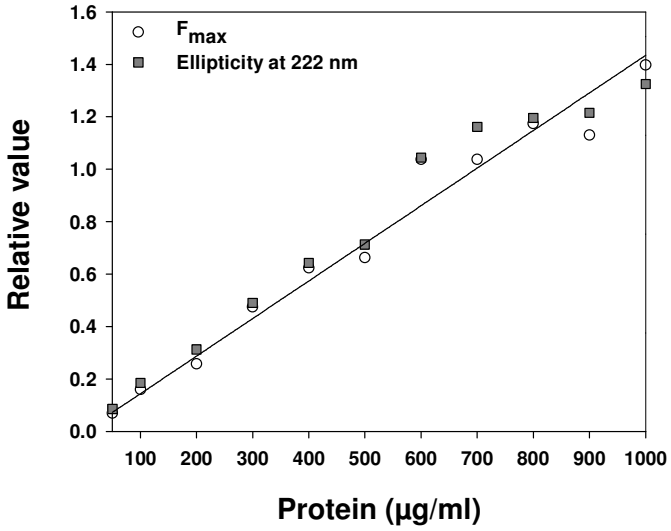

Figure 4.13 EcA2(W66Y) at different protein conc. in 0.8 M Gu.HCl at pH 8.0, 25 °C.

EcA2(Y176S)

A third and much more complicated type of behavior was exhibited by variants EcA2(Y176S) and EcA2(W66Y/Y181W). Here the onset of denaturation was shifted to lower denaturant concentrations. Moreover, the denaturation curves were distinctly asymmetric, indicating the formation of an intermediate species. Therefore, three or four-state models with two or three denaturation equilibria (section 3.17.2) were employed in these cases, yielding separate values of $\Delta G(H_2O)$ and m for each of the equilibria.

The replacement of Y176 by serine in mutant EcA2(Y176S) results in a drastically decreased stability of the enzyme and the appearance of at least two intermediates. In fluorescence spectra of EcA2(Y176S), the emission maximum slowly increased from 319 nm in the absence of Gu.HCl to ~ 330 nm between 0 and 0.6 M Gu.HCl and then shifted to 355 nm at 0.8 M Gu.HCl and above (Figure 4.14 A). In the denaturation profiles of EcA2(Y176S), as the Gu.HCl concentration increases (Figure 4.14 B), the first property to be modified is the activity: half of the initial activity is lost at 0.5 M Gu.HCl, and Y176S is completely inactivated above 0.7 M Gu.HCl. The changes in fluorescence and CD are biphasic: at 0.2–0.8 M Gu.HCl, a first change corresponds to a relative amplitude of 70-75 %, and a second occurs for the remaining 25-30 %. The denaturation parameters are summarized in table 4.5.

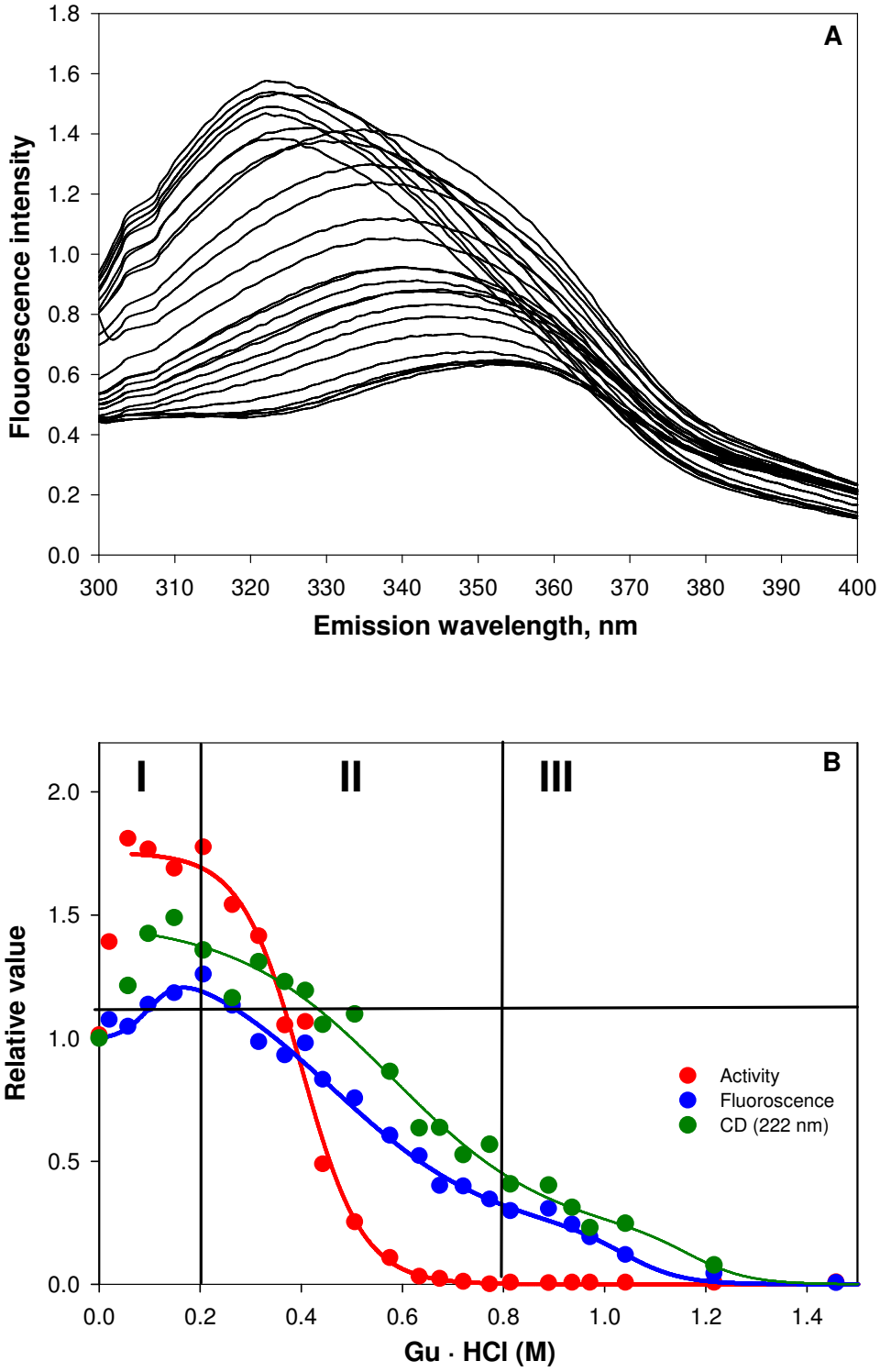

Figure 4.14 (A) Fluorescence spectra of EcA2(Y176S) at different concentrations of Gu.HCl. (B) Gu.HCl-induced denaturation curves of EcA2(Y176S). The appropriate fraction of denature protein (F_{app}) was plotted versus denaturant concentration (Gu.HCl). The data was measured at pH 8.0 and 25 ^{o}C. The CD and fluorescence curves are fits of the 3- and 4-state models, respectively. The activity vs. Gu.HCl profile was fitted according to the simple 2-state model.

Parameters	Fluorescence	CD	Activity
ΔG_{H2O} (1) (kJ/mol)	9	30	13
m (1) (kJ/mol/M)	-83.6	nc*)	nc*)
ΔG_{H2O} (2) (kJ/mol)	7	9	16.5
m (2) (kJ/mol/M)	-15.6	-15.8	-41
ΔG_{H2O} (3) (kJ/mol)	45	49	-
m (3) (kJ/mol/M)	-43	-41.9	-
X_n	1.4	-7.1	0.56
X_{i1}	1.7	-9.0	0.97
X_{i2}	0.80	-3.7	-
X_u	0.64	-2.9	0.010

Table 4.5 Result of denaturation curves (Figure 4.14 B) analysis for EcA2(Y176S) in Gu.HCl at pH 8.0, 25 °C. *) nc: no meaningful values could be calculated from the data.

Finding nonsuperimposable transition curves for different parameters shows that several intermediate protein forms are present at equilibrium depending on the Gu.HCl concentration:

$$N \overset{I}{\leftrightarrows} I_1 \overset{II}{\leftrightarrows} I_2 \overset{III}{\leftrightarrows} U$$

The N ⇆ I_1 step involves little change in activity, fluorescence and CD, the I_1 ⇆ I_2 step is related to the inactivation of protein and involves the most of the change in fluorescence as well as in CD, and complete change in fluorescence and CD occurs in the M ⇆ U step. Fluorescence measures the degree of shielding from solvent of Trp-66 (Brand & Witholt, 1967), and CD reflects the content of secondary structure (Adler *et al.,* 1973). The influence of Gu.HCl involves three successive steps: first, the protein first loses its activity, then it exposes its Trp-66 to solvent, and finally its secondary structure disappears. This data

suggest that I_1 is the dimeric species (active with a native fluorescence), I_2 is a folded monomer (retaining most of the secondary structure), and U is a largely unfolded monomeric state (both its CD and its intrinsic fluorescence indicate that U has retained some residual structure).

In order to clarify the nature of the intermediate a careful analysis of unfolding with CD-spectroscopy was performed. In the denaturation experiment using CD and fluorescence spectroscopy, a protein concentration of about 1 mg/ml was used at pH 8.0. The EcA2(Y176S) showed a typical far-UV CD spectrum observed for proteins with significant α–helical contents. The CD spectra of the Gu.HCl-treated protein showed a visible difference in the respective CD spectra. Because Gu.HCl was interfering with the CD spectra below 200 nm, only data in the range of 200-250 nm could be collected. In Figure 4.15 A & B the Gu.HCl denaturation curves at pH 8.0 with CD-spectroscopic and fluorimetric detection are shown. No significant changes in the CD and fluorescence spectra occurred between 0 and 0.6 M Gu.HCl. At 0.8-1.0 M Gu.HCl concentrations, both curves clearly represent a 2-3 step denaturation, with a prominent folding intermediate.

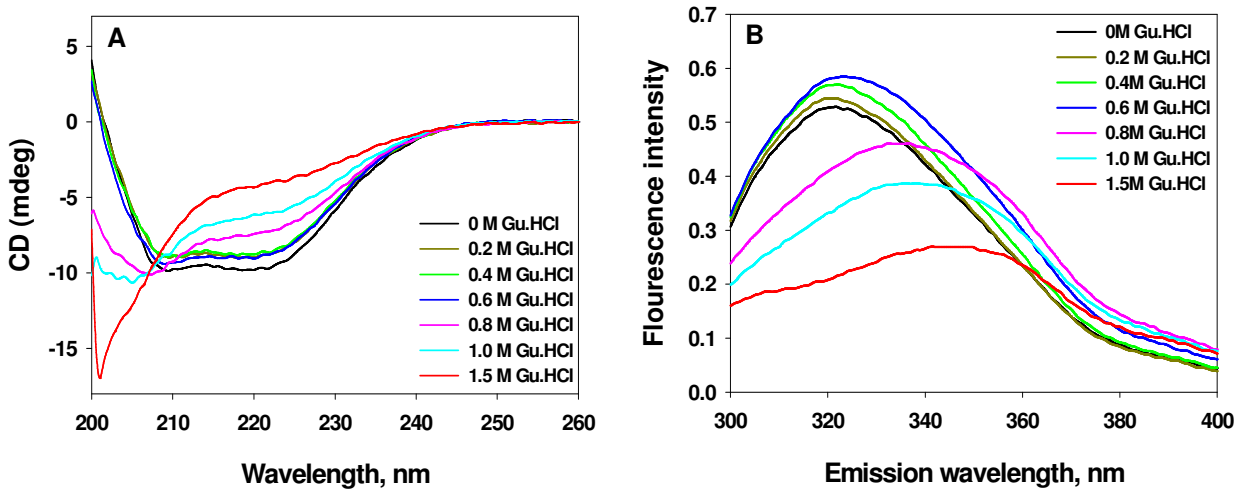

Figure 4.15 (A) Far-UV CD spectra and (B) fluorescence spectra of EcA2(Y176S) at different concentrations of Gu.HCl at pH 8.0, 25 °C.

In order to study the conformation of EcA2(Y176S) at different pH, we used emission maximum, fluorescence intensity, far-UV CD, and activity as a function of the molar

concentration of the Gu.HCl (Figure 4.16). There was not a significant difference in the emission maximum, fluorescence, and CD profiles at both pH tested. However, the EcA2(Y176S) was less stable at pH 5.0 and lost its activity already at very low (~0.15 M) concentrations of Gu.HCl.

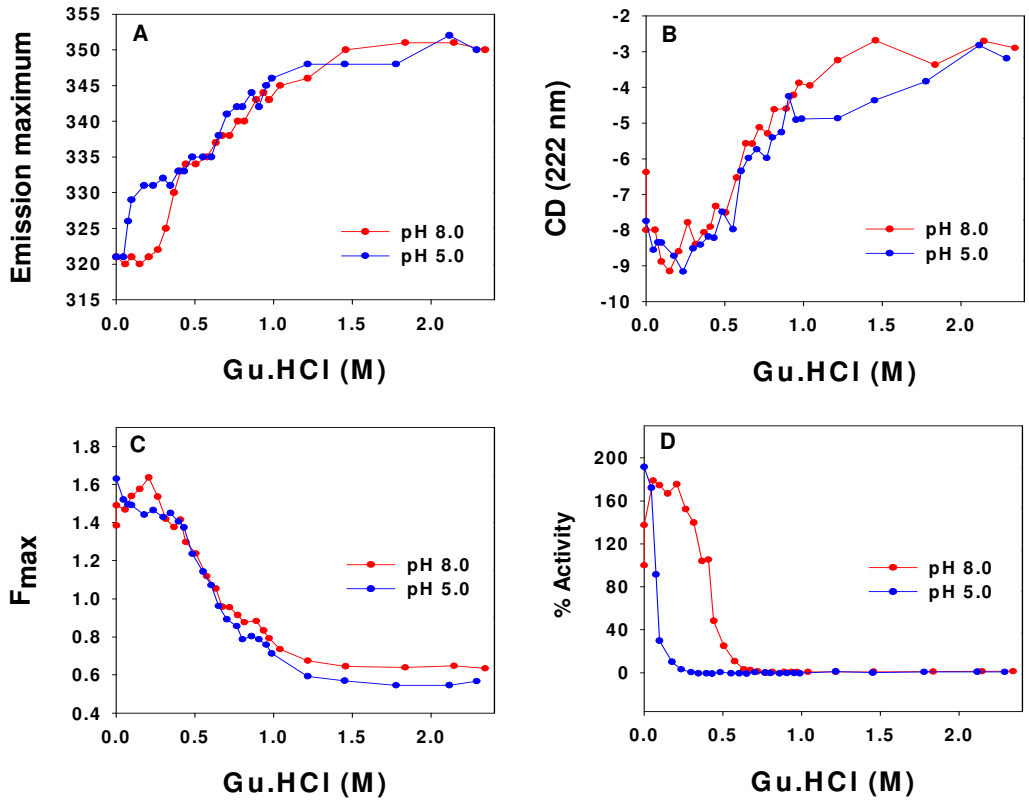

Figure 4.16 Gu.HCl-induced unfolding of EcA2(Y176S) at pH 5.0 & 8.0, 25 °C. (A), shift in the emission max (B), maximum fluorescence (C), ellipticity at 222 nm and (D), activity of the Gu.HCl treated protein.

EcA2(W66Y/Y181W)

In double mutant EcA2(W66Y/Y181W) a new tryptophan residue was placed at the dimer/dimer interface. The fluorescence emission spectrum of this variant was markedly different from that of EcA2(WT) (Figure 4.17 A). In the absence of Gu.HCl, maximum emission was seen at 347 nm, as compared to 319 nm for wild-type enzyme. Addition of Gu.HCl led to decreased quantum yields and, at the same time, blue-shifted the spectrum in a concentration-dependent manner.

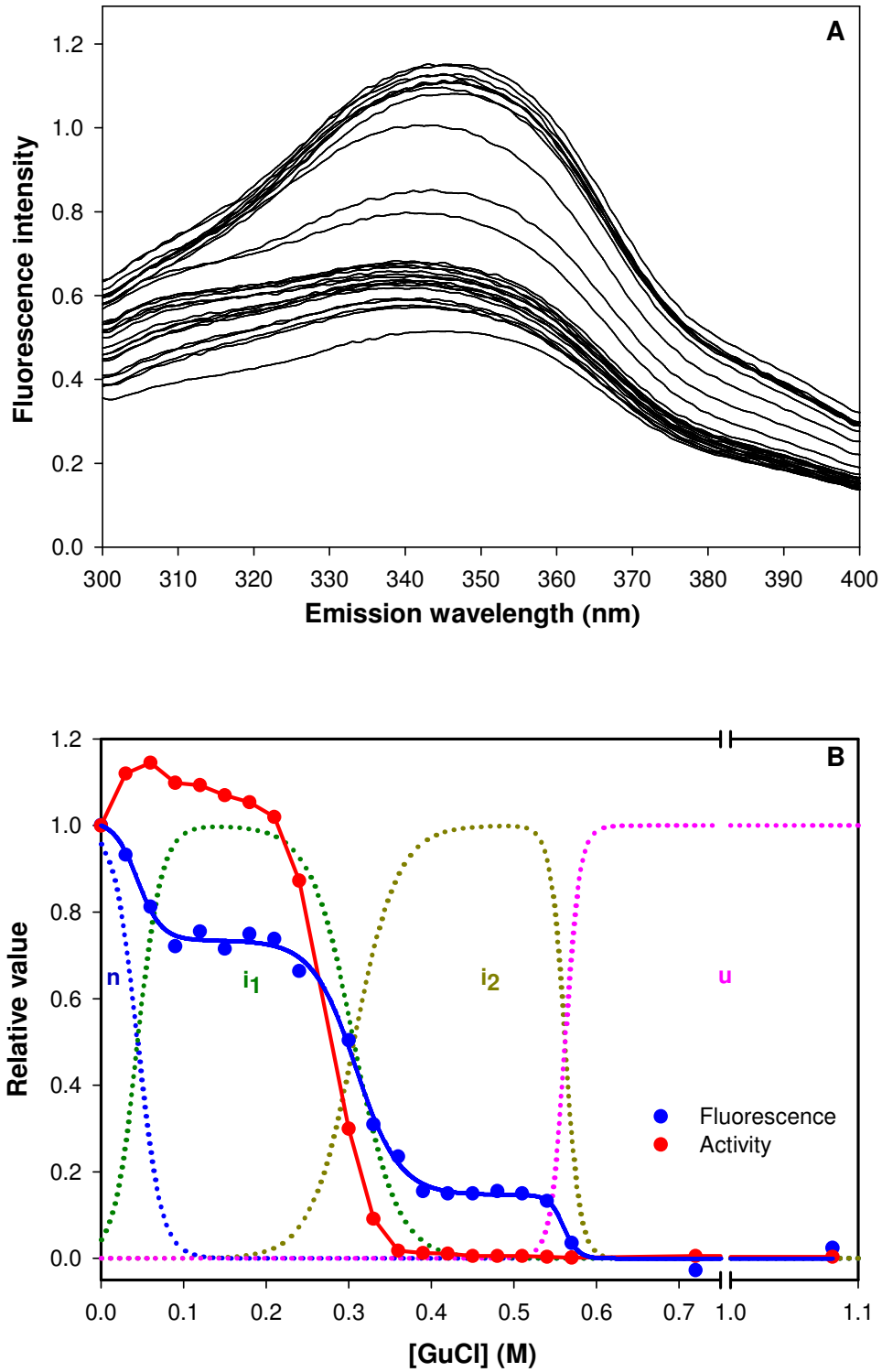

Figure 4.17 (A) Fluorescence spectra of EcA2(W66Y/Y181W) at different concentrations of Gu.HCl. The excitation wavelength was 285 nm. (B) Gu.HCl-induced denaturation curves of EcA2(W66Y/Y181W). The appropriate fraction of denatured protein (Fapp) was plotted vs. denaturant concentration. The data was measured at pH 8.0 and 25 ^{o}C. The curves correspond to three and four-state models of denaturation. The dotted lines indicate the calculated fractions of the various species (N, I_1, I_2 and U).

Parameters	Fluorescence	Activity
ΔG_{H2O} (1) (kJ/mol)	7.7	13
m (1) (kJ/mol/M)	-29.1	nc*)
ΔG_{H2O} (2) (kJ/mol)	158	16.5
m (2) (kJ/mol/M)	-173	-41
ΔG_{H2O} (3) (kJ/mol)	94	--
m (3) (kJ/mol/M)	-283	--
X_n	0.403	0.56
X_{i1}	0.355	0.97
X_{i2}	0.252	--
X_u	0.227	0.010

Table 4.6 Result of denaturation curves (Figure 4.17 B) analysis for EcA2(W66Y/Y181W) in Gu.HCl at pH 8.0, 25 °C. *) nc: no meaningful values could be calculated from the data

In the denaturation profiles (Figure 4.17 B), the first property to be modified is the activity: half of the initial activity is lost at 0.25 M Gu.HCl, and EcA2(W66Y/Y181W) is completely inactivated at concentrations above 0.4 M Gu.HCl. The changes in fluorescence were biphasic: at 0.1–0.3 M Gu.HCl, a first change corresponds to a relative amplitude of 50-55 %, and a second occurs for the remaining 45-50 %. The denaturation parameters are summarized in table 4.6. Thus, similar to EcA2(Y176S), double mutant EcA2(W66Y/Y181W) denaturation showed presence of two intermediates with strongly reduced stability.

In order to clarify the nature of the intermediates a detailed analysis of unfolding with CD-spectroscopical techniques was performed. In Figure 4.18 A and B, the Gu.HCl denaturation curves at pH 8.0 for CD-spectroscopic and fluorimetric detection are shown.

Both curves clearly represent a 2- or 3-step denaturation, with a prominent folding intermediate at Gu.HCl concentrations of 0.8 – 1.0 M.

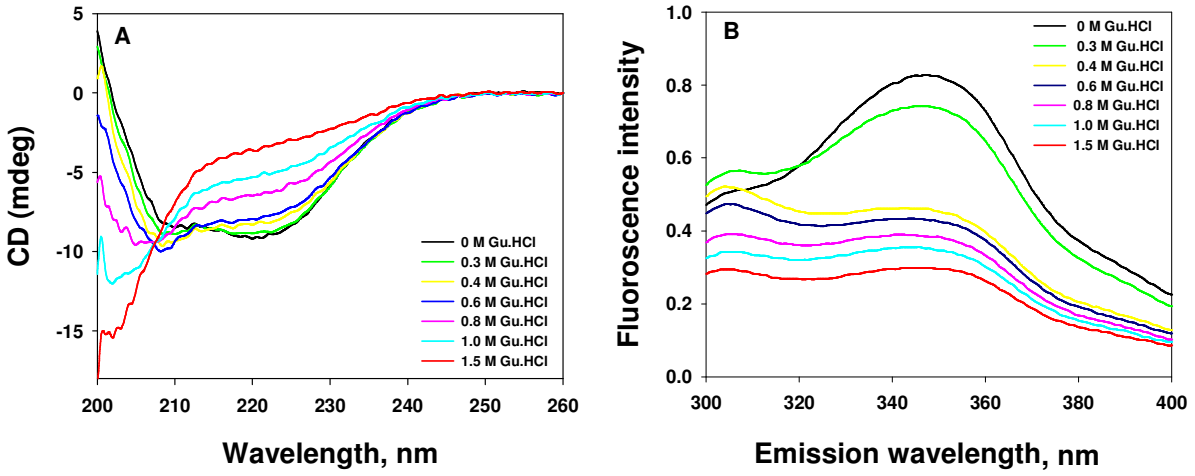

Figure 4.18 (A) Far-UV CD spectra and (B) fluorescence spectra of EcA2(W66Y/Y181W) at different concentration of Gu.HCl at pH 8.0, 25 °C.

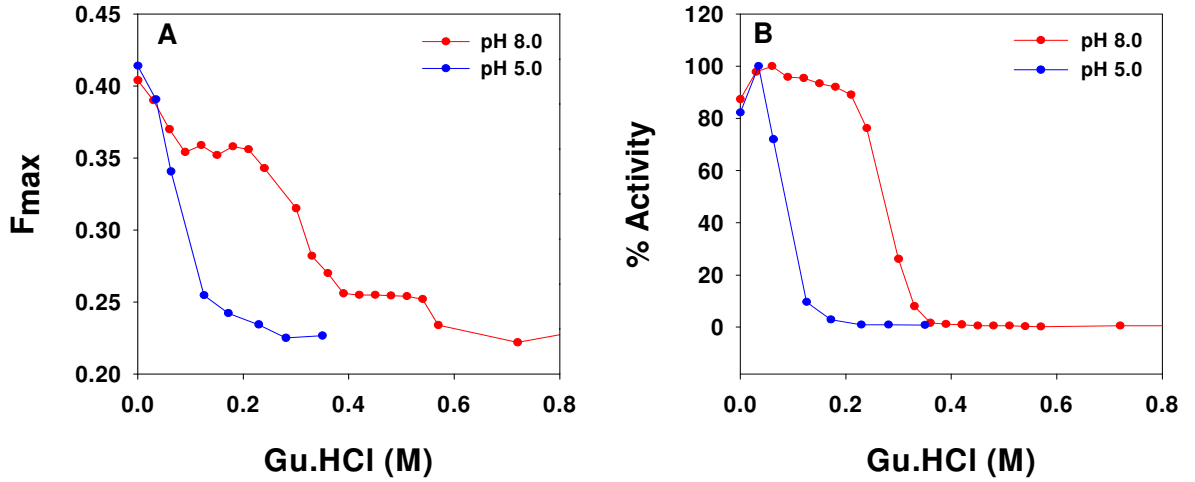

Figure 4.19 Gu.HCl-induced unfolding of EcA2(W66Y/Y181W) at different pH 5.0 and 8.0. (A), maximum fluorescence (B), activity of the Gu.HCl treated protein.

In order to study the conformation of EcA2(W66Y/Y181W) as a function of pH, we used fluorescence intensity, and activity as a function of the molar concentration of the

Gu.HCl (Figure 4.19). EcA2(W66Y/Y181W) was found to be less stable at pH 5.0, where it lost its activity at very low concentrations of Gu.HCl (~0.15 M).

EcA2(D188N)

Variant EcA2(D188N) showed fluorescence spectra similar to those of EcA2(Y176S) with a gradual increase of the emission maximum from 319 nm to 350 nm (Figure 4.20 A). In the denaturation experiment (Figure 4.20 B), half of the initial activity was lost at 0.6 M Gu.HCl, and D188N was completely inactivated above 0.9 M Gu.HCl. The changes in fluorescence and emission maximum were biphasic: at 0.3–0.6 M Gu.HCl, a first change corresponded to a relative amplitude of 50-55 %, and a second occured for the remaining 45-50 %. The denaturation parameters are summarized in table 4.7.

Thus, similar to EcA2(Y176S) and EcA2(W66Y/Y181W) denaturation, mutant EcA2(D188N) showed the presence of two intermediates with strongly reduced stability.

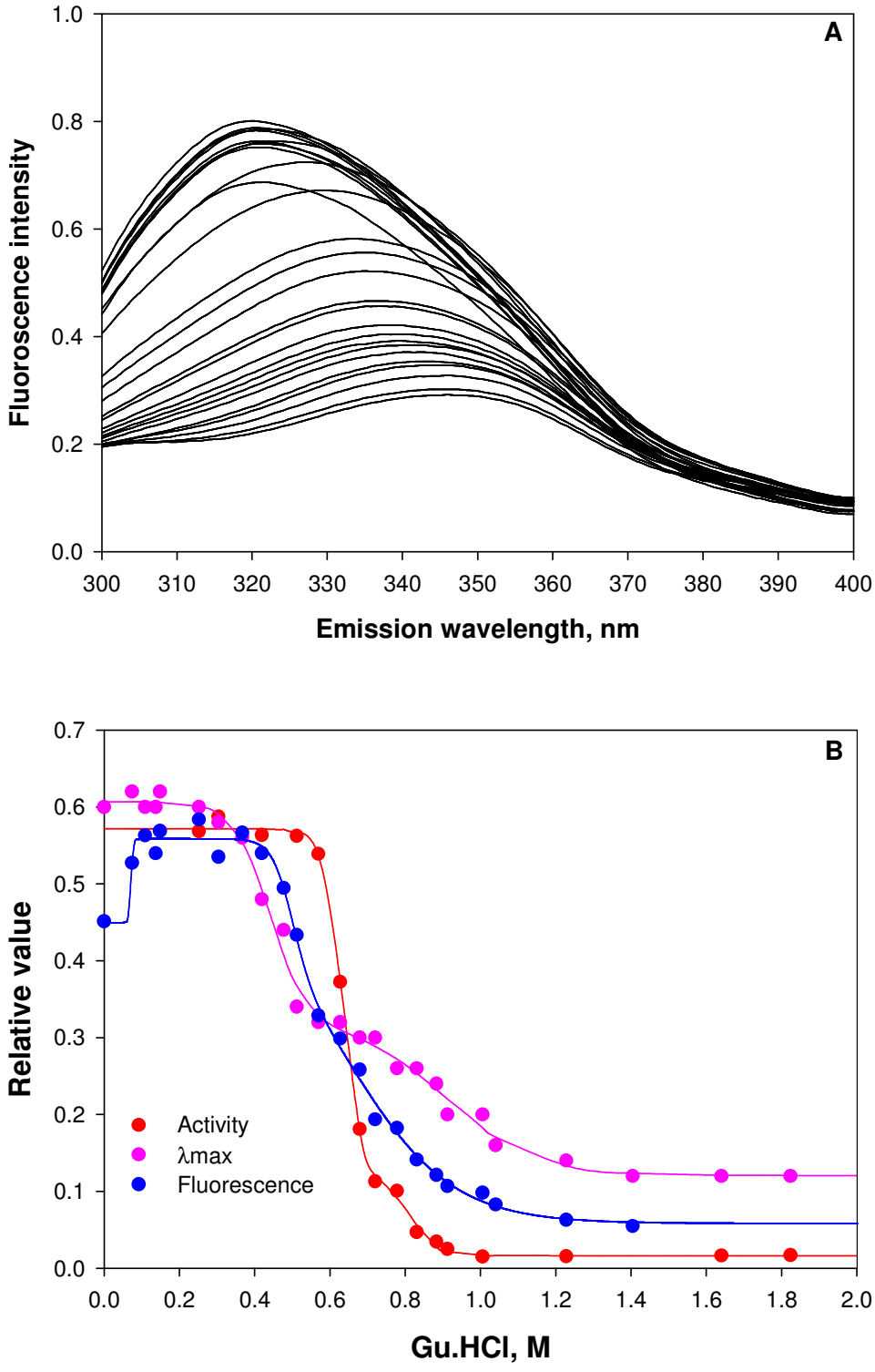

Figure 4.20 (A) Fluorescence spectra of EcA2(D188N) at different concentrations of Gu.HCl. The excitation wavelength was 285 nm. (B) Gu.HCl-induced denaturation curves of EcA2(D188N). The appropriate fraction of denature protein (Fapp) was plotted versus denaturant concentration (Gu.HCl). The data was measured at pH 8.0 and 25 ^{o}C. The curves correspond to three and four-state of denaturation.

Parameters	Fluorescence	Activity	λ(max)
ΔG_{H2O} (1) (kJ/mol)	54.5	60.2	22.4
m (1) (kJ/mol/M)	nc*)	-63.8	-19.0
ΔG_{H2O} (2) (kJ/mol)	42.3	94.8	50.9
m (2) (kJ/mol/M)	84.7	-77.6	-20.95
ΔG_{H2O} (3) (kJ/mol)	11.9	--	--
m (3) (kJ/mol/M)	18.3	--	--
X_n	0.69	0.572	320.7
X_{i1}	0.78	0.108	334.9
X_{i2}	0.71	--	--
X_u	0.35	0.016	344.9

Table 4.7 Result of denaturation curves (Figure 4.20 B) analysis for EcA2(D188N) in Gu.HCl at pH 8.0, 25 °C.)*nc: no meaningful values could be calculated from the data

EcA2(D156N)

Variant EcA2(D156N) showed fluorescence spectra similar to EcA2(Y176S) and EcA2(D188N) with a slow increase of the emission maximum from 319 nm to 350 nm (Figure 4.21 A). As the Gu.HCl concentration increased (Figure 4.21 B), half of the initial activity was lost at 0.45 M Gu.HCl, and D156N was completely inactivated above 0.6 M Gu.HCl. The changes in emission maximum and fluorescence were biphasic: at 0.2–0.7 M Gu.HCl, a first change corresponded to a relative amplitude of 70-75 %, and a second occurs for the remaining 25-30 %. The denaturation parameters are summarized in table 4.8. Again, the denaturation profiles of mutant EcA2(D156N) indicated presence of two intermediates with strongly reduced stability.

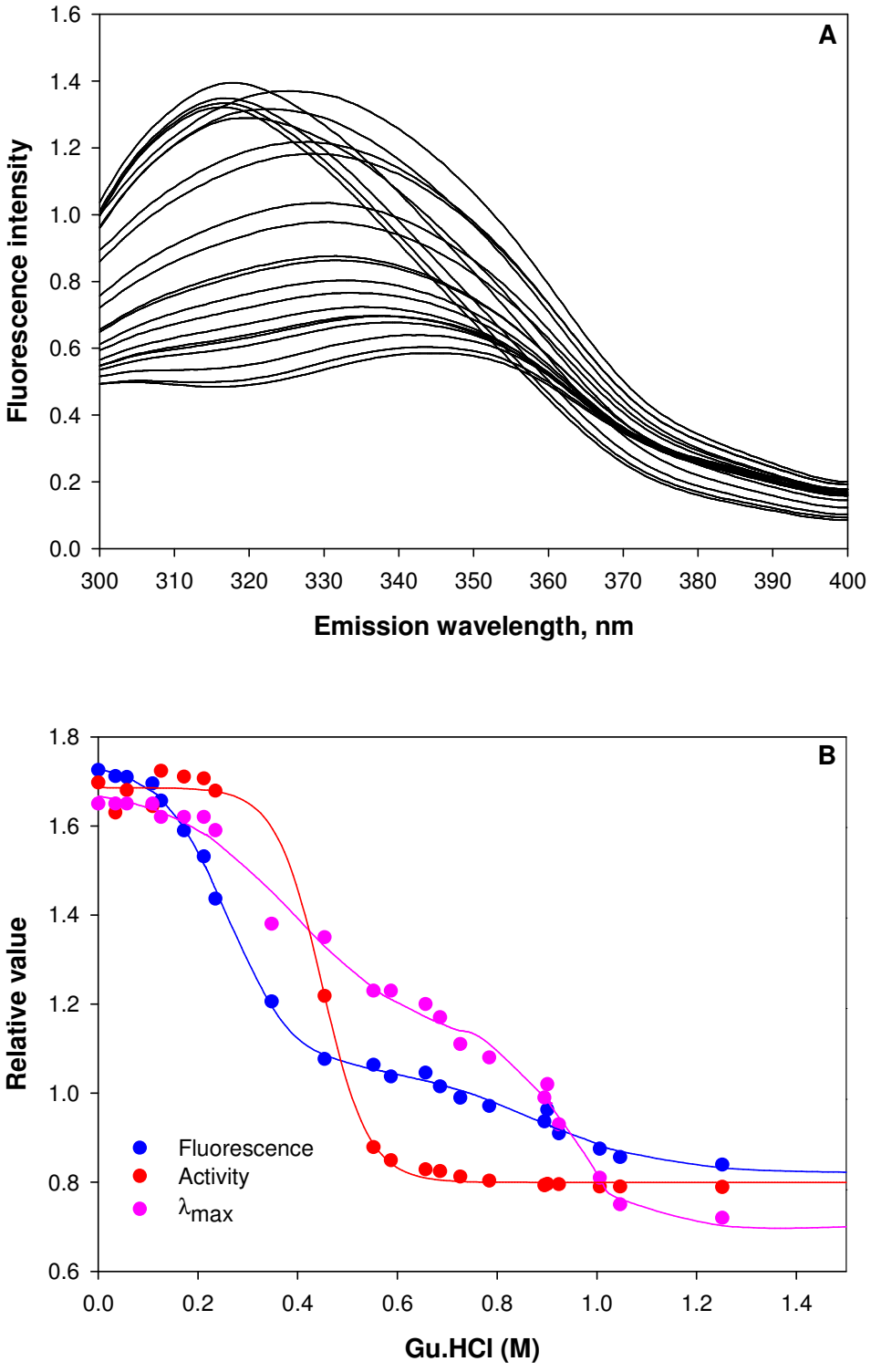

Figure 4.21 (A) Fluorescence spectra of EcA2(D156N) at different concentrations of Gu.HCl. The excitation wavelength was 285 nm. (B) Gu.HCl-induced denaturation curves of EcA2(D156N). The appropriate fraction of denatured protein (F_{app}) was plotted versus denaturant concentration (Gu.HCl). The data was measured at pH 8.0 and 25 ^{o}C. The curves correspond to 3 and 4-state of denaturation.

Parameters	Fluorescence	Activity	λ(max)
ΔG_{H2O} (1) (kJ/mol)	9.7	24.0	8.0
m (1) (kJ/mol/M)	-17.3	-53.5	-39.0
ΔG_{H2O} (2) (kJ/mol)	37.7	--	20.4
m (2) (kJ/mol/M)	-19.8	--	-41.3
X_n	1.741	0.89	314.7
X_i	1.062	--	333.7
X_u	0.821	0.016	347.7

Table 4.8. Result of denaturation curves (Figure 4.21 B) analysis for EcA2(D156N) in Gu.HCl at pH 8.0, 25 °C.

4.4.2 Gel filtration studies

Changes in oligomerisation state and shape of our EcA2 variants as a function of denatuarnt concentration were monitored by size-exclusion chromatography (SEC).

SEC permits one to evaluate dimensions of protein molecule in different conformers (Ackers, 1967, 1970; Davies, 1983; Corbett & Roche, 1984; Uversky, 1993) with high accuracy at low concentration (~ 0.01-0.001 mg/ml). It was shown (Corbett & Roche, 1984; Uversky *et al.,* 1992, 1993; Uversky, 1993) that a chromatographic FPLC column does not shift the equilibrium between the native, molten globule, and unfolded states and therefore can be safely applied to study the transitions between these states.

Application of size-exclusion chromatography is most promising for studying "all-or-none" transitions between two states of different compactness, like native-coil (Corbett & Roche, 1984; Uversky, 1993) and molten globule-coil (Uversky *et al.,* 1992, 1993) transitions. Moreover, SEC in principle provides a possibility to study separately the properties of "compact" and "less compact" molecules by collecting a corresponding fraction from the column (Uversky *et al.,* 1992, 1993) or by combining SEC with structural methods, e.g. with fluorescence. This is a new kind of information since traditional methods (e.g. CD, viscosity, etc) provide us with the data averaged over all conformations which exist within the transition region.

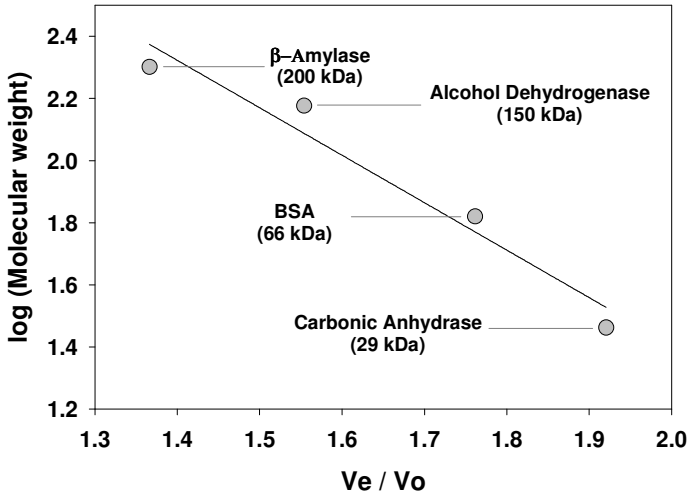

Figure 4.22 Typical standard curve for gel filtration

$$\log(M_r) = -1{,}53 \cdot \frac{V_e}{V_o} + 4{,}46$$

	Calculated Molecular weight	Elution volume, V_e
Tetramer	138.4 kDa	12.2
Dimer	69.2 kDa	13.8
Monomer	34.6 kDa	15.4

Table : 4.9 Calculated elution volume (V_e) from standard protein (Figure 4.22).

Protein samples (1 mg/ml) were incubated for 3 hrs with different concentration of Gu.HCl and injected into a Superdex 200 HR 20/30 column connected to a Äkta Explorer 100 FPLC system, preequilibrated and eluted with different concentration of Gu.HCl in 50 mM Hepes buffer of pH 8.0 at a flow rate of 0.5 mL/min. Elution was monitored by absorbance at 280 nm. The standard molecular mass protein (1 mg/ml) run in the presence of 50 mM Hepes pH 8.0 buffer were β–amylase (200 kDa), alcohol dehydrogenase (150 kDa), BSA(66 kDa) and carbonic anhydrase (29 kDa). The elution volume of tetramer, dimer and monomer were calculated (Table 4.10) with standard proteins (Figure 4.22):

$$\log(M_r) = m \cdot \frac{V_e}{V_o} + b,$$

where V_e is the elution volume and V_o is the exclusion volume of dextran blue (V_o= 8.05 ml).

EcA2(WT)

The quaternary structure of EcA2(WT) was monitored by gel filtration experiment in the presence of increasing amounts of Gu.HCl as described above (Figure 4.23). At concentrations between 0 M - 0.8 M Gu.HCl, the protein peak first shifted to higher elution volumes, indicating the formation of dimers at 0.6-0.8 M Gu.HCl. At Gu.HCl concentrations higher than 0.8 M, the elution volume gradually decreased to values similar to those observed in the absence of Gu.HCl. This was accompanied by a distinct broadening of the peak. Peaks corresponding to monomers were not observed in any of the experiments. This surprising behaviour may be caused by the formation of aggregates of denatured protein (see Discussion).

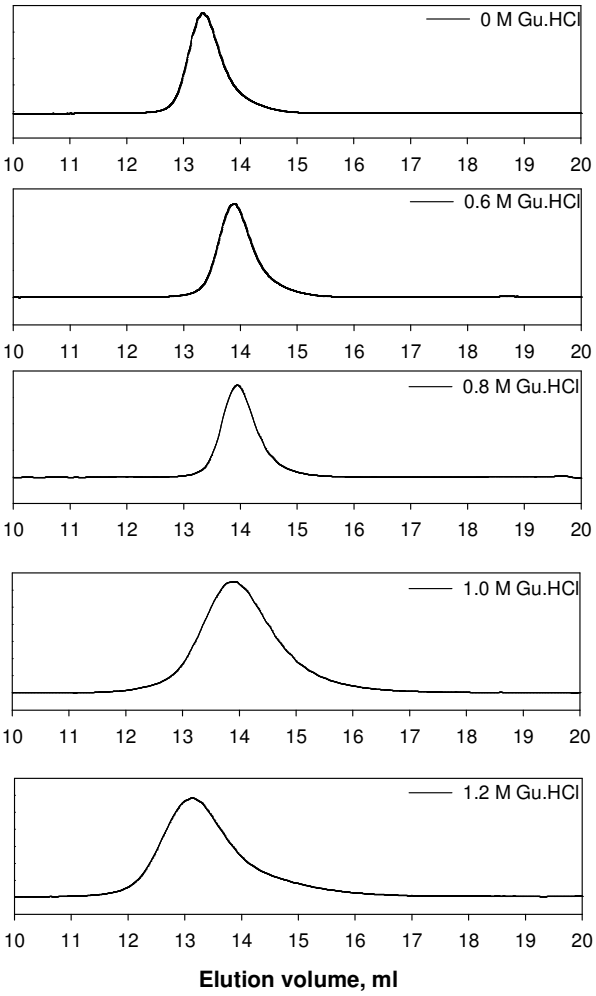

Figure 4.23 Gel filtration of EcA2(WT) in presence of Gu.HCl in 50 mM Hepes (pH 8.0). Molarity of Gu.HCl is indicated on the Figure.

EcA2(W66Y)

As shown in Figure 4.24, similar results were obtained with variant EcA2(W66Y). Again the elution volume first significantly increased and then decreased again at high Gu.HCl concentrations without showing any evidence of monomer formation. Aggregation at high Gu.HCl concentrations seemed to be even more pronouncing with this mutant.

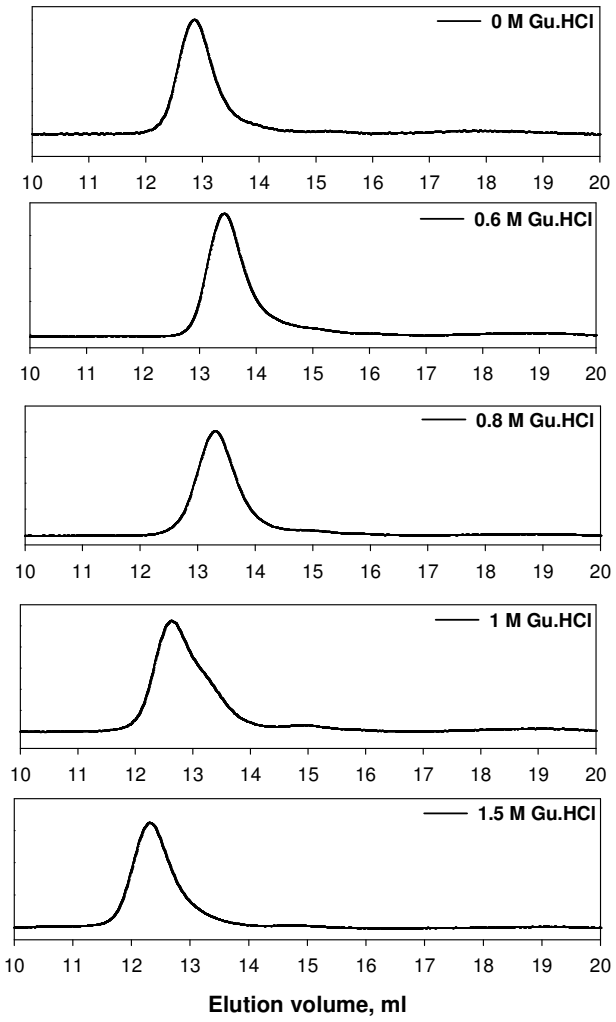

Figure 4.24 Gel filtration of EcA2(W66Y) in presence of Gu.HCl in 50 mM Hepes (pH 8.0). Molarity of Gu.HCl is indicated on the Figure.

EcA2(W66Y/Y181W)

A completely different behavior was seen with variant EcA2(W66Y/Y181W). At 0.2-0.4 M Gu.HCl, the elution volume of protein was markedly higher than in the absence of denaturant, indicating that the enzyme had dissociated into smaller fragments. From their size they might correspond to dimers (peak at V_e = 13.7) and monomers (peak at V_e = 15.8). At 0.4 M Gu.HCl, all of the protein appeared to be in a monomeric state, while at 0.8 M Gu.HCl and above aggregation took place as seen with the other enzyme forms.

The total area of the peaks was approximately same in all experiments, suggesting that no loss of protein occurred during the FPLC runs. The various protein forms were analyzed for activity separately. It was found that the first peak eluting by 0.2 M Gu.HCl

(V_e=13.6 ml) was fully active, suggesting that the dimers formed were active. By contrast, the putative monomer peak eluted by 0.4 M Gu.HCl was inactive. The peaks appearing at 0.8 M -1.5 M Gu.HCl did not show any activity as well.

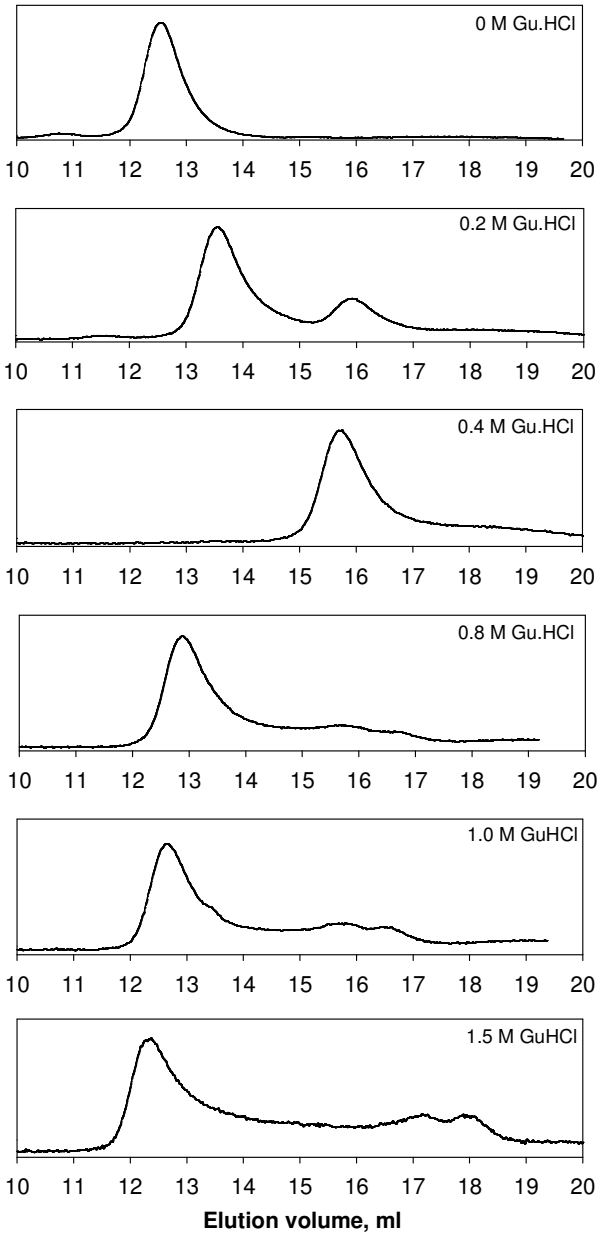

Figure 4.25 Gel filtration of EcA2(W66Y/Y181W) in the presence of Gu.HCl in 50 mM Hepes (pH 8.0). Molarity of Gu.HCl is indicated on the Figure.

EcA2(Y176S)

Variant EcA2(Y176S) showed behavior similar to EcA2(W66Y/Y181W). Again, the native protein appeared to dissociate into dimers and monomers at 0.2 M Gu.HCl (Figure 4.26) while, a single peak at V_e~12.5 ml was eluted by 1.5 M Gu.HCl. Thus, the gel filtration data confirmed the presence of dimers at low Gu.HCl concentrations, which is in agreement with the Gu.HCl-denaturation profiles of EcA2(Y176S) (Figure 4.14 B).

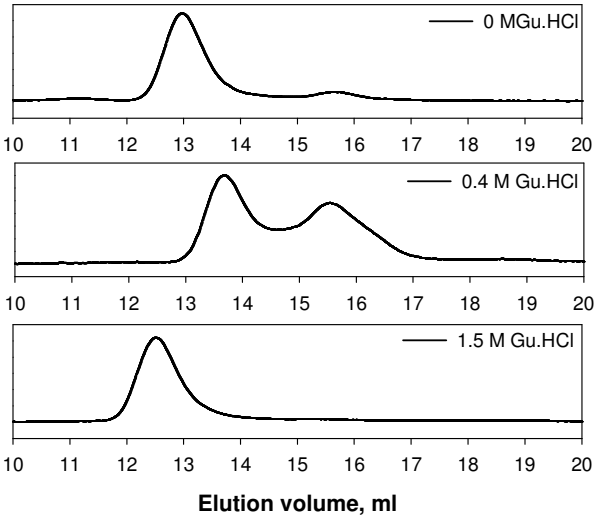

Figure 4.26 Gel filtration of EcA2(Y176S) in presence of Gu.HCl in 50 mM Hepes (pH 8.0). Molarity of Gu.HCl is indicated on the Figure.

EcA2(D156N)

As above, this variant dissociated into putative dimers and monomers at 0.4 M Gu.HCl (Figure 4.27). At 0.6 M Gu.HCl concentration, these peaks appeared to merge into a third species with an apparent mass between monomer and dimer (V_e ~13.3-14.5 ml), while aggregates formed above 0.8 M Gu.HCl. Again, this results agree with the Gu.HCl-denaturation profiles of EcA2(D156N) (Figure 4.21 B).

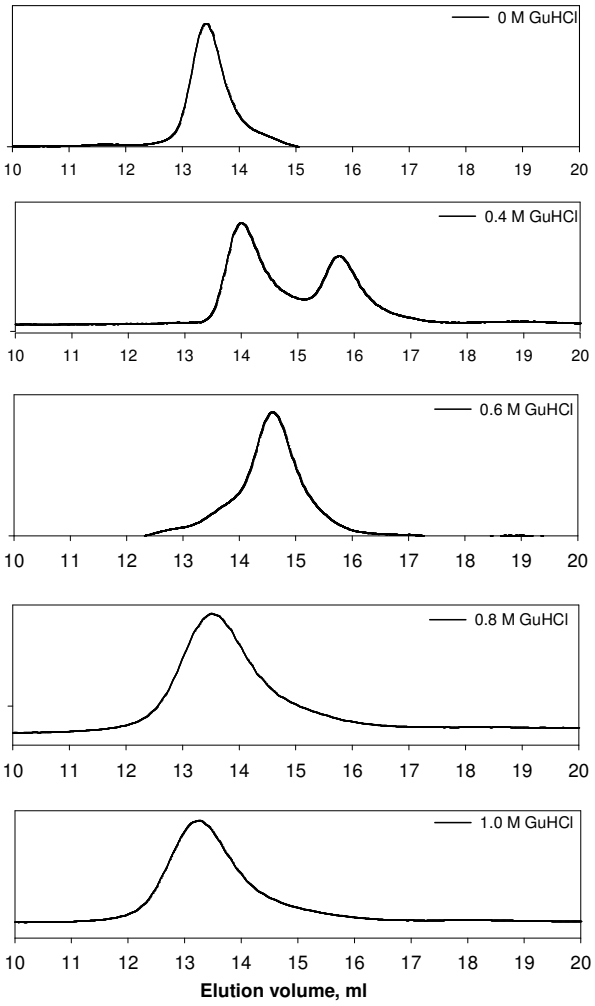

Figure 4.27 Gel filtration of EcA2(D156N) in presence of Gu.HCl in 50 mM Hepes (pH 8.0). Molarity of Gu.HCl is indicated on the Figure.

EcA2(D188N)

The results obtained with EcA2(D188N) are shown in Figure 4.28. With this variant, a more complex pattern was observed, indicating that the preparation used was not homogeneous or already partially degraded. The peak at about 17.2 ml was present at all Gu.HCl concentrations and thus appears to be a due to contaminant. Notwithstanding this problem, the general pattern observed with this mutant was rather similar to that seen with EcA2(D158N).

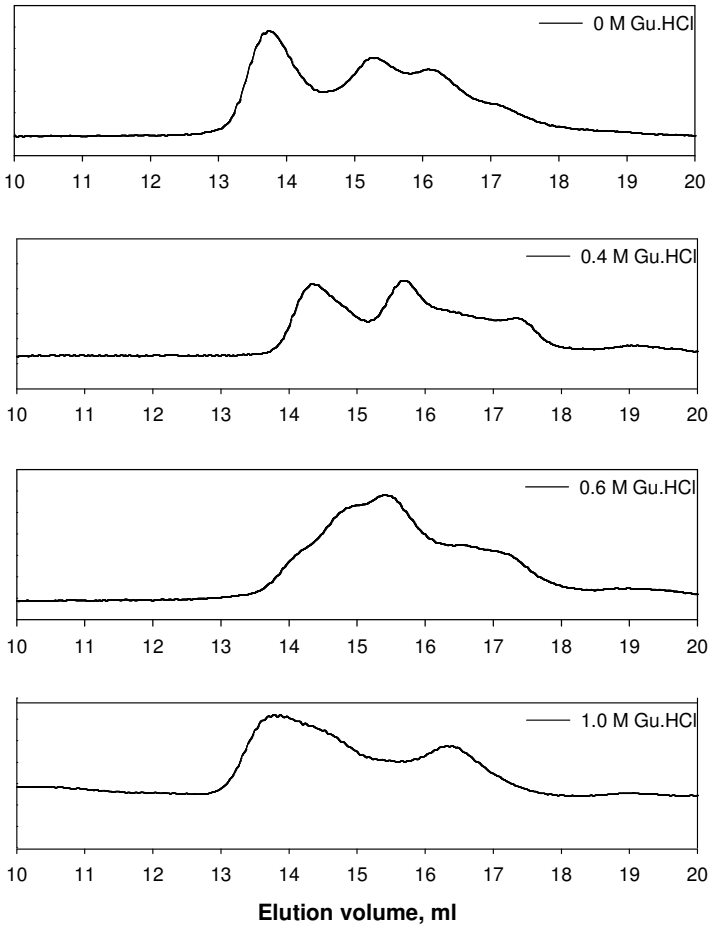

Figure 4.28 Gel filtration of EcA2(D188N) in presence of Gu.HCl in 50 mM Hepes (pH 8.0). Molarity of Gu.HCl is indicated on the Figure.

4.4.3 Thermal denaturation studies

To understand the effects of temperature and pH on the protein stability, thermal denaturation studies were carried out with wild type EcA2 and its mutants. Heating disrupts the folded structure of an enzyme because of increased vibrational and rotational motions of atoms. Three methods were used to monitor thermal denaturation of the protein, namely activity measurements, CD spectroscopy (CD) and differential scanning calorimetry (DSC).

4.4.3.1 Thermal denaturation as monitored by activity

For thermal denaturation, lower protein concentrations are required than for chemical denaturation. Therefore an enzyme concentration of 0.1 mg/ml was used for these experiments.

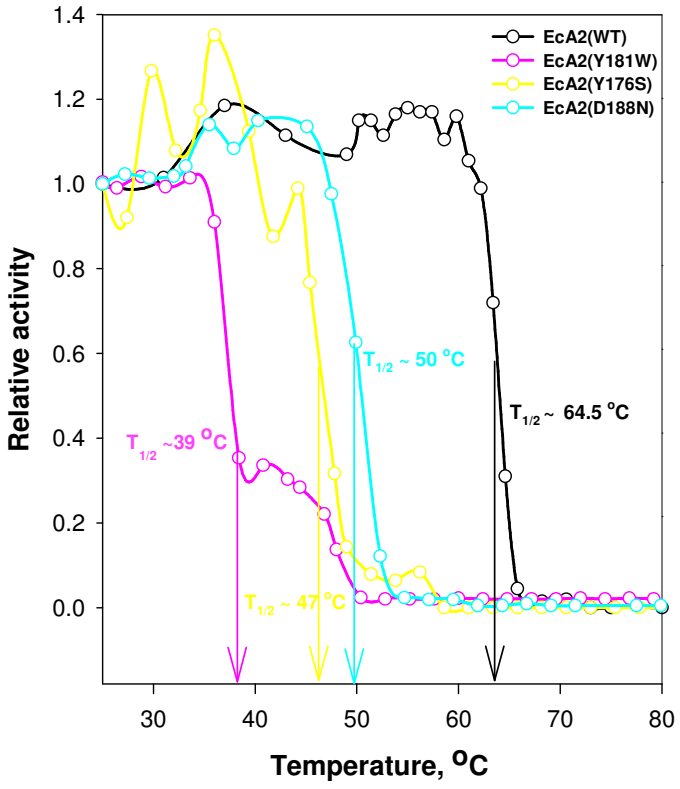

Figure 4.29 Thermal denaturation profiles of EcA2(WT) & its mutants monitored by activity.

In order to follow thermal denaturation by activity measurements, the enzyme was first dialyzed against the respective buffer solution and then slowly heated from 25 °C to 85 °C at a constant rate of 1 °C/min (cf. section 3.17.2). The residual activity of small

aliquots removed from the sample during heating was immediately measured with 1 mM AHA as described in section 3.16.3.

The resulting profiles for EcA2(WT) and several mutants are compared in figure 4.30. In each case, the temperature $T_{1/2}$ at half-denaturation was estimated from the inflection point of the profiles.

While most variants were inactivated within a narrow temperature range of about 5 °C, variant EcA2(Y181W) showed a more complex profile that indicates formation of an active intermediate at temperatures between 35 and 40 °C. Total denaturation took place between 45 and 50 °C.

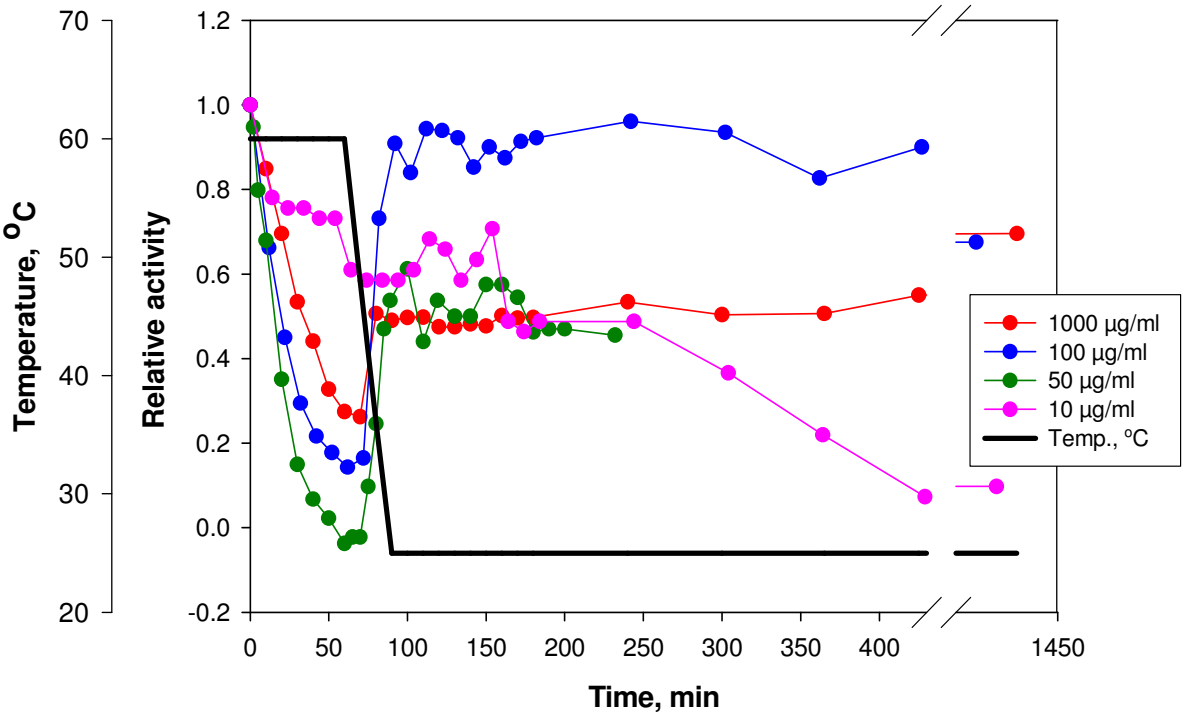

Figure 4.30 Thermal renaturation of EcA2(WT) at different protein concentration monitored by activity.

To check whether thermal denaturation was reversible, the experiment was modified as follows: EcA2(WT) solutions with concentrations between 10-1000 µg/ml were incubated at 60 °C for 60 min and then cooled down to 25 °C at a constant rate of 1.2 °C/min. As

shown in figure 4.30, the enzyme solution at 100 µg /ml regained up to 90% of its original activity, whereas only ~50% recovery was observed at lower and higher protein concentrations. Unexpectedly, the most dilute solution (10 µg/ml) was inactivated at the lowest rate and did not significantly regain activity after cooling.

4.4.3.2 Thermal denaturation monitored by Circular Dichroism (CD)

In addition to tryptophan fluorescence, CD spectroscopy was used to evaluate the effect of the mutations on the structure and stability of EcA2(WT). Far-UV CD spectroscopy is useful to monitor secondary structure, especially α-helical structure that comprises a large fraction of the EcA2(WT) fold.

Far-UV CD spectra of predominantly helical proteins have characteristic double minima at 208 and 222 nm and a maximum at 193 nm. Near-UV spectroscopy is sensitive to the local conformation around aromatic residues. Completely unfolded polypeptides have weak near-UV signal, but when the aromatic residues are well packed within a hydrophobic core, their CD signal is usually larger than when those same residues are solvent-exposed and mobile. Thus, near-UV CD spectroscopy provides a sensitive measure of the tertiary structure of proteins and is useful for the qualitative assessment of the packing of the aromatic residues.

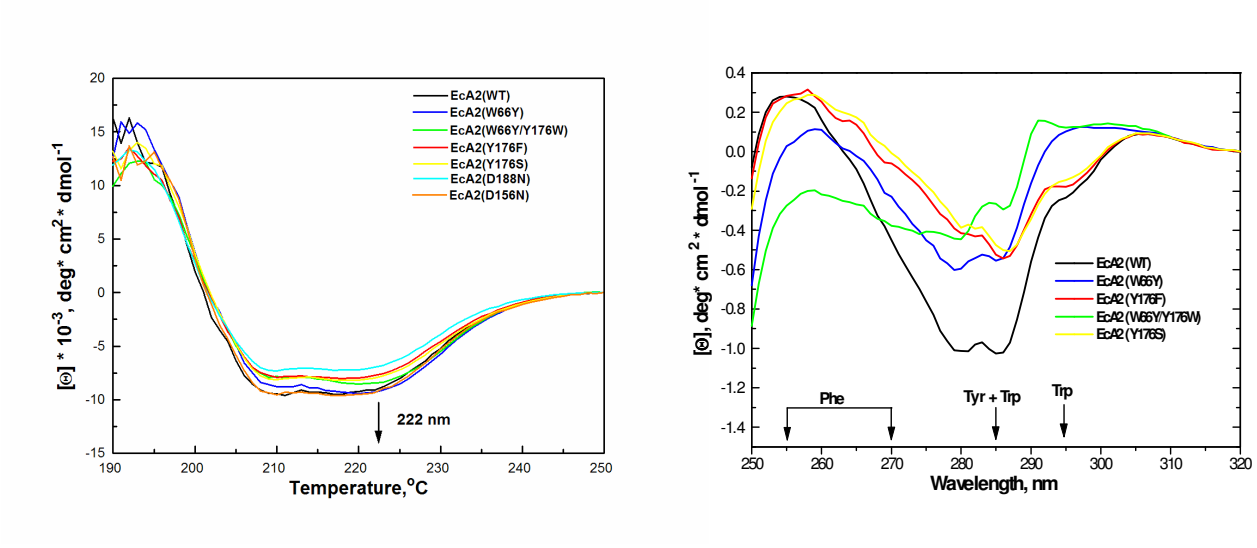

Figure 4.31 UV CD spectra of wild-type and mutant proteins. (A) Far-UV CD spectra of EcA2(WT) and its mutants. (B) Near-UV CD spectra of EcA2(WT) and its mutants.

CD spectroscopy is useful for distinguishing between protein states that are fully folded, partially folded or completely unfolded. Completely unfolded proteins lack secondary and tertiary structure and thus have little CD signal in the near-UV. The far-UV signal of completly unfolded proteins can vary in intensity, but generally has a characteristic "random coil" spectrum with a minimum near 203 nm. Molten globule folding intermediates contain secondary structure, yet lack a compact well defined hydrophobic core, a characteristic of natively folded proteins. As a result, molten globules have a significant far-UV CD signal with little near-UV CD signals. Hence, both near- and the far-UV CD spectroscopies are necessary to distinguish between an unfolded protein, a molten globule, and a folded protein.

Figure 4.31 show far-UV and near-UV CD spectra recorded with wild-type and mutant EcA2 forms. Figure 4.31 A shows far-UV CD wavelength scans from 190 nm to 250 nm. The samples contained ~0.1 mg/ml protein in 20 mM PBS, pH 8.0 in 2 mm tightly sealed quartz cuvettes. The spectra were recorded at 25 ^{o}C, which was the standard temperature in our CD experiments. The spectra shows negative peaks at 222 nm and 208 nm, which are the characteristic for α-helices. Based on the CD intensity, the α-helical content in this protein was estimated to be about 30 % (section 3.20.2). In their native state, EcA2(WT) and its mutants have similar amounts of helical structure.

In addition, near-UV CD spectra were recorded in the range of 250-320 nm. The samples contained ~3.4 mg/ml protein in 20 mM PBS, pH 8.0. They were placed in 5 mm pathlength quartz cuvettes and the spectra were recorded at 25 ^{o}C. The results are shown in figure 4.31 B. A well-defined negative trough with a double minimum at 280 nm and 285 nm indicates orientational ordering of a significant fraction of the Tyr and Trp groups present in wild type EcA2. The spectrum of W66Y had a similar shape, suggesting comparable Trp and Tyr packing in wild type and the mutant. In contrast, the near-UV CD spectrum of EcA2(W66Y/Y176W) where a new tryptophan residue had been inserted at the dimer-dimer interface was significantly different from the others.

A series of far-UV CD spectra were recorded at several constant temperatures from 25-73 ^{o}C (Figure 4.32). The CD spectral changes upon thermal denaturation of the protein reflect the transition from a natively folded to an unfolded state, as indicated by the large negative peak at 203 nm observed above 63 °C, which is characteristic of a random coil. As already mentioned, the ellipticity minima at 208 and 222 nm in the native spectrum are

characteristic of a high degree of α-helical secondary structure, and the isochromatic point observed near 208.5 nm suggests significant population of only two alternative conformations (α-helix and random coil).

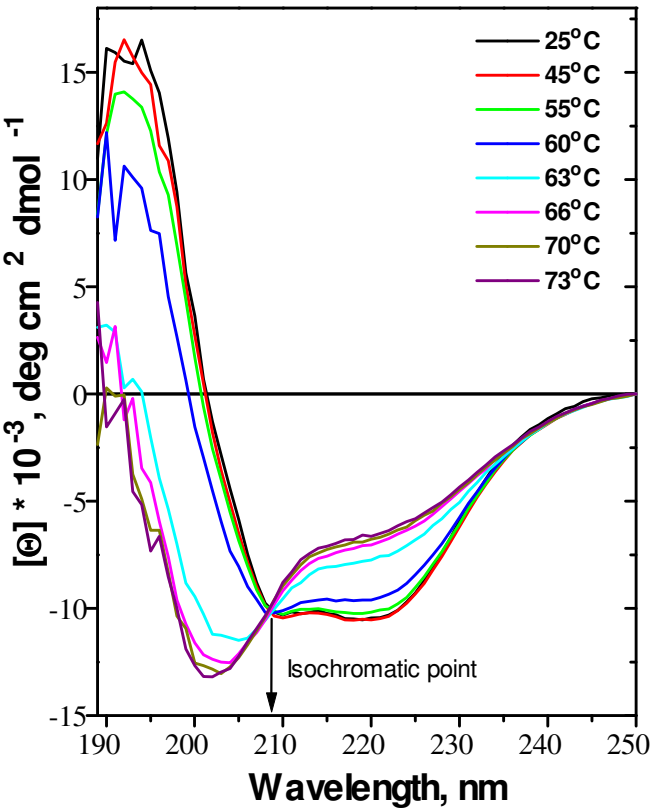

Figure 4.32 Far-UV CD spectra of EcA2(WT) recorded at several constant temperatures from 25-73 °C.

Another interesting observation was that, at different heating rates, the thermal unfolding and refolding curves of wild type protein were significantly different. The $\Theta_{222}(T)$ melting curves were recorded during heating and cooling from 25 °C to 85 °C at rates from 80 °C/h to 11 °C/h (Figure 4.33 A). As the heating rate decreased, the melting curves of EcA2(WT) showed a low-temperature shift, with the midpoint T_m of the heat unfolding reduced from ~ 67 °C (ν = 80 °C/h, red) to ~ 63 °C (ν = 11 °C/h, blue). Furthermore, the cooling curves (corresponding to refolding of the protein) showed a large scan rate dependence and displayed hysteresis at any scan rate explored. This indicates a slow irreversible transition with high activation enthalpy and precludes equilibrium

thermodynamic analysis of this transition. Therefore, the EcA2(WT) unfolding was a non-equilibrium transition at any scan rate explored.

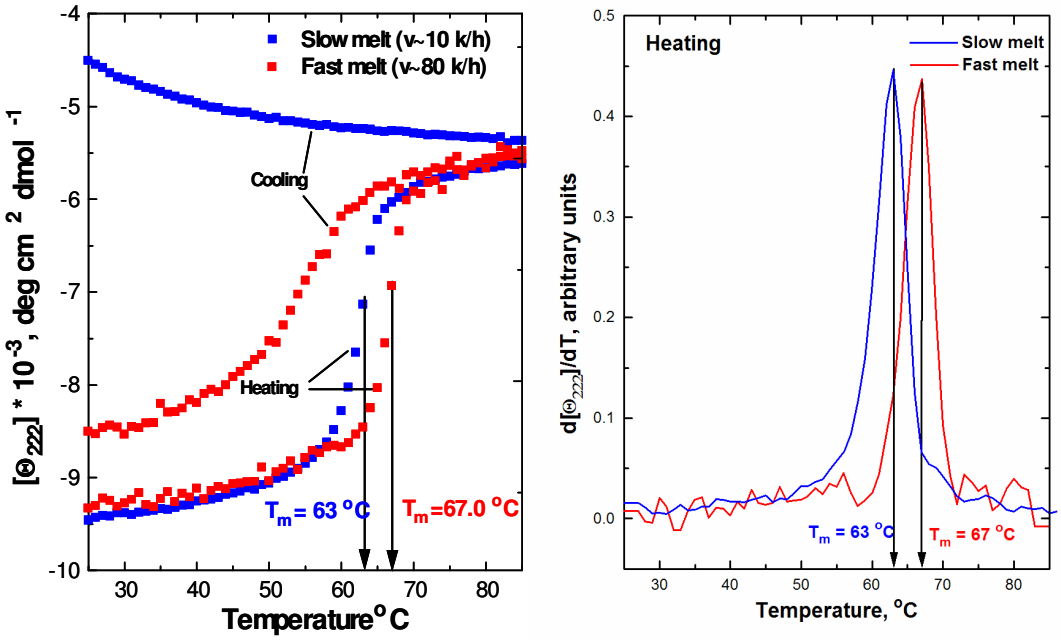

Figure 4.33 (A) Thermal unfolding and refolding of EcA2(WT). The thermal transition was monitored by CD at 222 nm upon heating and cooling at rate ν ~ 11 °C /h (blue) and ν ~ 80 °C /h (red). Arrows indicate the midpoint T_m of the protein unfolding. (B) First derivative function $d[\Theta_{222}]/dT$ of the heat unfolding curves. The peak positions shown by arrows indicate the apparent melting temperatures T_m.

In Figure 4.34, $\Theta_{222}(T)$ melting curves are shown for EcA2(WT) and all mutants studied during heating from 25 °C to 85 °C at a rate of 80 °C/h. Most mutants had lower T_m values as compared to EcA2(WT). In contrast, the melting curve (Figure 4.34, red curve) of EcA2(Y176F) was shifted to higher temperatures (T_m = 71 °C) suggesting higher thermal stability of this mutant. Again, hysteresis was observed in the thermal unfolding data of all mutants protein, indicating irreversibility of the unfolding transition.

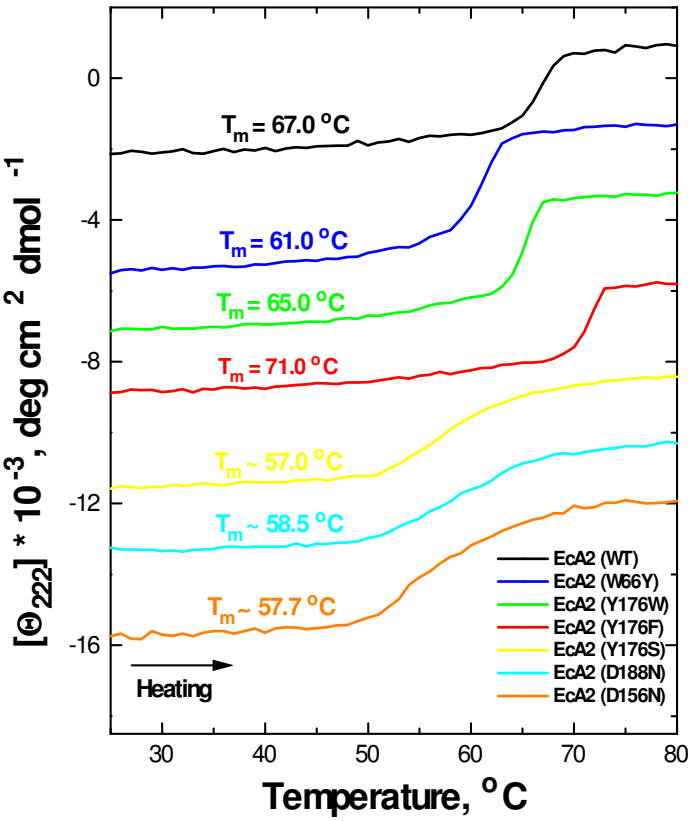

Figure 4.34 Thermal melts of EcA2(WT) & its mutants monitored by CD at 222 nm.

Figure 4.35 (inset) shows the far-UV CD wavelength scan of wild type protein at 25 °C in 20 mM PBS (pH 6.5-8.0) or 20 mM sodium acetate buffer (pH 5.0). The spectra at both pH values fully overlapped and showed major negative peaks at 222 nm and 208 nm, indicating that the secondary structure of the protein remained invariant in the pH range analyzed.

Nevertheless, the thermal unfolding profiles of EcA2(WT) showed significant differences at different pH (Figure 4.35), suggesting reduced protein stability at lower pH. Hysteresis was seen at all pH values examined.

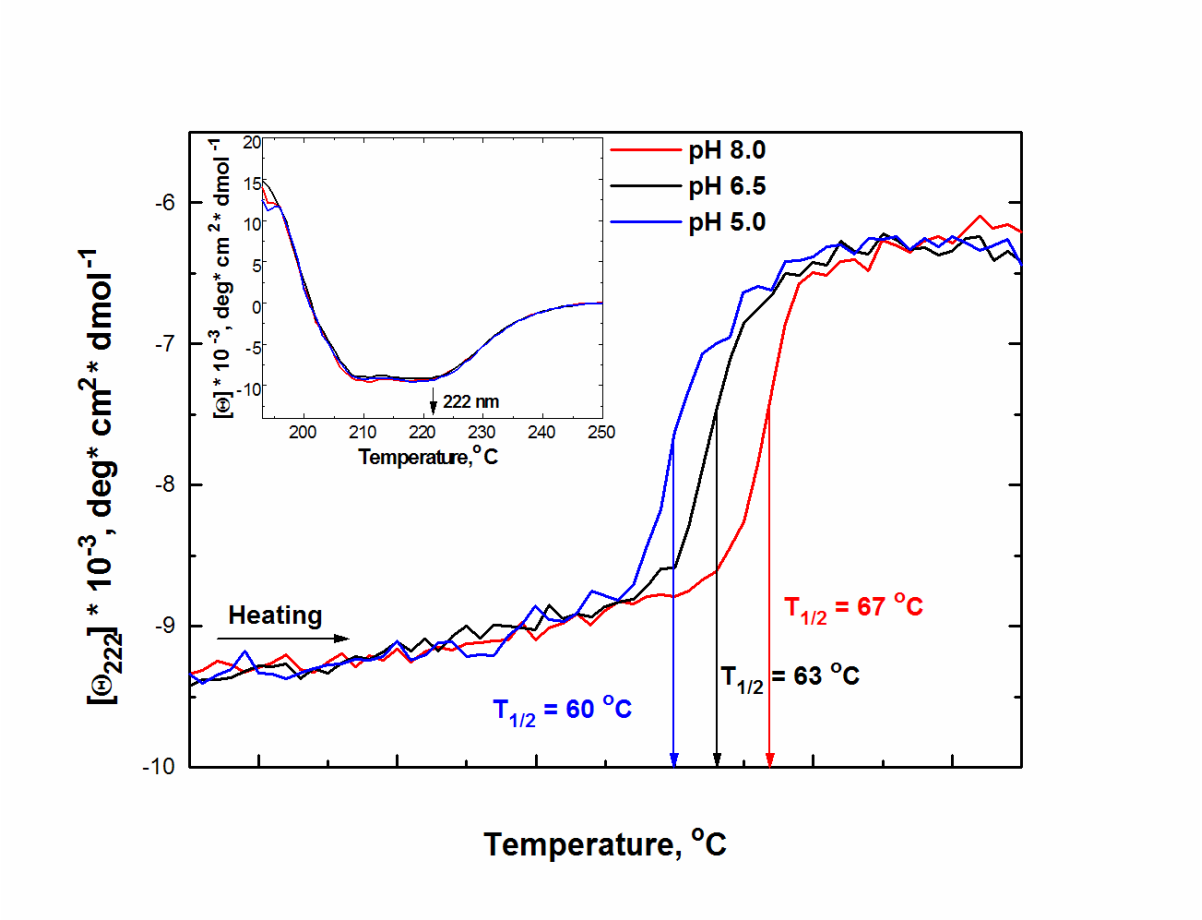

Figure 4.35 Thermal melting curves of EcA2(WT) at different pH monitored by CD at 222 nm. **Inset:** Far-UV CD spectra of EcA2(WT) at different pH.

In addition to measuring CD, the spectropolarimeter was also used to record the voltage applied to the dynodes of the UV detector photomultiplier (dynode voltage, *V*). The dynode voltage increases nearly linearly with any reduction in the light intensity at the detector which may result from light scattering and/or absorption.

The melting temperatures indicated by the CD (Figure 4.34) and light scattering melting curves of the proteins (Figure 4.36) are similar, indicating that protein unfolding leads to aggregation. Thus, the physical origin of the irreversible heat-induced protein unfolding appears to be aggregation of the unfolded protein.

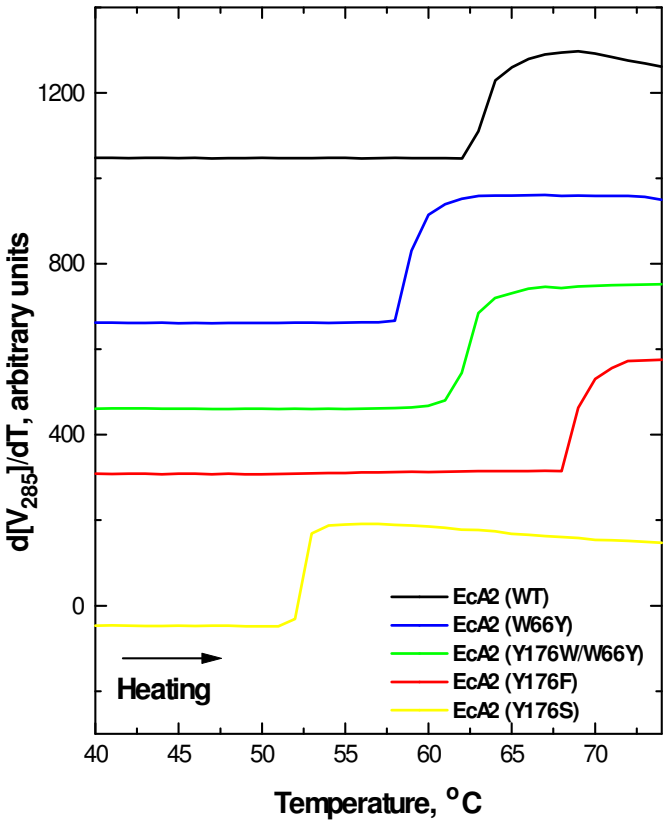

Figure 4.36 Thermally induced changes in the light scattering of EcA2(WT) and its mutants monitored by dynode voltage.

4.4.3.3 Thermal denaturation monitored by Differential Scanning Calorimetry (DSC)

The vast majority of stability studies have focused on the thermodynamic characterization of small, monomeric globular proteins (Privalov *et al.,* 1979; Murphy *et al*, 1992). There are much fewer studies on oligomeric systems because of the high degrees of irreversibility in unfolding and the complexity of the overall process (Jaenicke *et al.,* 2000). DSC is one of the most powerful methods for the characterization of protein stability (Plum *et al.,* 1995). For a thermodynamically reversible transition, the technique provides several pieces of information: the melting temperature T_m at which the maximum excess heat capacity is observed; the area under the curve, obtained by integration, giving the calorimetric enthalpy of denaturation (i.e., transition heat per molecule); the width of the

peak (in °C) at half the maximal excess heat capacity, which is an indication of the co-operativity of the protein structural change and is related to the vant Hoff's enthalpy of the transition (heat unfolding per cooperative unit); and the change in heat capacity of the protein during the heat unfolding transition that is also obtainable from the data. In addition, programs are available to analyze the composition of the denaturation curves by deconvolution analysis. Since thermal unfolding of EcA2 is thermodynamically irreversible due to aggregation, only a limited number of parameters (such as apparent T_m and apparent ΔH_{cal}) can be obtained by DSC.

EcA2(WT)

Figure 4.37 illustrates typical high-resolution calorimetric data for EcA2(WT) solubilized in 20 mM PB (pH 8.0) at different protein concentrations. The Cp(T) data were recorded upon heating from 10-80 ^oC. To facilitate direct comparison of the DSC and CD data (inset, Figure 4.37), similar heating rates (80-90 $^oC/h$) were used in both experiments. The first DSC scan shows a peak at 66.0 ^oC, which is close to the apparent T_m = 67 ^oC determined from the CD melting curve, $d\Theta_{222}(T)/dT$. T_m remained invariant with changes in the protein concentrations in the range tested, indicating the absence of the effects of protein aggregation on the peak position. No transitions were seen upon rescanning of these samples, indicating irreversibility of the thermal unfolding.

Figure 4.38 shows the data fit for the transition in EcA2(WT) over the temperature range 10-80 ^oC based on a 2-state model of denaturation. In figure 4.38 A, the DSC data was normalized on the basis of tetrameric structure. $\Delta H_{Cal}/\Delta H_{VH}$ for the transition was nearly 4, suggesting that one tetramer comprises about 4 cooperative units, i.e., the cooperative unit may be the monomer. Indeed, when the DSC data were normalized to the monomer concentration (Figure 4.38 B), the ratio $\Delta H_{cal}/\Delta H_{VH}$ was close to unity, confirming that the cooperatively unfolding unit in this transition is a monomer. Thus, it appears that the monomers in tetrameric EcA2(WT) unfold nearly independently of each other.

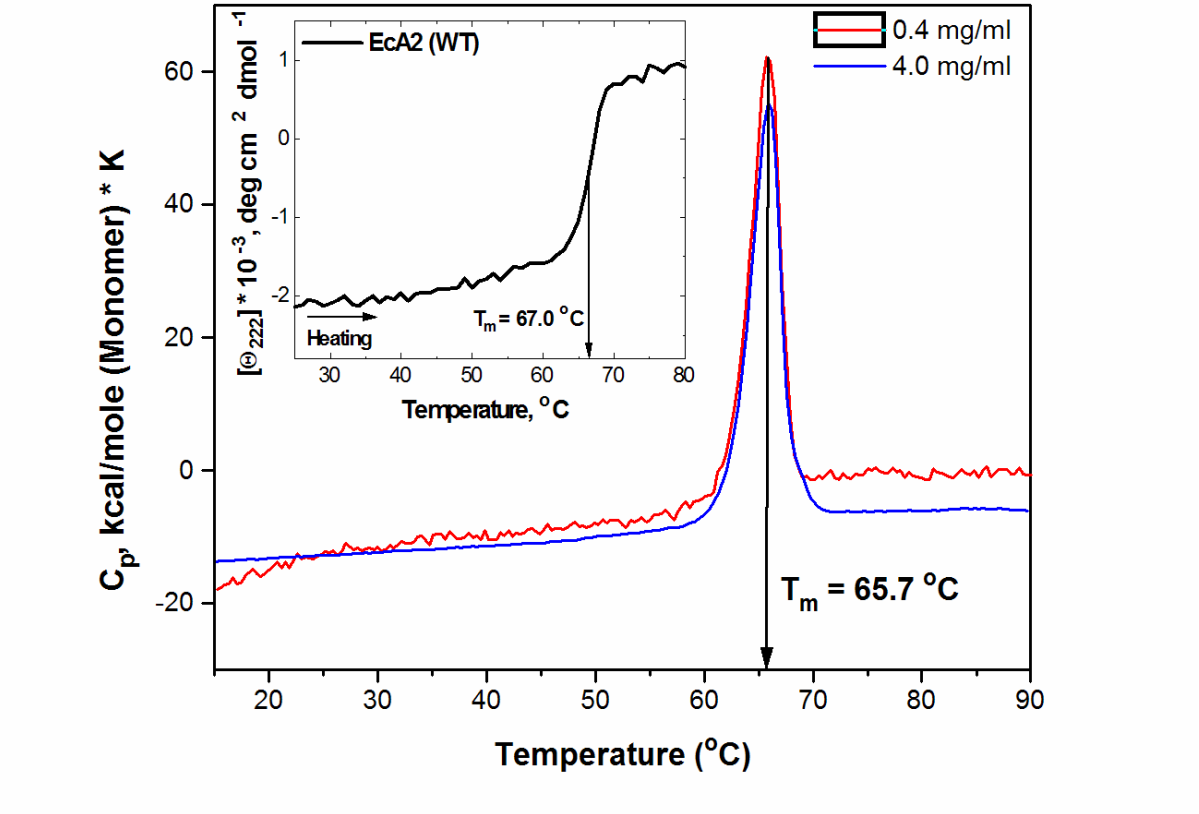

Figure: 4.37 Thermal denaturation of EcA2(WT) monitored by DSC at different protein concentrations at pH 8.0.
Inset: Melting of the α-helical structure of EcA2(WT) measured by the intensity of the 222-nm CD band.

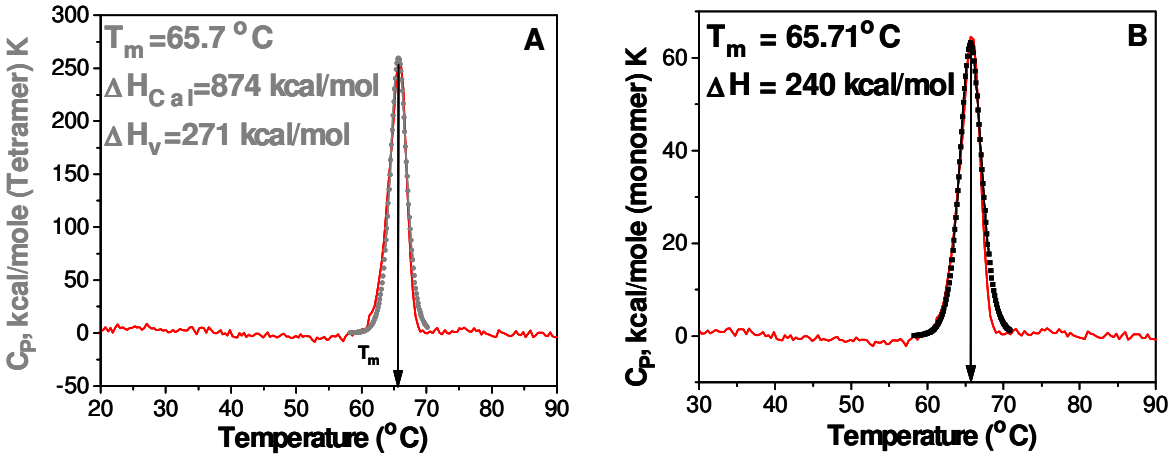

Figure: 4.38 Result of fitting the Cp(T) data (red) by a single Gaussian function using a 2-state model; (A) data were normalized on tetramer concentration (B) data were normalized on monomer concentration.

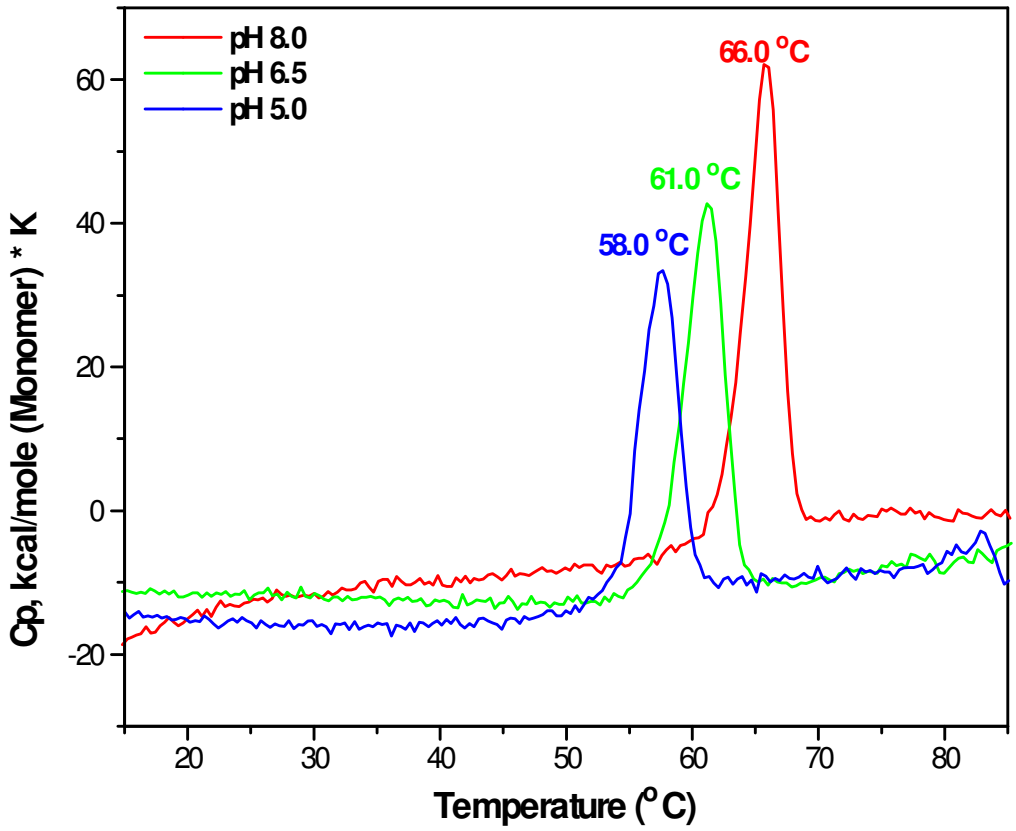

Figure: 4.39 Thermal denaturation of EcA2(WT) monitored by DSC at different pH.

The thermal stability of EcA2(WT) in the pH range 5.0-8.0 was monitored by DSC (Figure 4.39). Similar to the irreversible unfolding observed in our CD and light scattering experiments, the thermal unfolding monitored by DSC was irreversible at all pH's examined, as indicated by the absence of the transition from consecutive DSC scans recorded from the same sample. In the pH range 5.0-8.0, T_m increased with increasing pH, from 58.0 ^oC at pH 5.0 to 67.0^oC at pH 8.0. The highest ΔH_{cal} values (240 kcal/mol) were observed at pH 8.0, which decreased to 197 kcal/mol at pH 5.0. This suggests that the increase in protein stability upon increase in pH from 5 to 8 is mainly enthalpy driven. The irreversible nature of the thermal transitions prevented further analysis of the data, such as direct determination of the heat capacity increment ΔCp associated with the transition.

Figure 4.40 shows that the enthalpies and T_m of EcA2(WT) obtained by DSC & CD are linear functions of pH. All thermodynamic parameter determined for EcA2(WT) are summarized in table 4.10 at different pH.

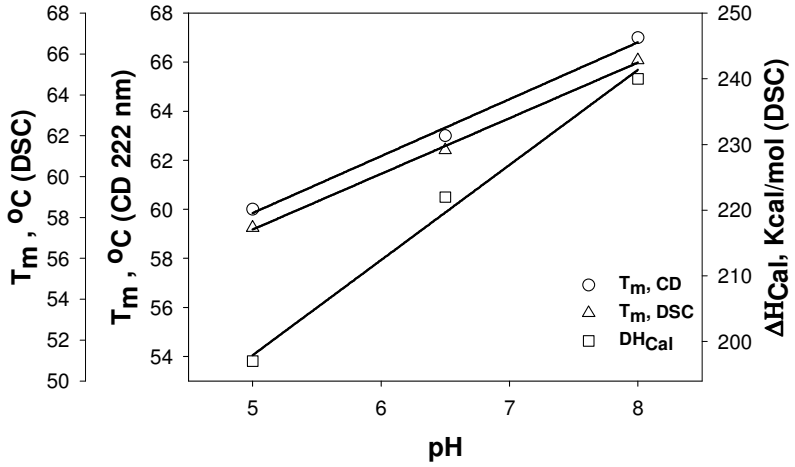

Figure: 4.40 Enthalpies & T_m of EcA2(WT) obtained by CD & DSC plotted as a function of pH.

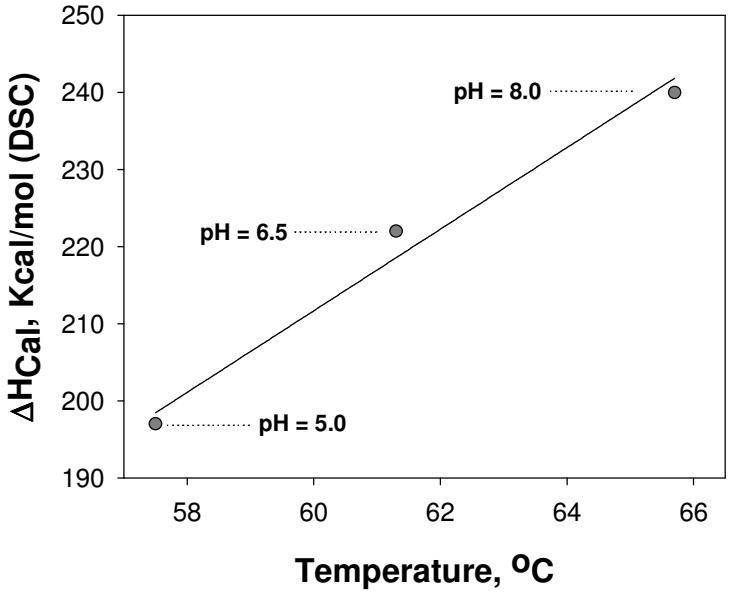

Figure 4.41 Enthalpies of EcA2(WT) at different pH obtained by DSC plotted against the temperature of denaturation. The slope of the least-squares line indicates the change in heat capacity associated with denaturation, ΔC_p = 5.3 kcal mol^{-1} K^{-1}

Figure 4.41 illustrates that the calorimetric enthalpy (per monomer) associated with the thermal unfolding of EcA2(WT) at different pH was an approximately linear function of T_m. This behavior is expected for a two-state transition and has been observed for a variety of small globular proteins (Privalov, 1979). The positive slope of this plot (about 5.3 kcal mol^{-1}

K^{-1} for wild-type protein) represents the difference in the heat capacity at constant pressure (ΔC_p) between the folded and the unfolded states of the molecule (heat capacity increment). Indeed, by definition $\Delta C_p = d\Delta Hcal/dT$, which is the slope of the plot $\Delta H_{cal}(T)$. The value of ΔC_p is proportional to the magnitude of the hydrophobic interactions in the folded state of a protein (the "hydrophobic effect"). The observed value of ΔC_p~5.3 kcal/(mol·K) assessed from our measurements at various pH is typical for the unfolding of proteins of this size, indicating the consistency of our analysis.

pH	**T_m (^oC) determined by CD (v~80 ^oC/h)**	**T_m (^oC) determined by DSC (v~90 ^oC/h)**	**ΔH_{Cal} (kcal/mol) per monomer determined by DSC (v~80 ^oC/h)**
5.0	60.0 ^oC	58.0 ^oC	197
6.5	63.0 ^oC	61.0 ^oC	222
8.0	67.0 ^oC	66.0 ^oC	240

Table 4.10 Apparent thermodynamic parameters for the thermal denaturation of EcA2(WT) as a function of pH.

EcA2(Y176F)

In the case of variant EcA2(Y176F), a series of DSC experiment similar to those described for EcA2(WT) were carried out. The DSC scan shows a peak at 71.0 ^oC (Figure 4.42), which is very close to the apparent T_m = 70.7 ^oC determined from the CD melting curve, $d\Theta_{222}(T)/dT$ (inset, Figure 4.42). Thus, the DSC peak corresponds to protein unfolding transition. Compared to the WT, this mutant shows similar ΔH_{cal} but significantly higher T_m, suggesting increased thermal stability due to the Y176F substitution.

Because of the irreversible nature of the transition, (inset, Figure 4.42), no further thermodynamic analysis of this transition was carried out.

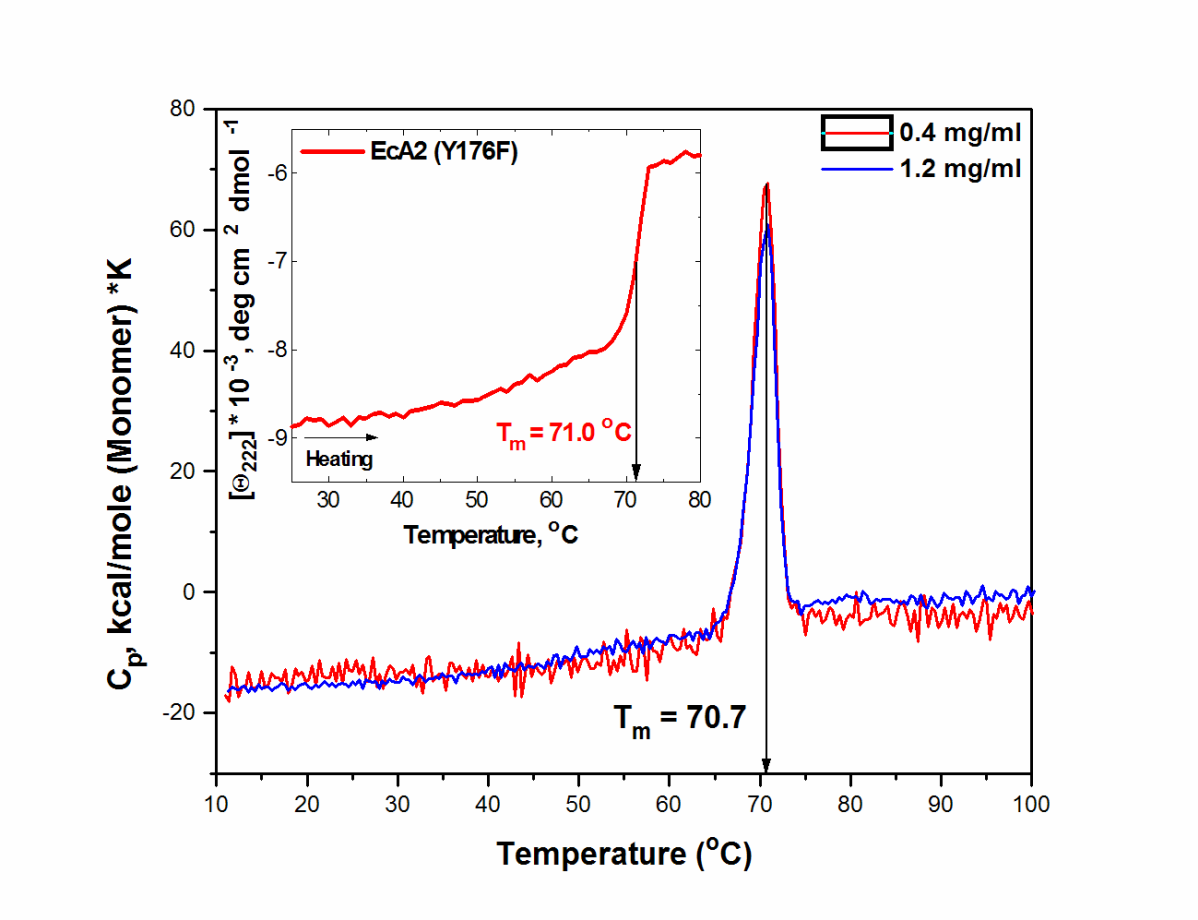

Figure 4.42 Thermal denaturation of EcA2(Y176F) monitored by DSC at different protein concentrations at pH 8.0. **Inset:** Melting of the α-helical structure of EcA2(Y176F) measured by the intensity of the 222-nm CD band.

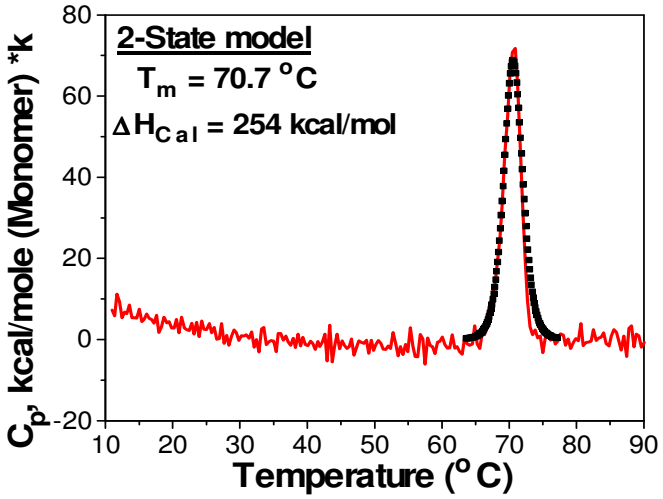

Figure 4.43 Result of fitting the Cp(T) data (red) by a single Gaussian function using a 2-state model (black); the data were normalized to monomer concentration.

EcA2(W66Y)

The DSC scan of EcA2(W66Y) mutant shows a peak at 60.2 ^{o}C (Figure 4.44), which is similar to the apparent T_m = 61.0 ^{o}C determined from the CD melting curve, $d\Theta_{222}(T)/dT$ (inset, Figure 4.44). Therefore, this DSC peak probably reflects protein secondary structural unfolding.

EcA2(W66Y/Y176W)

Double mutant EcA2(W66Y/Y176W) showed a DSC peak centered at 65.0 ^{o}C (Figure 4.47), which is identical to the apparent T_m = 65.0 ^{o}C determined from the CD melting curve, $d\Theta_{222}(T)/dT$ (inset, Figure 4.46). Thus, this DSC peak corresponds to protein secondary structural unfolding. An additional high-temperature peak observed at ~72 ^{o}C at a relatively high protein concentration of 1.2 mg/ml (Figure 4.46, blue curve), which apparently results from aggregation of thermally denatured protein.

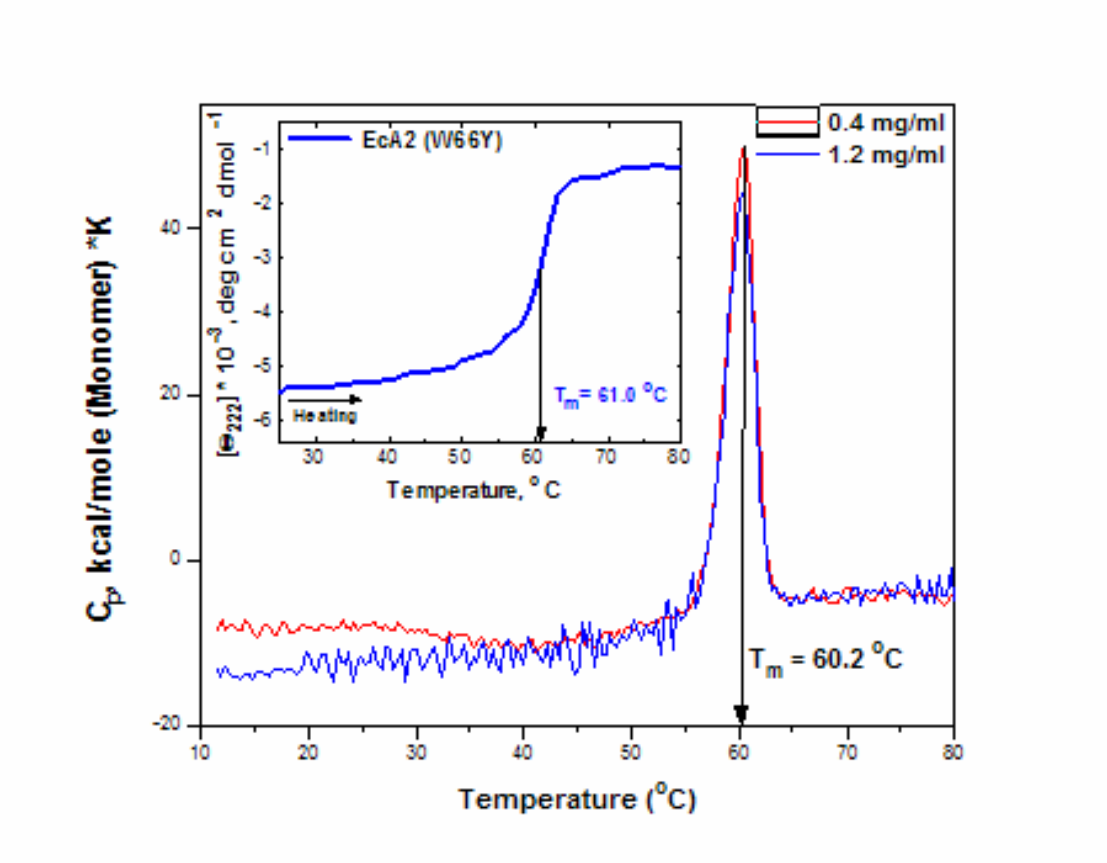

Figure 4.44 Thermal denaturation of EcA2(W66Y) monitored by DSC at different protein concentrations pH 8.0. **Inset:** Melting of the α-helical structure of EcA2(W66Y) measured by the intensity of the 222-nm CD band.

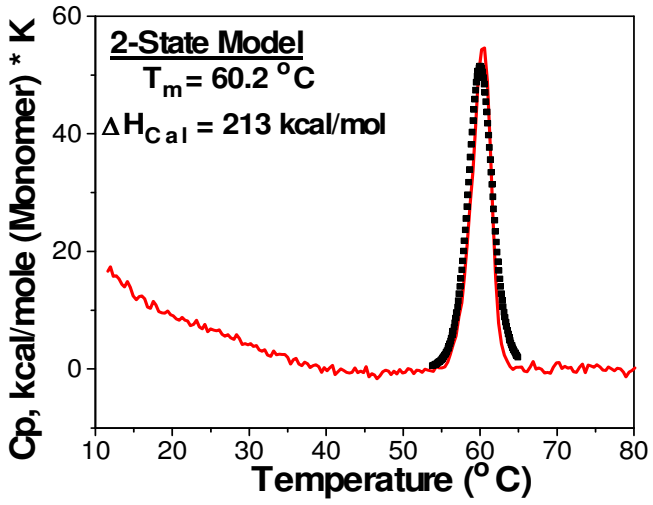

Figure 4.45 Result of fitting the Cp(T) data (red) by a single Gaussian function using a 2-state model (black); the data were normalized to monomer concentration.

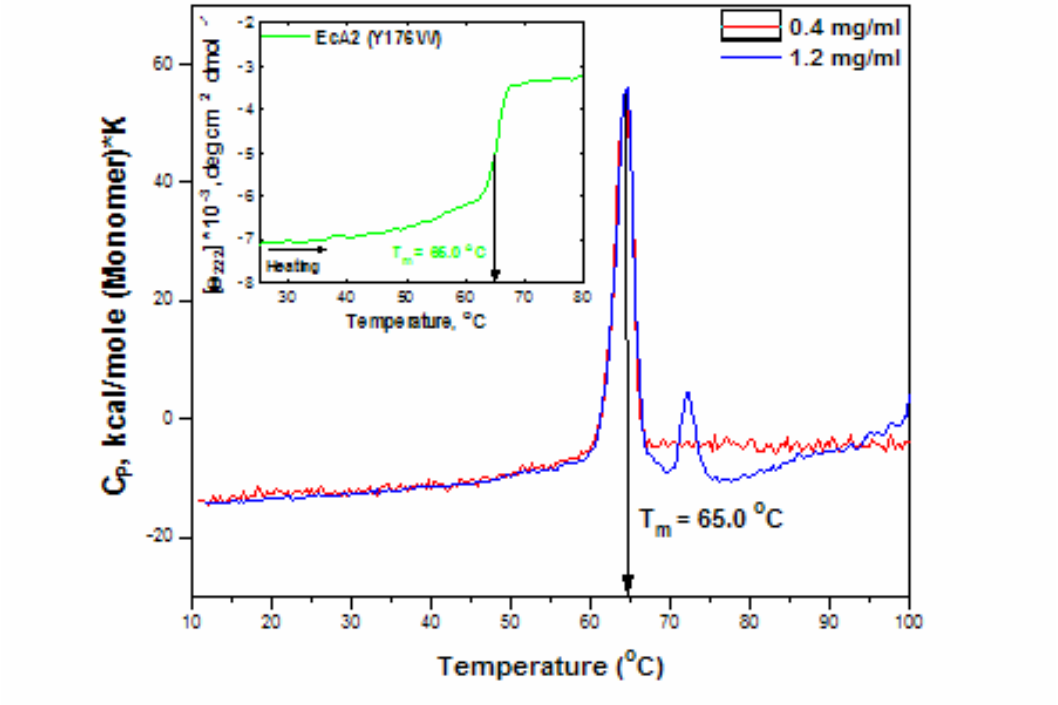

Figure 4.46 Thermal denaturation of EcA2(W66Y/Y176W) monitored by DSC at different protein concentrations pH 8.0. **Inset:** Melting of the α-helical structure of EcA2(W66Y/Y176W) measured by the intensity of the 222-nm CD band.

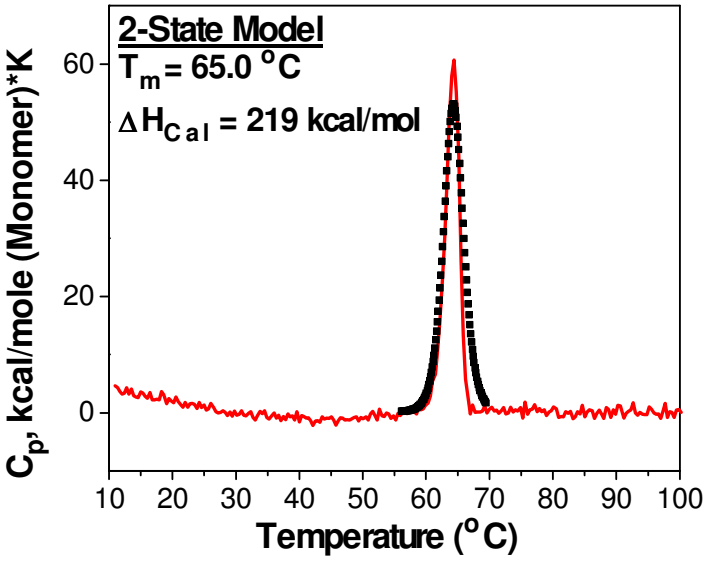

Figure 4.47 Result of fitting the Cp(T) data (red) by a single Gaussian function using a 2-state model (black); the data were normalized to monomer concentration.

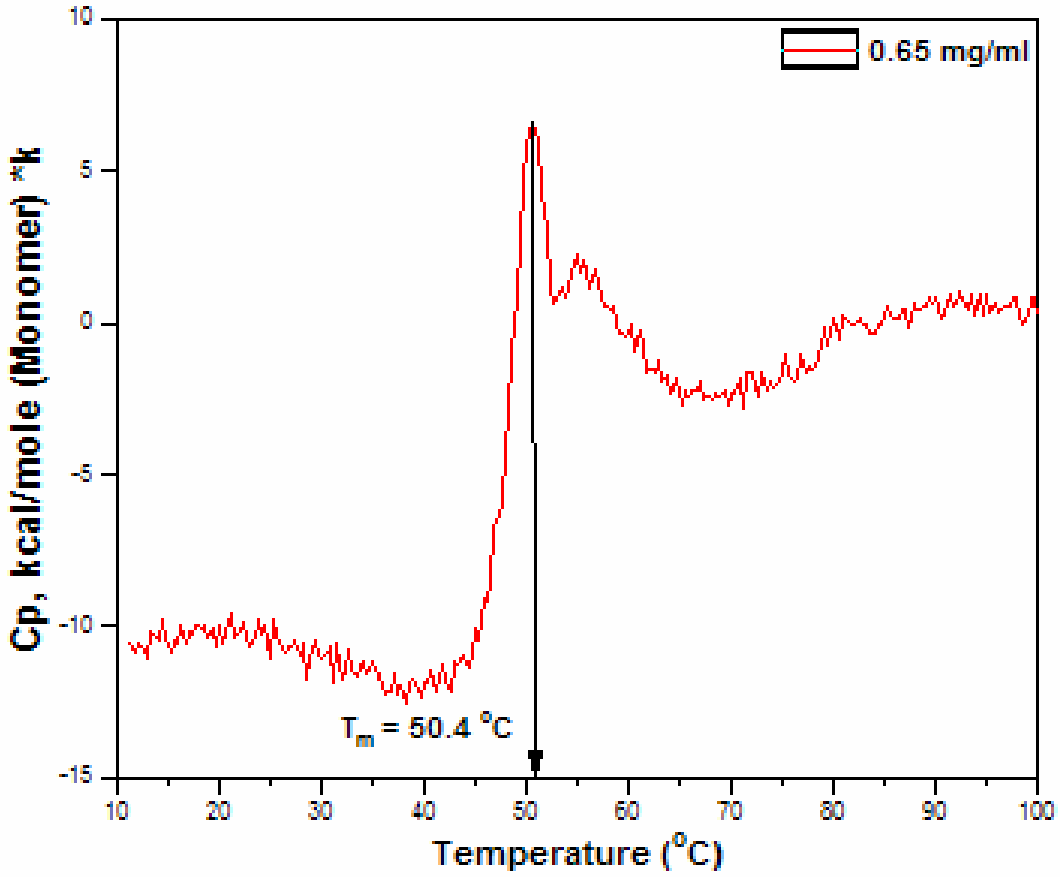

Figure 4.48 Thermal denaturation of EcA2(W66Y/Y181W) monitored by DSC.

EcA2(W66Y/Y181W)

With double mutant EcA2(W66Y/Y181W) and direct heating from 10 to 80 °C, a double peak endotherm was observed (Figure 4.48). The first peak had T_m at 50.4 °C, while the second was centered at 55 °C. Similar to other EcA2 proteins, no transitions were seen upon sample rescanning, indicating that unfolding was irreversible due to aggregation.

EcA2(Y176S)

With EcA2(Y176S) at concentrations of 0.15–2.4 mg/ml, the thermal transition recorded at a heating rate of 90 °C/h was resolved into three peaks (Figure 4.49). The T_m of the 1st peak was ~51 °C, which remained constant over the protein concentrations range

tested. The second peak shows variable amplitude and peak temperatures (from 56-52 °C) for different protein concentrations. An additional high-temperature peak was observed at the highest protein concentration of 1.2 mg/ml (Figure 4.49, blue curve), apparently resulting from aggregation of thermally denatured protein. At protein concentrations above 1.2 mg/ml, this additional peak broadened and shifted to lower temperatures (Figure 4.49, blue, magenta and dark yellow). High-temperature protein aggregation precludes accurate determination of ΔCp in this and other DSC data.

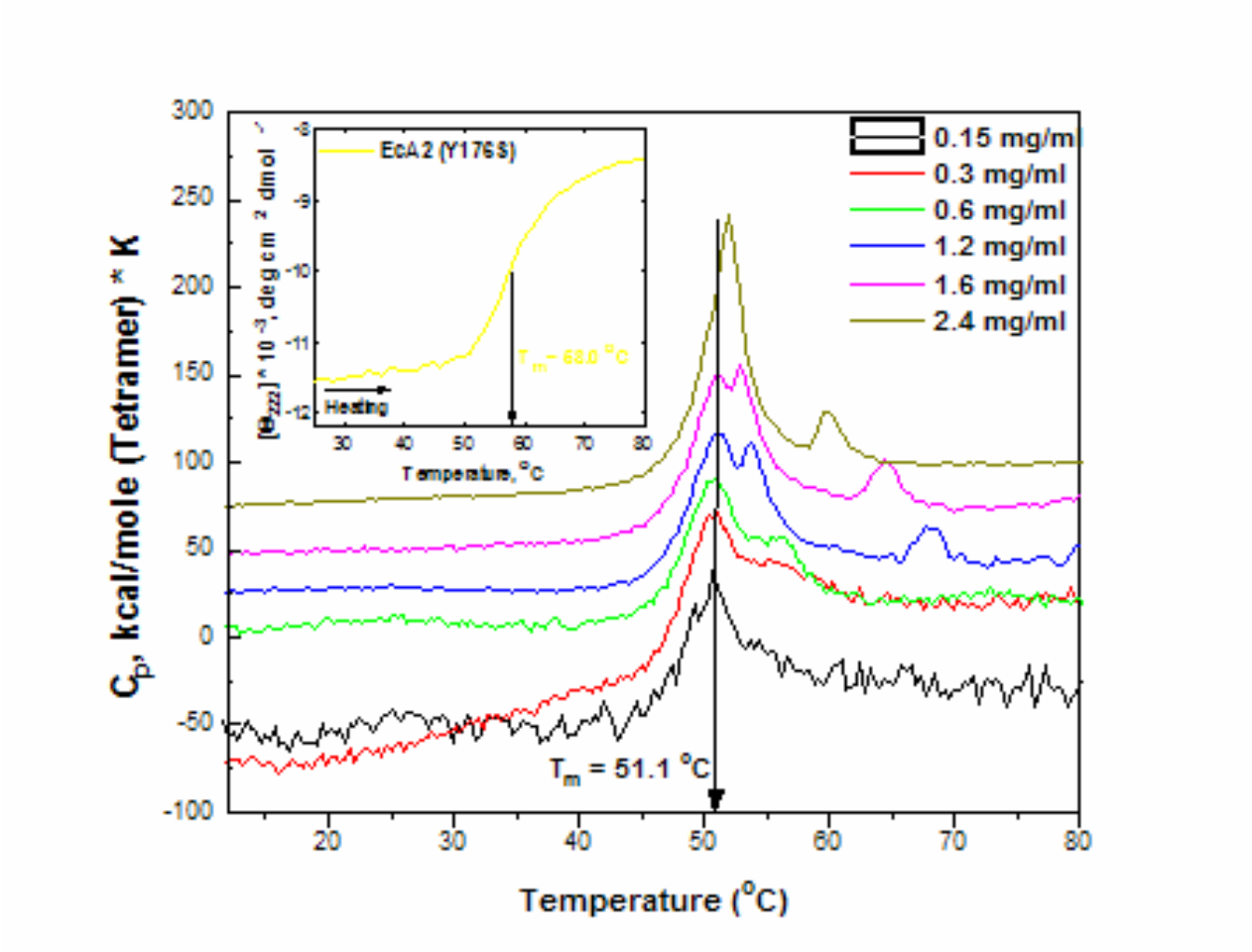

Figure 4.49 Thermal denaturation of EcA2(Y176S) monitored by DSC at different protein concentrations at pH 8.0. All curves are shifted along the Y axis to avoid overlaps. **Inset:** Melting of the α-helical structure of EcA2(Y176S) measured by the intensity of the 222-nm CD band.

To monitor the heat-induced changes in particle size, we utilized dynode voltage *V(T)* measurement in the near-UV CD experiment as outlined in Material and Methods (Section 3.20.1). The heating rate (80 °C/h) used for these CD experiments closely resembles that

used in the DSC experiments, thereby facilitating the direct correlation of the $C_p(T)$ and $V(T)$ data. The dynode voltage $V(T)$ recorded upon heating at 80 °C/h from 20 to 80 °C remained constant up to 52 °C but showed a large increase from 53 to 57 °C followed by a plateau (Figure 4.36, yellow). This heat-induced increase in turbidity could not be reversed upon cooling, suggesting that it reflects an irreversible increase in the particle size due to protein aggregation.

The irreversible increase in turbidity occured in the same temperature range as the second calorimetric transition. Consequently, the second calorimetric transition is accompanied by an irreversible aggregation. Thus, the correlation of the DSC and dynode data suggests that the first concentration-independent calorimetric peak may involve protein unfolding, while the second concentration-dependent peak involves aggregation. However, correlation with the far-UV CD melting curve (T_m~57 ^oC) recorded upon heating of EcA2(Y176S) at similar heating rate (inset, Figure 4.49) indicates that the first peak is not accompanied by any large cooperative α-helical unfolding. We conclude that

(i) the first DSC peak, which does not involve substantial secondary structure unfolding and thus remains "silent" in far-UV CD, apparently corresponds to the onset of the protein unfolding

(ii) the gradual heat-induced reduction in the protein α-helical content observed at high temperatures reflects complete unfolding of aggregated protein that is irreversible upon cooling.

EcA2(D188N)

The thermal transition of variant EcA2(D188N) was resolved into two peaks (Figure 4.51). The position of the first peak at T_m ~51.7 ^oC remained constant over the protein concentration range tested. The second peak showed variable amplitude and T_m (from 56-52 ^oC) for different protein concentrations, and thus is probably related to aggregation. Correlation of these data with the far-UV CD melting curve (T_m~58.5) recorded upon heating of EcA2(D188N) (inset, Figure 4.50) shows that the first peak corresponds to the onset of the unfolding transition and is not accompanied by any large cooperative α-helical unfolding, and the second DSC peak corresponds to protein unfolding and aggregation observed by CD in the same temperature range. Thus, similar to EcA2(Y176S), EcA2(D188N) appears to be

highly prone to aggregation that occurs shortly after the onset of the unfolding transition and does not require substantial protein unfolding.

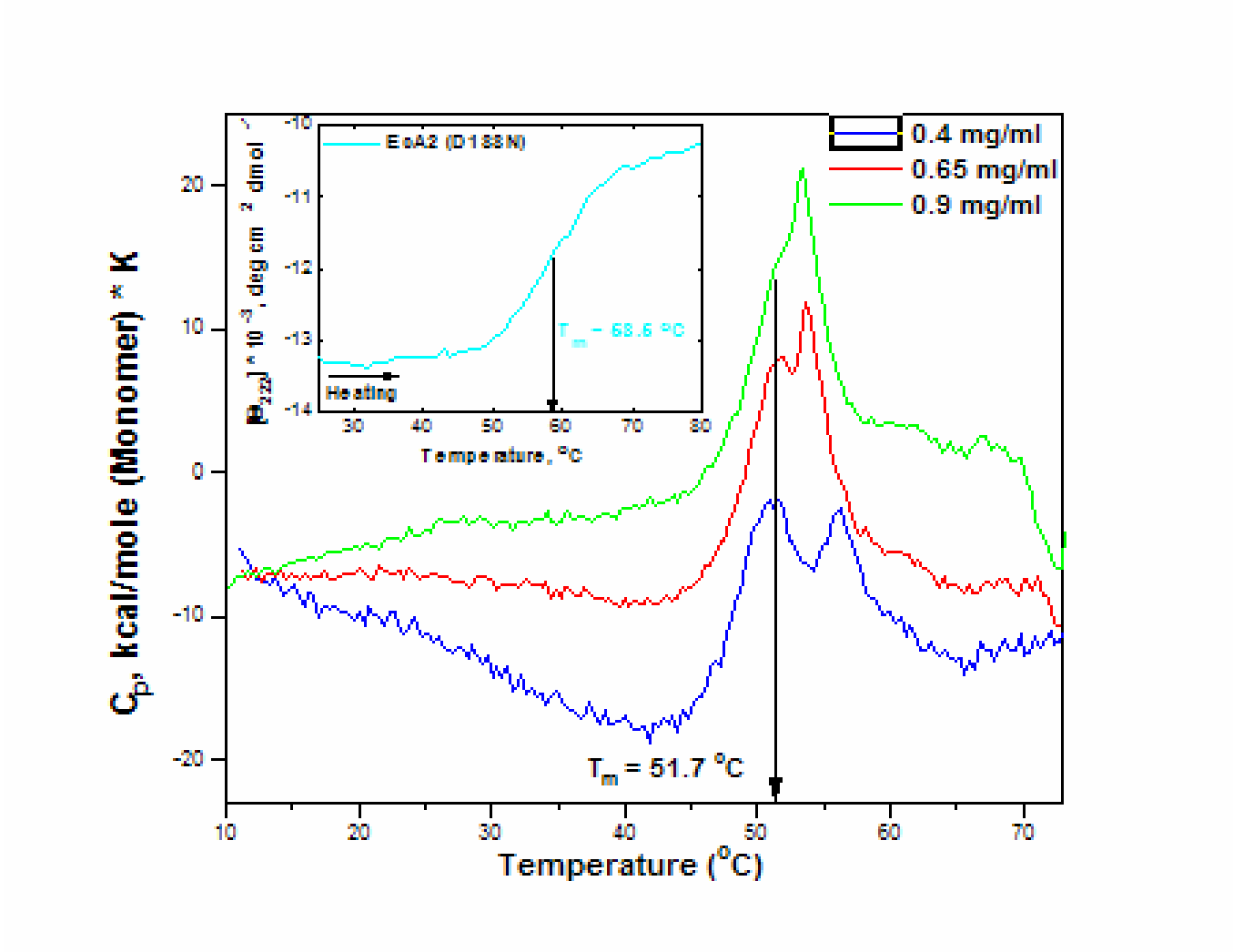

Figure: 4.50 Thermal denaturation of EcA2(D188N) monitored by DSC at different protein concentrations, pH 8.0. All curves are shifted along the Y axis to avoid overlaps. **Inset:** Melting of the α-helical structure of EcA2(D188N) measured by the intensity of the 222-nm CD band.

EcA2(D156N)

Mutant EcA2(D156N) also exhibited two DSC peak (Figure 4.51). The T_m of the first one was ~52.4 ^{o}C, which remained constant over the whole protein concentration range tested. The second peak showed variable amplitude and peak temperatures (from 56-52 ^{o}C) for different protein concentrations. Correlation of these data with the far-UV CD melting curve (T_m~57.7) recorded upon heating of EcA2(D156N) (inset, Figure 4.51) showed that the

first peak is not associated with any large cooperative α-helical unfolding. Thus, similar to EcA2(Y176S) and EcA2(D188N), the first calorimetric peak in EcA2(D156N) appears to correspond to the onset of the protein unfolding, and the second DSC peak reflects aggregation of the unfolded protein.

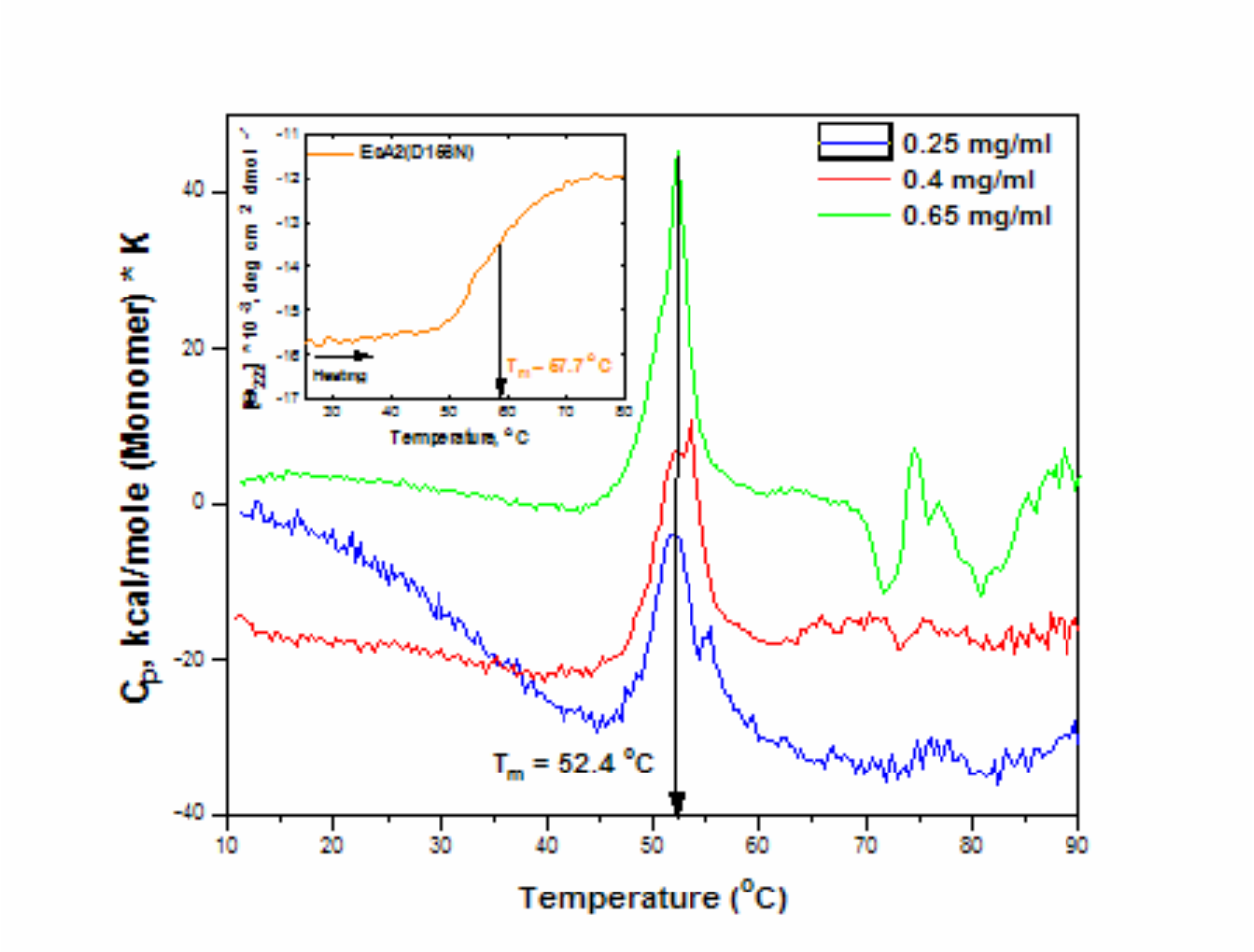

Figure 4.51 Thermal denaturation of EcA2(D156N) monitored by DSC at different protein concentrations, pH 8.0. All curves are shifted along the Y axis to avoid overlaps.
Inset: Melting of the α-helical structure of EcA2(D156N) measured by the intensity of the 222-nm CD band.

Figure 4.52 shows the calorimetric enthalpy (per monomer) of the thermal unfolding of EcA2(WT) and selected mutants as a function of the apparent melting temperature T_m measured by DSC. This dependence was nearly linear and had a positive slope, indicating that the mutation-induced changes in the protein thermal stability (as assessed by increase in Tm) had enthalpic origin (as assessed by ΔH_{cal}). Thus, the mutations affect the interatomic interactions in the folded state and hence protein stability. Assuming

that the mutations cause minimal effects on the burial of the hydrophobic residues in the folded state (and thus on ΔCp), the slope of the plot ΔHcal/(Tm) provides an estimate of the ΔCp of EcA2. This estimate, ΔCp~4.2 kcal/mol K, is in good agreement with the heat capacity increment estimated from the pH-dependence of the apparent T_m and ΔH_{cal} of EcA2(WT) (Figure 4.41) confirming the validity of our approach.

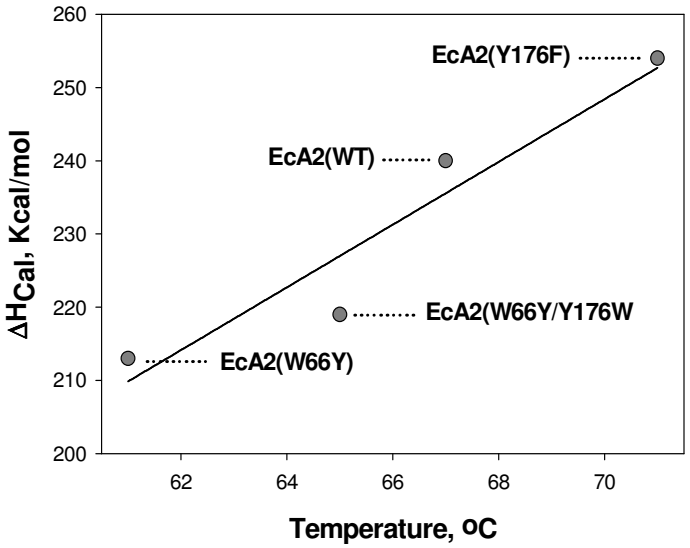

Figure 4.52 Enthalpies of EcA2(WT) and its mutant obtained by DSC plotted against the temperature of denaturation. The slope of the least-squares line indicates the change in heat capacity associated with denaturation, ΔC_p = 4.2±2 kcal mol^{-1} K^{-1}.

The apparent thermodynamic parameters of EcA2(WT) and its mutants monitored by activity, CD, and DSC are summarized in table 4.11.

Mutants	T_m (^oC) determined by activity (v~60 ^oC/h)	T_m (^oC) determined by CD (v~80 ^oC/h)	T_m (^oC) determined by DSC (v~90 ^oC/h)	ΔH_{Cal} (kcal/mol) per monomer determined by DSC (v~90 ^oC/h)
EcA2(WT)	64.5 ^oC	67.0 ^oC	66.0 ^oC	240
EcA2(W66Y)	--	61.0 ^oC	61.0 ^oC	213
EcA2(W66Y/ Y181W)	39 ^oC	--	1st peak - 50.4 ^oC), 2nd peak - T_m is conc. dependent	--
EcA2(W66Y/ Y176W)	--	65.0 ^oC	65.0 ^oC	219
EcA2(Y176F)	--	71.0 ^oC	71.0 ^oC	254
EcA2(Y176S)	47 ^oC	57.0 ^oC	1st peak - 51.1 ^oC, 2nd peak - T_m is conc. dependent	--
EcA2(D188N)	50 ^oC	58.5 ^oC	1st peak 51.7 ^oC, 2nd peak - Tm is conc. dependent	--
EcA2(D156N)	--	57.7 ^oC	1st peak - 52.4 ^oC, 2nd peak - T_m is conc. dependent	--

Table 4.11 Apparent thermodynamic parameters for the thermal denaturation of EcA2(WT) & its mutants monitored by activity, CD, and DSC.

5. Discussion

Subunit interactions within proteins are central to enzyme catalysis and enzyme regulation. Most enzymes are oligomers and may consist of an equilibrium mixture of various molecular forms which is modulated by ligands and other factors. Association-dissociation processes as well as conformational changes at subunit-subunit interfaces constitute most efficient mechanisms for allosteric control. Thus, an important goal of modern enzymology is to understand the role of subunit interactions in more detail in oligomeric enzymes (Jaenicke, 1987; Jameson and Seifried, 1999; Jaenicke and Lillie, 2000). Today, site-directed mutagenesis has become a standard technique in many laboratories, and recent advances in the spectroscopic and thermodynamic methods greatly facilitate the analysis of mutant proteins.

The aim of the present study was to analyze the molecular basis of the interactions between the subunits of *E. coli* asparaginase II (EcA2). As the clinical use of EcA2 is limited by the low stability of the enzyme in the systemic circulation, this matter is not only interesting for scientific reasons but also a better understanding of the subunit interactions in EcA2 might provide a basis for the construction of enzyme variants with increased stability and thus a extended lifetime in the patient's bloodstream.

5.1 Experimental approach

In the first part of this work, we collected data on the stability of wild type EcA2 using both chemical and thermal denaturation methods. In addition to fluorescence emission intensity (the only indicator of conformation used in previous experiments), we also employed enzyme activity, fluorescence emission spectra, circular dichroism (CD) and differential scanning calorimetry (DSC) as conformational probes. In addition, we examined the enzyme's quaternary structure at different denaturant concentrations using size exclusion chromatography (SEC).

We then analyzed the stability of number of mutants with amino acid replacements at the dimer-dimer interface. Here, we concentrated on residues at the A/D (or B/C) interface, since some information on the role of residues at the A/B interface was already available (see Introduction).

5.1.1 Spectroscopic properties of EcA2

EcA2 is readily amenable to spectroscopic studies using tryptophan fluorescence as the probe. Wild-type EcA2 contains eleven tyrosines, three histidines, and a single tryptophan residue (W66) per monomer. This single tryptophan greatly facilitates the interpretation of fluorescence data. Its unusually short wavelength of maximum emission (318-320 nm) may be attributed to the low polarity in the environment of this residue (Shifrin *et al.,* 1971). Shifrin *et al*. were the first to describe a red shift of fluorescence emission upon urea-induced denaturation of the EcA2 tetramer (Shifrin *et al.,* 1971). In 1974, these authors further reported that the refolding of the monomer is complete within seconds, whereas the reaggregation of the subunits into the active tetramer is much slower (Shifrin *et al.,* 1974). However, in Shifrin's experiments with urea no intermediate states of folding were detected except tetramers and monomers.

Later, equilibrium denaturation experiments with guanidine hydrochloride (Gu.HCl) carried out in our laboratory demonstrated that some EcA2 mutants [e.g., EcA2(H87A), EcA2(H183L), EcA2(Y181S)] may show complex denaturation profiles that indicate the occurrence of intermediates of dissociation and/or unfolding (Derst *et al.,* 1994). In one extreme case, EcA2(D124A), it was established by sedimentation equilibrium ultracentrifugation that even in the absence of denaturant a large fraction of this variant dissociated into dimers and monomers (Schubert *et al.,* 1996). However, the EcA2 mutants used in these early experiments had been constructed to identify catalytically important residues and no systematic attempt was made to relate these data to tetramer stabilization

Tryptophan W66 is located in a microenvironment that responds to changes in the active-site region in a very sensitive manner. This fact has not only be utilized to monitor denaturation and refolding but also used in a number of other ways, e.g., to study ligand binding to EcA2 (Harms *et al.,* 1991), to estimate the pK_a of the nearby residue H87 (Wehner *et al.,* 1992, Homer *et al.,* 1972), or to follow the movement of a flexible loop that closes the active site during catalysis (Aung *et al.,* 2000).

5.1.2 Equilibrium denaturation

Equilibrium denaturation studies are very useful to explore the structure, stabilization, and folding of small, monomeric proteins (Tanford, 1968; Pace, 1986, 1990; Timasheff,

1992). The methods for analyzing the energetics of reversible unfolding of proteins by thermal or chemical denaturant techniques (Privalov, 1979; Pace, 1986; Privalov & Gill, 1988) and the conclusions that can be drawn from thorough analysis of a few model proteins (Pace, 1986, 1990; Pace *et al.,* 1990) have been reviewed.

The range of stabilities calculated for monomers is between 6 and 14 kcal/mol (25 -70 kJ/mol) and represents the small difference between multiple non-covalent interactions favoring the folded protein structure and unfavorable entropic terms. Such studies have been particularly useful for analysis of packing forces in protein interiors (Alber & Matthews, 1987; Matsumura *et al.,* 1988), the testing of the globular folding of mutant proteins (Fersht *et al.,* 1992), and the functional interaction of residues (Carter *et al.,* 1984). However, application of similar techniques to oligomeric proteins has, until recently, been less common, despite the potential for providing additional information on subunit interactions. Classically, the kinetics of folding pathways have been used to determine the relationship of folding to activity of oligomeric proteins and to obtain information on the folding process itself (Jaenicke, 1987; Garel, 1992; Price, 1992). On the other hand, the inherent thermodynamics of conformational stability of these oligomeric proteins can be deduced from equilibrium denaturation studies.

In the present study, we induced denaturation of EcA2 by guanidine hydrochloride (Gu.HCl) and routinely followed the process by measuring the fluorescence of W66. In many cases, the effects of the denaturant on secondary structure were also monitored by CD spectroscopy. The denaturation curves for the mutants described here followed a two-state, three-state or even four-state mechanism of denaturation. Equilibrium constants K_D and the corresponding free enthalpies of folding in the absence of denaturant ΔG_{H2O}, were obtained by direct fits of appropriate model equations to the denaturation curves. As an additional parameter, constant m was derived from the curves which depends on the change in exposure to solvent of functional groups when the protein unfolds (Pace, 1986).

5.1.3 Thermal denaturation

Thermal denaturation is another approach to characterize the stability of a protein. The method used here (i.e. monitoring activity while slowly heating enzyme solutions) provides results that cannot be directly compared to the results of chemical denaturation,

because activity may already be lost due to a local conformational change in the active site while the proteins as a whole is still folded. Still, the mid-denaturation temperature T_m (the temperature at the inflection point of the activity vs. T profile) is useful to compare the stabilities of different enzyme forms.

By contrast, thermal denaturation monitored by CD can provide useful information on the temperature range where gross changes in secondary structure occur. Still more valuable are calorimetric techniques i.e. differential scanning calorimetry (DSC) that - at least in favorable cases - provide true thermodynamic parameters related to protein stability.

5.2 Expression and purification of EcA2 mutants

The mutant used in this work were expressed and purified by a standard protocol developed by Harms *et al*. (1991). The liberation of the periplasmic enzymes by osmotic shock is a purification step with a rather selective character. In this way, the periplasmic EcA2 is separated from most cellular protein in a very simple manner. Another important step is chromatofocusing in the pH range 6 - 4.5, where EcA2 is unusually stable while most other enzymes are denatured. The purified EcA2 forms were at least 95 % pure as judged from the elution profiles and SDS gels. For mutants with low activity, re-chromatofocusing was very important to remove traces of asparaginase activity following the main peak. The nature of this additional active species is still not clear. It could be due to small amounts of contaminating wild type enzyme or due to traces of asparaginase isozyme I which should be present in the BL21Ω host cells.

5.3 Dissociation and unfolding of wild-type EcA2

5.3.1 Denaturation profiles

The Gu.HCl-induced unfolding transitions when monitored by activity and fluorescence intensity (cf. Figure 4.5) indicate that denaturation of EcA2 (WT) is not a one-step process, i.e. the profiles indicate the existence of at least one intermediate form at Gu.HCl concentrations between 0.6 and 0.9 M. This putative intermediate is detectable in the profiles obtained from fluorescence intensity and activity measurements but not seen in the profiles of λ_{max} and CD vs. Gu.HCl concentration indicating that this EcA2 form (or forms)

is (are) largely folded and active. This suggests that the intermediates might be "intimate" dimers (A/C and B/D, respectively) whereas folded monomers are unlikely to retain activity since the active sites are disrupted when monomers form (see below).

As already mentioned, the shifts of the CD and λ_{max} profiles to higher Gu.HCl concentrations (cf. Figure 4.5 B) are expected, since in both spectroscopic techniques the native state yields a much higher signal than the denatured one and thus dominates the combined signal of both states (Eftink, 1998). When the fraction of denatured state (F_{app}) is estimated from linear combinations of spectra that represent the fully native and fully denatured states, the CD and λ_{max} profiles coincide with those obtained from F_{max} and activity (not shown).

5.3.2 Sedimentation and gel filtration data

The results of our sedimentation equilibrium centrifugation experiments (Figure 4.9) also suggest that the EcA2 tetramer largely dissociates into smaller fragments before unfolding occurs. When considering figure 4.9 it has to be taken into account, however, that the method employed is a much simplified form of the sedimentation equilibrium technique (see 3.19). The apparent molecular mass calculated from these data, therefore, does not necessarily reflect the size distribution of the EcA2 fragments in an accurate manner.

At first sight, the results of our gel filtration experiments with wild type EcA2 (Figure 4.23) seem to be inconsistent with the sedimentation equilibrium centrifugation data. As judged from their elution volumes, the peaks seen at Gu.HCl concentrations of 0.6 M and 0.8 M seem to be dimers, while no protein was detected at the position where native monomers should have appeared ($V_e \approx 15.5$ ml). The gradual shift of the peaks eluted at 1.0 and 1.2 M Gu.HCl to lower elution volume and their considerable broadening is also unexpected and needs explanation.

The observed pattern probably results from two effects. First, it was shown in several cases that with increasing denaturant concentrations the volume of denatured proteins also considerably increases. This expansion leads to a higher Stokes radius and thus to a lower elution volume in gel filtration experiments although the molecular mass of the protein does not change (Winzor, 2003). So, for instance, Gualfetti *et al*. (1999) found that the Stokes radius of the monomeric tryptophan synthase α-subunit increased by about 50% between

0 M and 8 M urea, leading to a several-fold increase in apparent molecular weight. Similar findings were reported by Lee *et al.* (2003) for the Gu.HCl induced denaturation of δ-crystallin and by Alcaraz *et al.* (2004) for rusticyanin and by McDuff *et al.* (2004) for α-urease.

Denaturants like Gu.HCl also can induce protein aggregation. This was for instance shown for lactate dehydrogenase from *B. megaterium* (Kotik *et al.,* 1993) and for other proteins as well. The formation of protein aggregates not only leads to an increase of the apparent mass but also to a characteristic broadening and tailing of the peaks eluted from gel filtration columns (Winzor, 2004).

Thus, we assume that at intermediate Gu.HCl concentrations wild type EcA2 dissociates into monomers that appear at unusually low elution volumes due to expansion and aggregate when fully denatured at 1 M Gu.HCl and above. Indeed, Kendrick *et al.* (1998) working with interferon-γ showed that Gu.HCl-induced expansion of the protein surface was a prerequisite for aggregation. Our thermal denaturation data confirm that fully denatured EcA2 subunits readily aggregate (see below).

This fact would also explain our finding that the position of the denaturation profiles of EcA2 (i.e. the Gu.HCl concentration at half denaturation)) does not depend on protein concentration as would be expected for a simple T ↔ 4 M equilibrium (cf. Figure 4.8). It also means, however, that the $\Delta G(H_2O)$ values calculated from the profiles must not be considered as true thermodynamic parameters, since the denaturation process is not fully reversible.

5.3.3 Thermal denaturation

Denaturation of wild-type EcA2 was followed by three different methods, i.e. loss of activity, CD spectroscopy, and by heat generation measured by DSC. All of these approaches yielded comparable values for the temperature of half-denaturation (T_m) between 63 and 67 °C (Figure 4.29, 4.33, and 4.37, Table 4.11). This indicates an "all-or-none" behavior, i.e. both activity and secondary structure were lost concomitantly in a narrow temperature range of about 5 °C. Several observations show that heat denaturation of EcA2(WT) is not an equilibrium process: The value of T_m depended on the heating rate, a sharp increase of the dynode voltage of the CD spectrometer indicated that a part of the denatured protein

immediately aggregated (Figure 4.36) and the melting curves exhibited hysteresis at any of the scan rates used.

Interestingly, a set of CD spectra recorded at constant temperatures around T_m exhibited a distinct isochromatic point at about 209 nm (Figure 4.32). This strongly suggests that in thermal denaturation only two EcA2 conformations were distinguished by CD spectroscopy, the native one with characteristic minima at 222 and 208 nm and a fully denatured species with a minimum at 201 nm. If there were any intermediates during heating their secondary structures would not significantly deviate from those of the native or the unfolded form. The single symmetric peak seen in DSC experiments (Figure 4.37) is also consistent with the absence of significantly populated intermediate states.

Although the irreversibility of the thermal melting process does not allow a rigorous thermodynamic analysis, some interesting semi-quantitative estimates could be obtained. So, the cooperative unit of unfolding seems to be the EcA2 monomer. The enthalpy change associated with the unfolding of this unit, ΔH, is about 250 kcal/mol (Figure 4.38), and the difference of the heat capacities of unfolded and native state (the heat capacity increment ΔC_p) is about 5 kcal/(mol·K) as estimated by two different methods (cf. Figs. 4.40 and 4.52).

5.3.4 pH-dependence of EcA2(WT) stability

Although there is no significant change in the secondary structure distribution of wild-type EcA2 between pH 5 and pH 8 (see Figure 4.35) both chemical and thermal denaturation data indicate that the overall stability of the enzyme is almost constnt in that range with a slight increase of T_m and ΔH_{cal} with increasing pH (Table 4.10). By contrast, a rapid loss in stability sets in below pH 5, possibly brought about by the protonation of aspartate and glutamate residues that contribute to the stabilization of the native conformation. The DSC data further suggest that the increase in protein stability upon increase in pH from 5 to 8 is mainly enthalpy-driven (Figure 4.41). The observed change of ΔH_{cal} may reflect deprotonation of residue H183 which has a pK_a of about 6.5 and is known to affect EcA2 stability (Wehner *et al.,* 1992).

5.4 Dissociation and unfolding of EcA2(W66Y)

The removal of W66, the main probe for fluorimetric measurement with wild type EcA2, leaves only the 11 tyrosine residues as fluorescent entities. As a probe for unfolding studies their cumulated fluorescence at 305 nm (cf. Figure 4.12) is as suitable as that of W66. In Gu.HCl-induced denaturation, EcA2 (W66Y) turned out to be slightly less stable than wild-type enzyme with a half denaturation point $[D]_{50\%}$ at 0.69 M Gu.HCl. at pH 8.0. Probably due to the large number of emitting residues which are distributed all over the structure, the denaturation profile was strictly symmetrical without any indication of an intermediate.

The behavior of EcA2(W66Y) in analytical gel filtration experiment were similar to that of wild-type enzyme (Figure 4.24). The results of thermal denaturation as monitored by CD and DSC yielded a slightly lower T_m of about 61 ^oC as compared to EcA2 (WT). However, the CD spectra of EcA2(W66Y) and EcA2(WT) were indistinguishable (Figure 4.31) and both the fluorescence emission and the ellipticity of the mutant protein were strictly proportional to its concentration in the range between 50 µg/ml and 1000 µg/ml, indicating that EcA2(W66Y) is stable down to low protein concentrations. Taken together, these findings suggest that the amino acid replacement W66→Y does not significantly affect the native tetrameric structure of EcA2. This is important as variant EcA2(W66Y) was used to construct double mutants in which tryptophan residues were introduced into positions 176 or 181 to serve as selective spectroscopic probes of dissociation-association phenomena affecting dimer-dimer contacts (see below).

5.5 The dimer-dimer interface

As already discussed in the introduction, EcA2 - although a homotetramer - should be regarded as a dimer of equivalent dimers. "Intimate" pairs are formed by subunits A and D or B and C, respectively. In the tetramer, the "intimate" dimers have two areas of contact that mainly involve residues 115-125 and 175-195, respectively. The number of direct interactions between the dimers is limited, whereas the subunits forming intimate pairs have more extended areas of contact. A comparison of the intimate pair BD and the loose pair AD is shown in Figure 5.1. From these relationships one would predict that during thermal or

chemical denaturation the EcA2 tetramer should first break up into the dimers AC and BD before these fragments dissociate to form monomers.

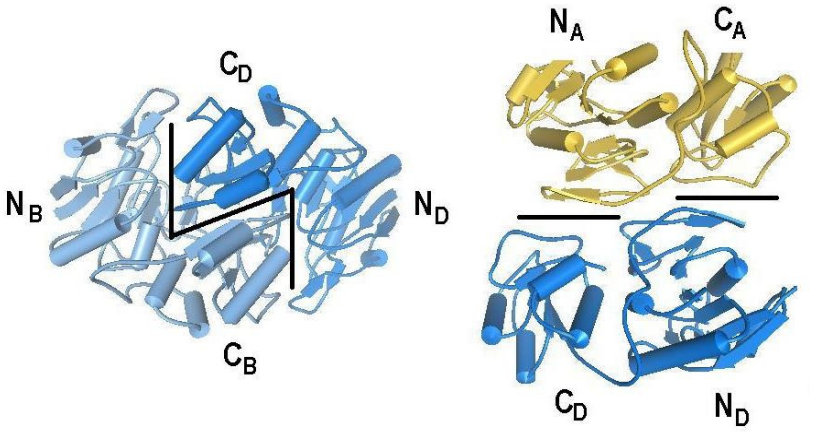

Figure 5.1 Interface regions of „intimate“ dimer (BD) compared with those of “loose” dimer (AD).

Contact sites are marked by black bars.

In the present work, we concentrated on the roles of individual amino acids at the dimer-dimer interface that connects A with D (or B with C). Figure 5.2 illustrates important interactions at the AD contact site in a highly schematic way.

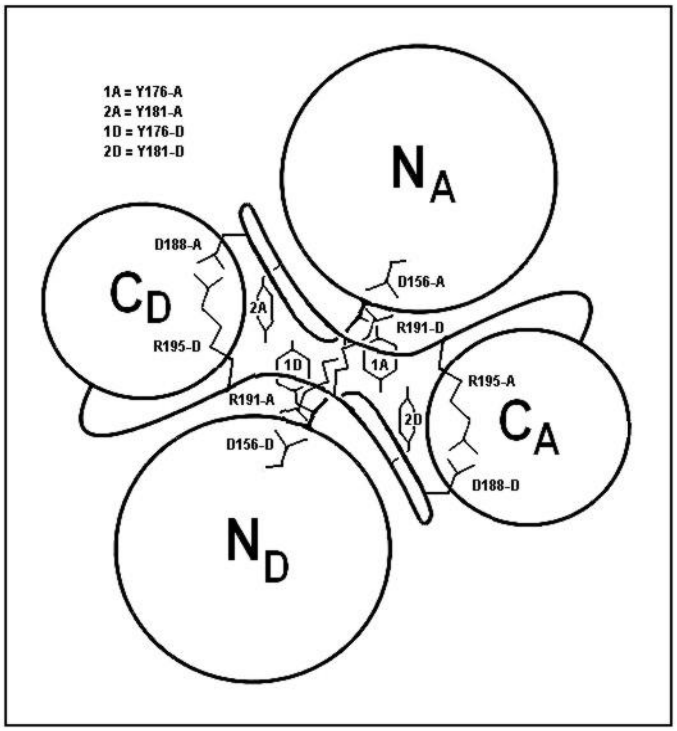

Figure 5.2 Stabilizing amino acid residues at the AD interface of EcA2(WT)

N_X = N-terminal domain of subunit X
C_X = C-terminal domain of subunit X

This interface area shows rotational symmetry and is largely made up by residues 175 - 195 of each monomer. They form hairpin-shaped loops with partial β-sheet conformation that are located on the surface of the larger N-terminal domains (N_A and N_D, respectively) and make contact with each other and with the smaller C-terminal domains of the opposing subunits C_D or C_A. The most conspicuous residues in this part of the protein are neighboring pairs of tyrosine residues, each one consisting of Y176 of one subunit and Y181 of the other (see also Figure 1.8). As judged from the crystal structure of the EcA2 tetramer, four additional pairs of charged residues appear to form salt bridges between the subunits. In the center of the interface area, residue R191 of one subunit is bound to D156 of the opposing monomer, while two more pairs made up from R195 and D188, respectively, are found at the outer limits of the contact area. In addition to tyrosines 176 and 181 which were replaced with various other amino acids, residues 156 and 188 were exchanged for isosteric but uncharged asparagine residues to examine the role of the respective salt bridges in tetramer stabilization.

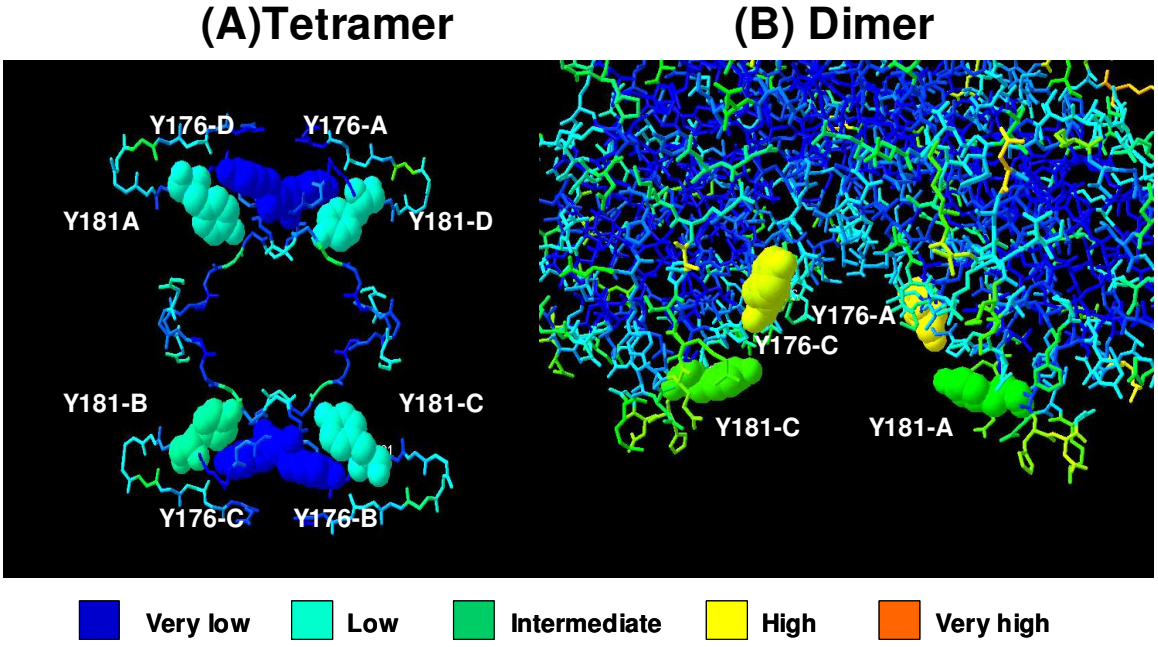

Figure 5.3 Solvent accessibility of tyrosine residues calculated from the crystal structure of EcA2 usinf DSSP.

Another factor with relevance for the interpretation of spectroscopic data is the accessibility of fluorophors in native, dissociated, and unfolded states of the protein. We, therefore

calculated the accessibility parameters of tyrosine Y176 and Y181 in the EcA2 tetramer and in the "intimate" dimers using DSSP (Kabsch and Sander, 1983). The results are presented in graphical form in Figure 5.3. Residue Y176 has very low accessibility in tetramer to become exposed to the solvent upon formation of intimate dimers. The accessibility of Y181 is low in the tetramer and somewhat higher in the dimer.

5.6 Role of Y176 and Y181 in tetramer stabilization

Several EcA2 variants afforded information on the role of Y176. EcA2(Y176S) and EcA2(Y176F) were thoroughly characterized in this study, while the properties of double mutant EcA2(W66Y/Y176W) have been described by Wendt (2002).

EcA2 (Y176S)

The replacement of Y176 with the much smaller serine resulted in a drastically decreased stability of the enzyme with the appearance of at least two intermediates. In contrast to the mutants described above, several parameters (activity, fluorescence and ellipticity) first increased with Gu.HCl concentrations between 0 and 0.2 M (Figure 4.14). Between 0.2 M and 0.6 M Gu.HCl enzymatic activity was lost while the spectroscopic parameters fell to 60-80% of their initial values. 1.2 M Gu.HCl was necessary for full denaturation.

The process taking place at low Gu.HCl concentration could be identified by means of analytical gel filtration: At 0.2 M Gu.HCl, only dimers were seen, while dimers and monomers were present at 0.4 M Gu.HCl (Figure 4.26). The elution volumes of these peaks were close to the expected values since the Gu.HCl concentrations required for dissociation were low enough not to cause significant expansion of the dissociated fragments (see above).

As already mentioned, at 0.2 M Gu.HCl the activity of EcA2(Y176S) was even higher than in the absence of denaturant indicating that the dimers formed were fully active "intimate" pairs which harbor two almost intact catalytic centers, while the active sites are disrupted in the loose pairs. The CD data are also consistent with dimer formation as no detectable loss of secondary structure took place below 0.4 M Gu.HCl (Figure 4.15).

The thermal melting curves of EcA2(Y176S) were characterized by a broad transition region covering more than 15 °C with a T_m of about 57 °C (Figure 4.34). Again, this is

consistent with the presence of unfolding intermediates (Figure 4.35). In DSC an complex pattern with three peaks was seen (Figure 4.49). The first one at 51 °C was independent of protein concentration and thus could be the result of a first-order process (e.g. dissociation of the tetramer into dimers or monomers), while the other two peaks were shifted to lower temperatures with increasing protein concentration. The assumption that the peak at 51 °C reflects dissociation rather than unfolding is also supported by melting experiments monitored by CD (Figure 4.49) which do not indicate significant loss of secondary structure below 55 °C. Taken together, these observations are consistent with the view that replacement of Y176 with a much smaller serine strongly impairs the subunit interactions at the AD interface leading to a spontaneous dissociation into dimers.

EcA2 (W66Y/Y176W)

A mutant with a single tyrptophan residues in position 176 - i.e. EcA2(W66Y/Y176W) -was constructed and analyzed by Wendt (2002) as an attempt to place a fluorescent residue at the dimer-dimer interface as a direct probe of the dissociation and association of the "intimate" dimers. This approach (i.e. the introduction of tryptophan residues as site-specific spectroscopic probes) has been successfully applied earlier, e.g., to monitor the loop movement in proteins (Atkinson *et al.,* 1988, Aung *et al.,* 2000)) or to characterize intermediates in protein folding pathways (Smit *et al.,* 1991).

Surprisingly, the fluorescence of W176 in EcA2(W66Y/Y176W) was not detectable in the folded protein, whereas spectra recorded at high Gu.HCl concentrations showed peaks typical of a tyrptophan residue in an aqueous environment. The absence of fluorescence in the native double mutant is probably due to strong quenching by neighboring residues. Especially acidic amino acids and their amides in the immediate vicinity can act as quenchers (Chen and Barkley, 1998). In fact, as illustrated by Figure 5.3, in the native state of EcA2 residue Y176 is surrounded by three such residues, i.e. D188, N175 and Q190.

As W176 in EcA2(W66Y/Y176W is spectroscopically "silent", Wendt (2002) used the combined tyrosine fluorescence at 305 nm to follow Gu.HCl-induced denaturation of this variant (cf. Figure 4.12). For the main unfolding step he found a $\Delta G(H_2O)$ of 56 kJ/mol, i.e. a value slightly higher than that obtained with wild-type EcA2. This suggests that W176 exerts the same stabilizing effect on the EcA2 tetramer as the native Y176. This notion is

fully supported by our DSC experiments which yielded a T_m of 65 °C for the double mutant (Figure 4.46) as compared to 67 °C for wild-type EcA2. An additional high-temperature DSC peak at ~72 °C at high protein concentrations probably resulted from aggregation of the thermally denatured protein.

EcA2 (Y176F)

Variant EcA2 (Y176F) was constructed to examine whether the phenolic hydroxyl group of Y176 is important for its stabilizing function. This appeared reasonable as in the wild-type tetramer a hydrogen bond connects this hydroxyl group with the backbone carbonyl group of the opposing D188 (see Figure 1.8). Surprisingly, the replacement did not impair stability but markedly increased it. The fluorescence spectrum of EcA2(Y176F) and its shift during denaturation were very similar to the situation with wild-type enzyme (Figure 4.10). The Gu.HCl-induced denaturation profiles also resembled those of EcA2(WT) but were shifted to higher Gu.HCl concentrations (1.2 M at pH 8.0), and a calculated $\Delta G(H_2O)$ of about 64 kJ/mol was markedly higher as well. In the gel filtration experiment no intermediates were observed. The results of thermal denaturation monitored by CD and DSC (Figs. 4.34 and 4.42) were in complete agreement with the chemical denaturation data, showing a higher T_m of 71 °C as compared to 65 °C for EcA2(WT). Thus, the hydroxyl group of Y176 is not only dispensable for tetramer stabilization, it even impairs the stability of the monomers.

An explanation for these findings is suggested by a closer look at the environment of Y176 in the EcA2 tetramer (Figure 5.4). The aromatic side chain of Y176 (here Y176-D is shown in blue) is located in a narrow cleft mainly formed by polar residues belonging to the "hairpin" of the opposing A-subunit (Y181-A, D188-A, Q190-A, and R191-A, yellow). The adjacent N175-D also contributes to the structure. Of course, exactly the same configuration of residues exists around Y176-A on the other side (not shown in Figure 5.4, see Figure 5.2). As the side chain of Y176 almost fills the cleft, it helps to lock the "hairpins" in the optimum position. Small side chains in position 176 like the hydroxymethyl group of a serine are unable to fill the cleft and thus cannot maintain the required local conformation. This weakens the subunit interactions at the AD and BC interfaces and promotes dissociation of the native tetramer into dimers AC and BD.

Our data further show that phenylalanine and tyrptophan - both aromatic residues of comparable size - can replace tyrosine at position 176. Why they also stabilize the EcA2 monomers against Gu.HCl-induced denaturation is difficult to explain on the basis of the available crystal structures. As shown in Figure 5.3, amino acid 176 is largely exposed to the solvent in dimers and monomers and thus should not significantly contribute to their stability. Probably the tertiary structure of isolated monomers differs from the conformation they adopt in the tetramer so that a less polar residues at position 176 can exert more favorable stabilizing interactions than a more polar tyrosine.

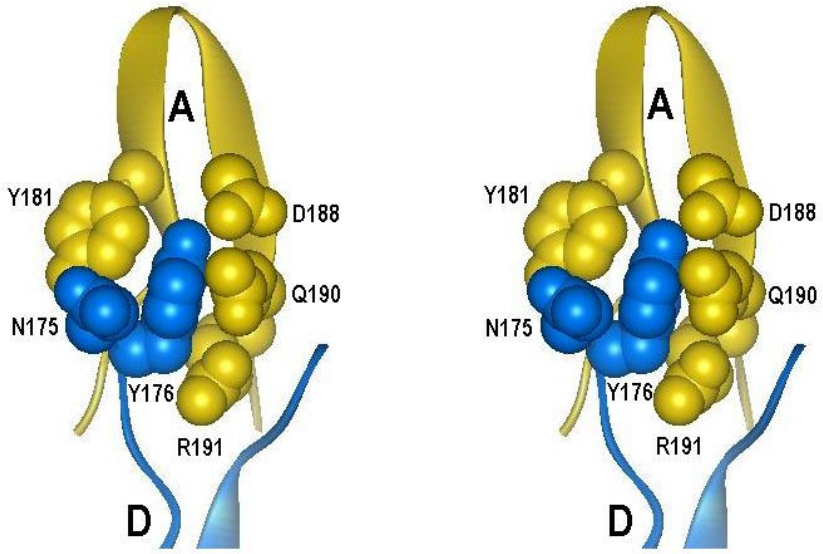

Figure 5.4 Environment of residue Y176 at the AD interface (stereo representation)

EcA2 (W66Y/Y181W)

Residue Y181 is not far from H183 which, in turn, is located at an interface where three subunits meet. As illustrated by Figure 5.3, Y181 almost touches Y176 on one side, whereas its other side is more easily accessible. Previous mutagenesis studies in our laboratory have shown that the mutation Y181F did not affect the stability of the enzyme, while - analogous to our results with Y176 - smaller and more polar side chains in this position labilize the entire structure. With both EcA2(Y181S) and EcA2(Y181C), the onset of denaturation was shifted to lower denaturant concentrations and both species exhibited complex denaturation curves with at least one intermediate (Derst *et al.,* 1994).

Adopting the same strategy as above, EcA2(W66Y) was used to construct double mutant EcA2(W66Y/Y181W) with a site-specific spectroscopic probe at the dimer-dimer interface. Again the resulting enzyme exhibited an unusual fluorescence emission spectrum with a maximum at 347 nm in the absence of denaturant. Addition of Gu.HCl did not cause a significant red shift, indicating that W181 remained in a distinctly polar environment irrespective of denaturant concentration applied (Figure 4.17). Fluorescence intensity, on the other hand, strongly varied with denaturant concentration, yielding denaturation profiles of very good quality. The profiles were complex but revealed at least two intermediates that were both stable within a range of 0.2 M Gu.HCl (Figure 4.17B). By gel filtration the intermediates were unequivocally identified as active dimers (i_1) which prevailed at 0.2 M Gu.HCl and folded monomers (i_2) at 0.4 M Gu.HCl (Figure 4.25). The fact that activity was totally lost during the transition from i_1 and i_2 (Figure 4.17B) again confirms that the EcA2 monomers are inactive even in the folded state.

Thermal denaturation of the mutant yielded a T_m of ~ 39 ^oC when monitored by activity. DSC, on the other hand, showed two peaks. The first one (at T_m~50.4) is probably related with the unfolding of the protein while the second one (at T_m~55.0) is due to the aggregation of the heat-denatured protein (Figure 4.48).

To summarize our data on the role of Y176 and Y181, it now seems established that at both positions aromatic residues are required to ensure sufficient stability of the EcA2 tetramer. The hydroxyl groups of either residue, on the other hand, are not essential. If the inter-subunit hydrogen bonds suggested by the crystal structure (Figure 1.8) really exist in solution, they do not appreciably contribute to the stability of the native enzyme.

5.7 Role of D156 and D188

EcA2 (D188N)

As already discussed in the introduction an electrostatic interaction connects D188(COO-) with R195(Gua+) at dimer–dimer interface (see also Figure 5.2). Replacement of D188 with an isosteric but uncharged asparagine resulted in destabilization of the tetrameric structure of the EcA2. Again, active dimers appeared as intermediates of denaturation (Figure 4.28). Similar to EcA2(Y176S) and EcA2(W66Y/Y181W), mutant EcA2(D188N) showed the presence of two intermediates with highly reduced stability. In

agreement with these data, thermal denaturation monitored by activity yielded a reduced T_m of ~ 50 ^oC. In DSC two endothermic peaks appeared. The first one at T_m~52 ^oC is probably related to the unfolding of the monomers while the second (T_m ~56-52 ^oC) indicates aggregation of the heat denatured protein. In summary, we conclude that the salt bridge between D188(COO-)---R195(Gua+) markedly contributes to the tetramer stability.

EcA2 (D156N)

Another electrostatic interaction at dimer–dimer interface involves D156(COO-) and R191(Gua+). The absence of this interaction in variant EcA2(D156N) had effects similar to those seen with EcA2(D188N): Chemical denaturation profiles indicated the presence of at least two intermediates (Figure 4.21), which were identified as dimers and monomers by analytical gel filtration (Figure 4.27). Thermal denaturation of EcA2 (D156N) monitored by activity showed a T_m at ~ 52.4 ^oC. As discussed above, the peaks seen in DSC probably reflect the unfolding process (at T_m ~ 51.7 °C) while the concentration-dependent signal at T_m~ 56-52 ^oC is caused by aggregation of the unfolded enzyme.

5.8 Interactions at dimer-dimer interfaces

From systematic surveys of subunit-subunit interfaces, some general rules on oligomer-stabilizing interactions have emerged Glaser *et al*. (2001) determined the residue-residue preferences in intermolecular interactions based on a large database of co-crystallized protein-protein interfaces. Their results revealed that the highest residue-residue preferences at the interface were for interactions between pairs of large hydrophobic residues, and the lowest preferences for interactions between pairs of small residues. Experimental studies by Vallone *et al.* have indicated that there is a correlation between the change in the free energy of association of the mutants and the change in buried hydrophobic surface area (Vallone *et al.,* 1998). Thus, the hydrophobicity of key residues at the subunit interface is expected to be the main driving force for protein-protein interactions.

Here, we show that some of the key interactions that stabilize the native EcA2 tetramer do not follow this rule. Although the interaction between Y181 and Y176 is predominantly hydrophobic in character, the cleft in which Y176 is inserted is mainly formed by polar side chains (see Figure 5.4). Moreover, as judged from our data the salt bridges

between D188 and R192 or D156 and R195, respectively, are at least as important in stabilizing EcA2 as the tyrosine-tyrosine interactions. In agreement with other studies, our results further demonstrate that point mutations at strategic positions can dramatically destabilize (or stabilize) large proteins. So, the removal of a single hydroxyl group per EcA2 monomer - as in EcA2(Y176F) - increased its stability against Gu.HCl-induced denaturation by 20 % and its melting temperature by 6 °C without affecting the catalytical properties of the enzyme. Thus it appears that biochemical evolution does not try to create proteins with the highest possible stability but prefers proteins that are flexible and just stable enough to fulfill their task in a natural environment. On the other hand, there are many applications of enzymes in biotechnology where maximum stability and resistance against denaturation are desirable. A better understanding of the factors that govern protein stability will help "protein engineers" to create enzyme variants with such properties.

Ackers GK. Analytical gel chromatography of proteins. Adv Protein Chem 1970;24:343-446.

Ackers GK. Molecular sieve studies of interacting protein systems. I. Equations for transport of associating systems. J Biol Chem 1967;242(13):3026-34.

Adler AJ, Greenfield NJ, Fasman GD. Circular dichroism and optical rotatory dispersion of proteins and polypeptides. Methods Enzymol 1973;27:675-735.

Alber T, Matthews BW. Structure and thermal stability of phage T4 lysozyme. Methods Enzymol 1987;154:511-33.

Alcaraz, L. A. and Donaire, A. Unfolding process of rusticyanin. Evidence of protein aggregation. 2004; 271: 4284–4292.

Aung HP, Bocola M, Schleper S, Rohm KH. Dynamics of a mobile loop at the active site of *Escherichia coli* asparaginase. Biochim Biophys Acta 2000;1481(2):349-59.

Bagert U, Rohm KH. On the role of histidine and tyrosine residues in *E. coli* asparaginase. Chemical modification and 1H-nuclear magnetic resonance studies. Biochim Biophys Acta 1989;999(1):36-41.

Bauer K. [On the biochemistry of asparginase]. Med Klin 1969;64(1):9-12.

Beumer-Jochmans MP. [The asparaginase activity and viability of BCG vaccines prepared under similar conditions but with different strains]. Ann Microbiol (Paris) 1973;124(2):289-92.

Biltonen RL, Freire E. Thermodynamic characterization of conformational states of biological macromolecules using differential scanning calorimetry. CRC Crit Rev Biochem 1978;5(2):85-124.

Biorad. Instruction manual for the Mini Protean cell™ 1987.

Blow DM, Birktoft JJ, Hartley BS. Role of a buried acid group in the mechanism of action of chymotrypsin. Nature 1969;221(178):337-40.

Bothwell MA, Howlett GJ, Schachman HK. A sedimentation equilibrium method for determining molecular weights of proteins with a tabletop high speed air turbine centrifuge. J Biol Chem 1978;253(7):2073-7.

Boyse EA, Old LJ, Campbell HA, Mashburn LT. Suppression of murine leukemias by L-asparaginase. Incidence of sensitivity among leukemias of various types: Comparative inhibitory activities of guinea pig serum L-asparaginase and *Escherichia coli* L-asparagianse. *J. Exp. Med.* 1967;125:17-31.

Bradford MM. A rapid and sensitive method for the quantitation of microgram quantities of protein utilizing the principle of protein-dye binding. Anal Biochem 1976;72:248-54.

Brand L, Witholt B. Methods Enzymol. 1967;11: 776-856.

Broome JD. Evidence that the L-asparaginase of guinea pig serum is responsible for its antilymphoma effects. II. Lymphoma 6C3HED cells cultured in a medium devoid of L-asparagine lose their susceptibility to the effects of guinea pig serum in vivo. J Exp Med 1963;118:121-48.

Campbell HA, Mashburn LT, Boyse EA, Old LJ. Two L-asparaginases from *Escherichia coli* B. Their separation, purification, and antitumor activity. Biochemistry 1967;6(3):721-30.

Capizzi RL. Asparaginase-methotrexate in combination chemotherapy: schedule-dependent differential effects on normal versus neoplastic cells. Cancer Treat Rep 1981;65(Suppl 4):115-21.

Carter PJ, Winter G, Wilkinson AJ, Fersht AR. The use of double mutants to detect structural changes in the active site of the tyrosyl-tRNA synthetase (*Bacillus stearothermophilus*). Cell 1984;38(3):835-40.

Cedar H, Schwartz JH. Localization of the two-L-asparaginases in anaerobically grown *Escherichia coli*. J Biol Chem 1967;242(16):3753-5.

Cedar H, Schwartz JH. Production of L-asparaginase II by *Escherichia coli*. J Bacteriol 1968;96(6):2043-8.

Chen, Y. and Barkley, M.D. Towards understanding tryptophan fluorescence in proteins. Biochemistry 1998;37: 9976-9982.

Chesney RH. *E. coli* L-asparaginase II production in the presence and absence of catabolic activating protein. FEMS Microbiol. Lett. 1983;17:161-162.

Clavell LA, Gelber RD, Cohen HJ, et al. Four-agent induction and intensive asparaginase therapy for treatment of childhood acute lymphoblastic leukemia. N Engl J Med 1986;315(11):657-63.

Clementi A. La desamidation enzymatique de l'asparagine chez les differentes especes anumales et la signification physiologique de sa presance dans l'organisme. Arch. Intern. Physiol. 1922;19:369-398.

Corbett RJ, Roche RS. Use of high-speed size-exclusion chromatography for the study of protein folding and stability. Biochemistry 1984;23(8):1888-94.

Dagert M, Ehrlich SD. Prolonged incubation in calcium chloride improves the competence of *Escherichia coli* cells. Gene 1979;6(1):23-8.

Daveis LC. J.Chromatogr. Sci. 1983;21:214-217.

de Crombrugghe B, Busby S, Buc H. Cyclic AMP receptor protein: role in transcription activation. Science 1984;224(4651):831-8.

Derst C, Henseling J, Rohm KH. Engineering the substrate specificity of *Escherichia coli* asparaginase. II. Selective reduction of glutaminase activity by amino acid replacements at position 248. Protein Sci 2000;9(10):2009-17.

Derst C, Henseling J, Rohm KH. Probing the role of threonine and serine residues of *E. coli* asparaginase II by site-specific mutagenesis. Protein Eng 1992;5(8):785-9.

Derst C, Wehner A, Specht V, Rohm KH. States and functions of tyrosine residues in *Escherichia coli* asparaginase II. Eur J Biochem 1994;224(2):533-40.

Derst, C. Ph.D. Thesis (Human Biology) Department of Medicine, Philipps University Marburg, 1995.

Ebright RH, Beckwith J. The catabolite gene activator protein (CAP) is not required for indole-3-acetic acid to activate transcription of the araBAD operon of *Escherichia coli* K-12. Mol Gen Genet 1985;201(1):51-5.

Eftink MR. The use of fluorescence methods to monitor unfolding transitions in proteins. Biochemistry (Mosc) 1998;63(3):276-84.

Fasman, D. G. Circular Dichroism and the Conformational Analysis of Biomolecules: New York: Plemum Press, 1996.

Fersht AR, Matouschek A, Serrano L. The folding of an enzyme. I. Theory of protein engineering analysis of stability and pathway of protein folding. J Mol Biol 1992;224(3):771-82.

Fraer DS, Burrell RC. Spectrophotometric method for determining hydroxylamine reductase activity in higher plants. Anal. Chem. 1955;27:1664-1665.

Freire E, Biltonen. RL. Statistical mechanical deconvolution of thermal transitions in macromolecules. I. Theory and application to homogenous systems. *Biopolms* 1978;17:463-479.

Freire E, Biltonen. RL. Statistical mechanical deconvolution of thermal transitions in macromolecules. 11. General treatment of cooperative phenomena. *Biopolymers* 1978;17:481-496.

Freire E, Biltonen. RL. Statistical mechanical deconvolution of thermal transitions in macromolecules. 111. Application to double-stranded to single-stranded transitions of nucleic acids. *Biopolymer* 1978;17:497-510.

Fukada H, Sturtevant JM, Quiocho FA. Thermodynamics of the binding of L-arabinose and of D-galactose to the L-arabinose-binding protein of *Escherichia coli*. J Biol Chem 1983;258(21):13193-8.

Garel JR. Folding of large proteins: Multidomain and multisubunit proteins. New York: Freeman, 1992.

Gralnik H, Henry P. L-Asparaginase induced coagulopathy. Proc Am Assoc Cancer Res 1969;10:32.

Greenquist AC, Wriston JC, Jr. Chemical evidence for identical subunits in L-asparaginase from *Escherichia coli* B. Arch Biochem Biophys 1972;152(1):280-6.

Gualfetti, P. J.; Iwakura, M.; Lee, J. C.; Kihara, H.; Bilsel, O.; Zitzewitz, J. A., and Matthews, C. R. Apparent radii of the native, stable intermediates and unfolded conformers of the α-subunit of tyryptophan synthase from *E. coli*, a TIM barrel protein. Biochemistry 1999;38:13367-13378.

Hanahan D, Meselson M. Plasmid screening at high colony density. Methods Enzymol 1983;100:333-42.

Harms E, Wehner A, Aung HP, Rohm KH. A catalytic role for threonine-12 of *E. coli* asparaginase II as established by site-directed mutagenesis. FEBS Lett 1991;285(1):55-8.

Harms E, Wehner A, Jennings MP, Pugh KJ, Beacham IR, Rohm KH. Construction of expression systems for *Escherichia coli* asparaginase II and two-step purification of the recombinant enzyme from periplasmic extracts. Protein Expr Purif 1991;2(2-3):144-50.

Harrison RW, Weber IT, Ammon HL, et al. Protein Structure, Folding and Design 1987;2:83-92 .

Haskell CM, Canellos GP, Leventhal BG, et al. L-asparaginase: therapeutic and toxic effects in patients with neoplastic disease. N Engl J Med 1969;281(19):1028-34.

Haskell CM, Canellos GP. l-asparaginase resistance in human leukemia--asparagine synthetase. Biochem Pharmacol 1969;18(10):2578-80.

Hill JM, Roberts J, Loeb E, Khan A, MacLellan A, Hill RW. L-asparaginase therapy for leukemia and other malignant neoplasms. Remission in human leukemia. Jama 1967;202(9):882-8.

Ho PP, Frank BH, Burck PJ. Crystalline L-asparaginase from *Escherichia coli* B. Science 1969;165(892):510-2.

Ho PP, Milikin EB. Multiple forms of L-asparaginase. Biochim Biophys Acta 1970;206(1):196-8.

Homer RB, Allsopp SR. An investigation of the electronic and steric environments of tyrosyl residues in ribonuclease A and Erwinia carotovora L-asparaginase through fluorescence quenching by caesium, iodide and phosphate ions. Biochim Biophys Acta 1976;434(2):297-310.

Homer RB. The pH dependence and quenching of the fluorescence of asparaginase from *Escherichia coli* B. Biochim Biophys Acta 1972;278(2):395-8.

Hortobagyi GN, Yap HY, Wiseman CL, et al. Chemoimmunotherapy for metastatic breast cancer with 5-fluorouracil, adriamycin, cyclophosphamide, methotrexate, L-asparaginase, Corynebacterium parvum, and Pseudomonas vaccine. Cancer Treat Rep 1980;64(1):157-9.

Jaenicke R, Lilie H. Folding and association of oligomeric and multimeric proteins. Adv Protein Chem 2000;53:329-401.

Jaenicke R. Folding and association of proteins. Prog Biophys Mol Biol 1987;49(2-3):117-237.

Jameson DM, Seifried SE. Quantification of protein-protein interactions using fluorescence polarization. Methods 1999;19(2):222-33.

Jayaraman PS, Peakman TC, Busby SJ, Quincey RV, Cole JA. Location and sequence of the promoter of the gene for the NADH-dependent nitrite reductase of *Escherichia coli* and its regulation by oxygen, the Fnr protein and nitrite. J Mol Biol 1987;196(4):781-8.

Jennings MP, Beacham IR. Analysis of the *Escherichia coli* gene encoding L-asparaginase II, ansB, and its regulation by cyclic AMP receptor and FNR proteins. J Bacteriol 1990;172(3):1491-8.

Jerlstrom PG, Bezjak DA, Jennings MP, Beacham IR. Structure and expression in *Escherichia coli* K-12 of the L-asparaginase I-encoding ansA gene and its flanking regions. Gene 1989;78(1):37-46.

Jerlström PG, Liy J, and Beacham IR. Regulation of *Escherichia coli* L-asparaginase II and L-aspartase by the fnr gene product. *FEMS Microbiol. Lett* 1987;41:127-130.

Kabsch, W. and Sander, C. Dictionary of protein secondary structure: pattern recognition of hydrogen-bonded and geometrical features. Biopolymers. 1983;22: 2577-637.

Kidd JG. Regression of transplanted lymphomas induced in vivo by means of normal guinea pig serum. II. Studies on the nature of the active serum constituent: histological mechanism of the regression: tests for effects of guinea pig serum on lymphoma cells in vitro: discussion. J Exp Med 1953;98(6):583-606.

Kim KW, Kamerud JQ, Livingston DM, Roon RJ. Asparaginase II of Saccharomyces cerevisiae. Characterization of the ASP3 gene. J Biol Chem 1988;263(24):11948-53.

Kotik, M. and Zuber, H. Mutations that significantly change the stability, flexibility and quaternary structure of the L-lactate dehydrogenase from *Bacillus megaterium*. Eur J Biochem 1993; 211:267-280.

Krishnan KS, Brandts. JE. Scanning calorimetry, vol. 49, 1978. *Methods Enzymol.* 49: 3-14.

Laemmli UK. Cleavage of structural proteins during the assembly of the head of bacteriophage T4. Nature 1970;227(5259):680-5.

Lee, H. J.; Lu, S. W., and Chang, G. G. Monomeric molten globule intermediate involved in the eqilibrium unfolding of tetrameric δ_2-crystallin. Eur J Biochem 2003; 270, 3988-3995.

Lubkowski J, Palm GJ, Gilliland GL, Derst C, Rohm KH, Wlodawer A. Crystal structure and amino acid sequence of Wolinella succinogenes L-asparaginase. Eur J Biochem 1996;241(1):201-7.

Maita T, Matsuda G. The primary structure of L-asparaginase from *Escherichia coli*. Hoppe Seylers Z Physiol Chem 1980;361(2):105-17.

Maita T, Morokuma K, Matsuda G. Amino acid sequence of L-asparaginase from *Escherichia coli*. J Biochem (Tokyo) 1974;76(6):1351-4.

Maniatis T, Frisch EF, Sambrook J. Molecular Cloning: A Laboratory Manual, New York 1989.

Mashburn LT, Wriston JC, Jr. Tumor Inhibitory Effect of L-Asparaginase From *Escherichia coli*. Arch Biochem Biophys 1964;105:450-2.

Matsumura M, Becktel WJ, Matthews BW. Hydrophobic stabilization in T4 lysozyme determined directly by multiple substitutions of Ile 3. Nature 1988;334(6181):406-10.

Mc Duff, F. O.; Doucet, A., and Beauregard, M. Low concentration of guanidine hydrochloride induces the formation of an aggregation-prone state in α-urease. Biochem Cell Biol 2004; 82, 305-313.

Minton MP, Bullmann HMS, Scawen MD, Atkins T, Gilbert HJ. Nucleotide sequence of the *Erwinia chrysanthemi* NCPPB 1066 L-asparaginase gene. Gene 1986;46:25-35.

Muller HJ, Boos J. Use of L-asparaginase in childhood ALL. Crit Rev Oncol Hematol 1998;28(2):97-113.

Nelson M, McClelland M. Use of DNA methyltransferase/endonuclease enzyme combinations for megabase mapping of chromosomes. Methods Enzymol 1992;216:279-303.

Nesbit ME, Ertel I, Hammond GD. L-Asparaginase as a single agent in acute lymphocytic leukemia: survey of studies form Childrens Cancer Study Group. Cancer Treat Rep 1981;65(Suppl 4):101-7.

Nozaki Y. The preparation of guanidine hydrochloride, Methods Enzymol. 1971;26, 43-50.

Oettgen HF, Old LJ, Boyse EA, et al. Inhibition of leukemias in man by L-asparaginase. Cancer Res 1967;27(12):2619-31.

Ortlund E, Lacount MW, Lewinski K, Lebioda L. Reactions of Pseudomonas 7A glutaminase-asparaginase with diazo analogues of glutamine and asparagine result in unexpected covalent inhibitions and suggests an unusual catalytic triad Thr-Tyr-Glu. Biochemistry 2000;39(6):1199-204.

Pace CN, Shireley BA, and Thomson JA. Measuring the conformational stability of a protein. In: Protein structure, a practical approach. Oxford: IRL Press, 1989.

Pace CN. Conformational stability of globular proteins. Trends Biochem Sci 1990;15(1):14-7.

Pace CN. Determination and analysis of urea and guanidine hydrochloride denaturation curves. Methods Enzymol 1986;131:266-80.

Palm GJ, Lubkowski J, Derst C, Schleper S, Rohm KH, Wlodawer A. A covalently bound catalytic intermediate in *Escherichia coli* asparaginase: crystal structure of a Thr-89-Val mutant. FEBS Lett 1996;390(2):211-6.

Plum GE, Breslauer KJ. Calorimetry of proteins and nucleic acids. Curr Opin Struct Biol 1995;5(5):682-90.

Price N. Folding and assembly of multi-subunit proteins. Cambridge, UK: Cambridge University Press, 1992.

Privalov PL, Gill SJ. Stability of protein structure and hydrophobic interaction. Adv Protein Chem 1988;39:191-234.

Privalov PL, Khechinashvili NN. A thermodynamic approach to the problem of stabilization of globular protein structure: a calorimetric study. J Mol Biol 1974;86(3):665-84.

Privalov PL, Potekhin SA. Scanning microcalorimetry in studying temperature-induced changes in proteins. Methods Enzymol 1986;131:4-51.

Privalov PL. Stability of proteins: small globular proteins. Adv Protein Chem 1979;33:167-241.

Qiagen „QIAprep® Miniprep Handbook 07/99“ 1999.

Rao JKM, Gribskov MR, Lubkowski J, Miller M, Swain AL, Wlodawer A. A comparison of crystal structures of bacterial L-asparaginases. New York: Academic Press, 1996.

Rigell CW, Saussure. Cd, Freire. E. Protein and lipid structural transitions in cytochrome c oxidase- dimyristoylphosphatidylcholine reconstitutions. *Biochemistry* 1985;24: *5638-5646.*

Rogers KS. L-asparaginase for treatment of lymphoid neoplasia in dogs. J Am Vet Med Assoc 1989;194(11):1626-30.

Russell L, Yamazaki H. The dependence of *Escherichia coli* asparaginase II formation on cyclic AMP and cyclic AMP receptor protein. Can J Microbiol 1978;24(5):629-31.

Schmid F. Spectral methods of characterizing protein conformational changes. In: Protein structure, a practical approach. Oxford: IRL Press, 1989.

Schubert, D., Derst, C. and Röhm, K. H. Abstract. Annual ABRF Meeting: Biomolecular Techniques, San Francisco, CA 1996.

Schwartz JH, Reeves JY, Broome JD. Two L-asparaginases from *E. coli* and their action against tumors. Proc Natl Acad Sci U S A 1966;56(5):1516-9.

Shifrin S, Luborsky SW, Grochowski BJ. L-Asparaginase from *Escherichia coli* B. Physicochemical studies of the dissociation process. J Biol Chem 1971;246(24):7708-14.

Shifrin S, Parrott CL, Luborsky SW. Substrate binding and intersubunit interactions in L-asparaginase. J Biol Chem 1974;249(5):1335-40.

Shifrin S, Parrott CL. In vitro assembly of L-asparaginase subunits. J Biol Chem 1974;249(13):4175-80.

Shirley BA. Protein conformational stability estimated from urea, guanidine hydrochloride, and thermal denaturation curves. In: Stability of protein pharmaceuticals, Part A: Chemical and physical pathways of protein degradation. New York: Plenum Press, 1972.

Sluyterman LA, Elgersma O. Chromatofocusing: isoelectric focusing on ion exchange columns I. General principles. J.Chromatogr. 1978;150:17-30.

Sluyterman LA, Wijdenes J. Chromatofocusing: isoelectric focusing on ion exchange columns. II. Experimental verification. *J. Chromatogr*. 1978;150:31-44.

Smith CJ, Clarke AR, Chia WN, Irons LI, Atkinson T, Holbrook JJ. Detection and characterization of intermediates in the folding of large proteins by the use of genetically inserted tryptophan probes. Biochemistry 1991;30(4):1028-36.

Soru E, Zaharia O. Immunoenzymology of L-asparaginase from the BCG strain of Mycobacterium bovis. Immunochemistry 1974;11(12):791-5.

Spiro S, Guest JR. Regulation and over-expression of the fnr gene of *Escherichia coli*. J Gen Microbiol 1987;133(12):3279-88.

Stratagene. „QuickChangeTM Site-Directed Mutagenesis Kit – Instruction Manual“ 1998.

Strickland EH. , vol. 2, 1974. CRC Critical Review Biochemistry. 1974; 2:113-175.

Stryckmans PA, Otten J, Delbeke MJ, *et al*. Comparison of chemotherapy with immunotherapy for maintenance of acute lymphoblastic leukemia in children and adults. Blood 1983;62(3):606-15.

Sun DX, Setlow P. Cloning, nucleotide sequence, and expression of the Bacillus subtilis ans operon, which codes for L-asparaginase and L-aspartase. J Bacteriol 1991;173(12):3831-45.

Swain AL, Jaskolski M, Housset D, Rao JK, Wlodawer A. Crystal structure of *Escherichia coli* L-asparaginase, an enzyme used in cancer therapy. Proc Natl Acad Sci U S A 1993;90(4):1474-8.

Tabor S, Richardson CC. A bacteriophage T7 RNA polymerase/promoter system for controlled exclusive expression of specific genes. 1985. Biotechnology 1992;24:280-4.

Tanford C. Protein denaturation. Adv Protein Chem 1968;23:121-282.

Teale FW, Weber G. Ultraviolet fluorescence of the aromatic amino acids. Biochem J 1957;65(3):476-82.

Timasheff SN. Water as ligand: preferential binding and exclusion of denaturants in protein unfolding. Biochemistry 1992;31(41):9857-64.

Tomao FA, Schwartz MK, Lash E, Oettgen H, Krakoff IH. Blod levels and distributions of L-asparaginase in man. Proc. Amer. Assoc. Cancer Res. 1969;10:94.

Unden G, Guest JR. Cyclic AMP and anaerobic gene expression in E. coli. FEBS Lett 1984;170(2):321-5.

Uversky VN, Semisotnov GV, Pain RH, Ptitsyn OB. 'All-or-none' mechanism of the molten globule unfolding. FEBS Lett 1992;314(1):89-92.

Uversky VN, Semisotnov GV, Ptitsyn OB. Biofizika 1993;38:37-46.

Uversky VN. Use of fast protein size-exclusion liquid chromatography to study the unfolding of proteins which denature through the molten globule. Biochemistry 1993;32(48):13288-98.

Wehner A, Derst C, Specht V, Aung HP, K.H. R. The catalytic mechanism of *Escherichia coli* asparaginase II. *Hoppe Seylers Z. Physiol. Chem* 1994;375:108.

Wehner A, Harms E, Jennings MP, et al. Site-specific mutagenesis of *Escherichia coli* asparaginase II. None of the three histidine residues is required for catalysis. Eur J Biochem 1992;208(2):475-80.

Wehner A. Vergeichenende kinetische and spektroskopische Untersuchungen an Mutanten der *E.coli*-Asparaginase II. Dissertation, Fachbereich Chemie, Universitaet Marburg. 1993.

Wendt, M. Diploma Thesis (Human Biology), Department of Medicine, Philipps University Marburg, 2002.

Whitecar JP, Jr., Bodey GP, Harris JE, Freireich EJ. L-asparaginase. N Engl J Med 1970;282(13):732-4.

Winzor, D. J. Analytical exclusion chromatography. J Biochem Biophys Methods. 2003;56, 15-52.

7. Summary

L-asparaginases (EC 3.5.1.1) catalyze the hydrolysis of L-asparagine to aspartic acid and ammonia. Asparaginases of bacterial origin have been used for over 40 years in the treatment of acute lymphatic leukemia (ALL). Asparaginase isoenzyme II from *Escherichia coli* (EcA2) is especially effective in cancer therapy. The enzyme, a homotetramer (138 kDa) made up from equivalent dimers, is also an ideal model compound to study folding/unfolding and association/dissociation phenomenon of a large oligomeric protein: It is readily amenable to site-directed mutagenesis, a single tryptophan residue per subunit simplifies spectroscopic analysis of conformational changes, and it spontaneously refolds after chemical denaturation. Our aim was to probe the molecular basis of the interactions between the EcA2 dimers by mutations, and to construct EcA2 variants with improved stability for possible application in leukemia treatment.

Using guanidine hydrochloride (Gu.HCl) equilibrium denaturation methods, we analyzed unfolding of wild-type EcA2 and a number of variants with amino acid replacements in the interior of the subunits or at the interfaces between the so-called intimate dimers. Enzymatic activity, fluorescence, and CD spectroscopy were used to monitor chemical denaturation by Gu.HCl. For wild-type EcA2 we found a highly cooperative transition from the folded to the denatured state. By gel filtration and sedimentation equilibrium ultracentrifugation, we showed that unfolding of the wild-type enzyme was preceded by dissociation into dimers and monomers. EcA2(WT) showed little change in stability between pH 5-8 but a rapid loss in stability below pH 5.

As compared to wild-type enzyme, variants with amino acid exchanges that weaken dimer-dimer interactions exhibited more complex denaturation profiles with one or two stable intermediate states. So, for instance, variants EcA2(Y176S) and EcA2(W66Y/Y181W) dissociate into fully active dimers at low Gu.HCl concentrations. On the other hand, variant EcA2(Y176F) shows higher structural stability and specific activity than the wild-type protein.

Thermal unfolding of EcA2 and its mutants was examined by differential scanning calorimetry (DSC) and CD. Correlation of DSC, CD, and light scattering data showed a single cooperative heat unfolding transition accompanied by irreversible protein aggregation,

which precluded quantitative thermodynamic analysis of the excess heat capacity data. DSC data of EcA2 (WT) suggested that the increase in protein stability upon an increase in pH from 5-8 is mainly enthalpy-driven. Consistent with the chemical unfolding data, mutant EcA2(Y176F) showed higher thermal stability (a higher melting temperature, T_m) than wild type enzyme while EcA2(Y176S) and EcA2(W66Y/Y181W) were much more heat-sensitive, indicating the preference for large hydrophobic side chains at this site. In addition, two salt bridges, D156···R191 and D188 ···R195, markedly contribute to the tetramer stability.

Our results demonstrate that even small changes at a subunit interface may markedly enhance or impair EcA2 stability without compromising its catalytic properties. Engineered enzyme variants with enhanced stability, such as EcA2(Y176F), are promising candidates for an improved asparaginase therapy of leukemias.

7. Zusammenfassung

L-Asparaginasen (EC 3.5.1.1) katalysieren die Hydrolyse von L-Asparagin zu Asparaginsäure und Ammoniak. Asparaginasen bakteriellen Ursprungs werden seit über 40 Jahren zur Behandlung der Akuten Lymphatischen Leukämie (ALL) eingesetzt. Das Isoenzym II der *E. coli*-Asparaginase (EcA2) ist dabei besonders wirksam. Die EcA2 ist ein Homotetramer, das aus zwei äquivalenten Dimeren aufgebaut ist. Zur Untersuchung von Faltung und Denaturierung bzw. Assoziation und Dissoziation oligomerer Proteine ist sie ein ideales Modellsystem: das Enzym kann problemlos durch Mutagenese modifiziert werden, ein einziger Tryptophanrest pro Untereinheit vereinfacht den spektroskopischen Nachweis von Konformationsänderungen, und das Protein renaturiert nach chemischer Denaturierung spontan. Das Ziel der vorliegenden Arbeit war es, durch systematische Mutagenese die molekularen Grundlagen der Wechselwirkungen zwischen den EcA2-Dimeren zu klären und stabilere EcA2-Varianten für mögliche Anwendungen in der ALL-Therapie zu konstruieren.

Zunächst untersuchten wir durch Gleichgewichtsdenaturierung mit Guanidin-hydrochlorid (Gu.HCl) als Denaturans die Entfaltung des Wildtypenzyms und einer Serie von EcA2-Varianten mit Aminosäureaustauschen im Inneren der Monomeren und an den Kontaktflächen zwischen den so genannten "intimen" Dimeren. Um die Denaturierung zu verfolgen wurden Aktivitätsmessungen sowie Fluoreszenz- und CD-Spektroskopie eingesetzt. Beim Wildtypenzym zeigte sich einen hoch kooperativer Übergang vom nativen in den denaturierten Zustand. Durch Gelfiltration und Gkeichgewichtssedimentation konnten wir allerdings zeigen dass der Denaturierung eine Dissoziation in Dimere und/oder Monomere vorausgeht. Die thermodynamische Stabilität des nativen Enzyms ist zwischen pH 5 und 8 nahezu konstant, während sie unterhalb von pH 5 rasch verloren geht.

Im Vergleich zum Wildtyp waren die Denaturierungsprofile von Mutanten mit modifizierten Dimer-Dimer-Kontakten deutlich komplexer und deuteten auf das Vorliegen von einem oder zwei stabilen Zwischenprodukten hin. So dissoziieren z.B. die Varianten EcA2(Y176S) und EcA2(W66Y/Y181W) schon bei sehr niedrigen Gu.HCl-Konzentrationen in aktive Dimere. Auf der anderen Seite war die Variante EcA2(Y176F) deutlich stabiler und auch aktiver als der Wildtyp.

Zur Untersuchung der Temperaturstabilität wurde die thermische Denaturierung der EcA2-Varianten durch Differential Scanning-Kalorimetrie (DSC) und CD-Spektroskopie

verfolgt. Ergänzt durch Lichtstreuungsexperimente, zeigten diese Daten, dass die native EcA2 bei etwa 65 °C in einem einzigen hooch kooperativen Prozess denaturiert um dann sofort irreversibel zu aggregieren. Wegen der Irreversibilität des Vorgangs war es nicht möglich, aus den Daten exakte thermodynamische Parameter abzuleiten. Diee DSC-Experimente zeigten weiter, dass die Zunahme der thermischen Stabilität des Wildtypenzyms zwischen pH 5 und 8 enthalpische Ursachen hat. In Übereinstimmung mit den Ergebnissen der chemischen Denaturierung war auch die thermische Stabilität der Variante EcA2(Y176F) im Vergleich zum nativen Enzym deutlich erhöht, während EcA2(Y176S) und EcA2(W66Y/Y181W) sehr viel labiler waren. Dies zeigt, dass für eine optimale Stabiliserung des EcA2-Tetrameren unpolare aromatische Reste in den Positionen 176 und 182 notwendig sind. Wir konnten außerdem zeigen, dass Salzbrücken zwischen den Aminosäuren D156 und R191 bzw. zwischen D188 und R195 ebenfalls entscheidend zur Stabilität daes nativen EcA2-Tetrameren beitragen.

Unsere Ergebnisse belegen, dass schon geringe Veränderungen der Kontakte zwischen den Untereinheiten die Stabilität der der EcA2 dramatisch erhöhen oder erniedrigen können ohne die katalytische Aktivität des Enzyms zu beeinträchtigen. Gezielt veränderte EcA2-Varianten wie z.B. EcA2(Y176F) sind viel versprechende Kandidaten für eine verbesserte Asparaginase-Therapie der ALL.

8. Appendix

8.1 Abbreviations

8.1.1 General

A	Absorption
Å	Ångstrom (10^{-8} cm)
Amp	Ampicillin
ansA	Gene of *E. coli* Asparaginase I
ansB	Gene of *E. coli* Asparaginase Il
*ansB**	Mutated gene of *E. coli* Asparaginase Il
APS	Ammonium persulfate
bp	Base pair
BSA	Bovine serum albumin
CD	Circular dichroism
(k)Da	(Kilo) Dalton
DMSO	Dimethylsulfoxide
DNA	Deoxyribonucleic acid
dNTP	Deoxynucleotide phosphate
dATP	Deoxyadenosine triphosphate
dGTP	Deoxyguanosine triphosphate
dCTP	Deoxycytosine triphosphate
dTTP	Deoxythymidine triphosphate
DSC	Differential scanning calorimetry
DTT	Dithiothreitol
E. coli	*Escherichia coli*
EDTA	Ethylenediaminetetraacetic acid
ε	Extinction coefficient
Gu.HCl	Guanidine hydrochloride
I_{XXX}	Fluorescence intensity at XXX nm
IP	Isoelectric point
L-AHA	L-aspartic acid β-hydroxamate

LB-Medium	Luria-Bertani medium
$\lambda_{EMM.}$	Wavelength of emission
M	Molar
MES	2-[N-Morpholino]-ethanesulfonic acid
mg	Miligram
min	Minute
MOPS	3-[N-Morpholino]-propane sulphonic acid
OD_{XXX}	Optical Density at XXX nm wavelength
PAGE	Polyacrylamide-Gel electrophoresis
PCR	Polymerase chain reaction
rpm	Revolutions per minute
SDS	Sodium dodecylsulphate
SDS-PAGE	Sodium dodecylsulfate polyacrylamide gel electrophoresis
TAE	Tris Acetate-EDTA
TCA	Trichloroacetic acid
TE	Tris-EDTA buffer
TEMED	N,N,N´,N´-Tetramethyl ethylenediamine
Tris	Tris-(hydroxymethyl)-aminomethane
U	Activity unit ($\mu mol.min^{-1}$)
UV	Ultra voilet
v/v	Volume by volume
w/v	Weight by volume
WT	Wild type

8.1.2 Amino acids

Amino acid	3-Letter-Code	1-Letter-Code
Alanine	Ala	A
Arginine	Arg	R
Asparagine	Asn	N
Aspartic acid	Asp	D
Cysteine	Cys	C
Glutamine	Gln	Q
Glutamic acid	Glu	E
Glycine	Gly	G
Histidine	His	H
Isoleucine	Ile	I
Leucine	Leu	L
Lysine	Lys	K
Methionine	Met	M
Phenylalanine	Phe	F
Proline	Pro	P
Serine	Ser	S
Threonine	Thr	T
Tryptophane	Trp	W
Tyrosine	Tyr	Y
Valine	Val	V

8.2 Curriculum Vitae

Name: VERMA, Shikha

Gender: Female

Date and Place of Birth: 07.03.1977 at Meerut, India

Educational Qualifications:

Primary Education:

1986-1991 J Kanya Inter College, Shamli, India

Secondary Education:

1991-1993 J Kanya Inter College, Shamli, India

Bachelor of Science:

July 1994-April 1997 Chaudhary Charan Singh University, Meerut, India

Master of Science:

Aug. 1997-Oct. 1999 Chaudhary Charan Singh University, Meerut, India

Research student:

April 2000–Jan. 2001 Philipps University Marburg, Germany
Institute of Pharmaceutical Technology and Biopharmacy

Ph.D. Student:

Jul. 2001-May. 2005 Institute of Physiological Chemistry, Philipps University Marburg (Molecular Enzymology, Prof. Röhm)
"Systematic Site-directed Mutagenesis to Characterize Subunits Interactions in *E. coli* asparaginase II, an Enzyme Used in Leukemia Treatment" supported for 3 years by a fellowship from Graduiertenkolleg "Protein Function at the Atomic Level".

Visiting Scholar:
Nov. 2003–April 2004 Department of Physiology and Biophysics, Boston University School of Medicine, Boston, USA.
Performed the thermal unfolding of *E. coli* asparaginase II and its mutants by using Circular Dichroism and Differential Scanning Calorimetry techniques.

8.3 Acknowledgements

I would like to thank and acknowledge the collective efforts of the following group of people for my doctoral thesis dissertation:

At the outset, I would like to thank and express my sincere appreciation and gratitude to my Ph.D. advisor Prof. Dr. Klaus Heinrich Röhm, who was not only an outstanding mentor professionally but also a constant pillar of support, advice, and ideas. He always encouraged me and provided unwavering support during this four year period of dissertation work. On many occasions when hurdles seemed insurmountable, his valuable advice on troubleshooting helped me overcome most challenges in science as well in life in general.

My heartfelt thanks to Prof. Olga Gursky, who allowed me to use her laboratory space, equipments, and for her tremendous help in CD, DSC experiments, and also extensive discussion in my thesis work.

My sincere thanks are also due to Prof. Dr. Monika Löffler for her unending support in all these years of my duration.

Also I would like to thank my colleagues, Micha, Elke, Bettina, Yvonne, Birgit, Ute, and all other people in Physiological Chemistry department for giving me a wonderful time in all these four years. Also my thanks are due to colleagues at the other end of the Atlantic specially Shobini, Sangeeta, and Shujun, in the laboratory of Prof. Gursky.

I would like to specially thank Dr. Mechthild Röhm for her affection, love, and care, which never let me miss my motherland and family.

Finally, I would also like to thank my entire family: my Mother and Father for raising me and teaching me to be a good person, my Brother and Sisters for their support in my life, and my Husband, for his persistent encouragement and unended support to make this work happen. I could not have come to this point without all these help.

8.4 Erklärung

Ich erkläre ehrenwörtlich, dass ich die dem Fachbereich Medizin zur Promotionsprüfung eingereichte Arbeit mit dem Titel "Systematic site-directed mutagenesis to characterize subunits interactions in *E. coli* asparaginase II, an enzyme used in leukemia treatment " im Institut für Physiologische Chemie, Arbeitsgruppe Molekulare Enzymologie unter der Leitung von Herrn Prof. Dr. Röhm ohne sonstige Hilfe selbst durchgeführt und bei der Abfassung der Arbeit keine anderen als die in der Dissertation angegebenen Hilfmittel benutzt habe. Ein Teil der Experimente wurde unter Anleitung von Frau Prof. Olga Gursky an der Boston University in Boston, MA durchgeführt.

Ich habe bisher an keinem in- und ausländischen Medizinischen Fachbereich ein Gesuch um Zulassung zur Promotion eingereicht noch die vorliegende oder eine andere Arbeit als Dissertation vorgelegt.

Teile der vorliegenden Arbeit wurden bereits wie folgt veröffentlich:

Posterpräsentationen

Verma S., Derst C., Wendt M.M., Gursky O., Röhm K.H. Chemical and thermal stabilities of type II asparaginases from *E. coli, E. chrysanthemi*, and *Pseudomonas* 7A. A comparative study.Nineteenth Symposium of the Protein Society *"Protein Structure, Function and Disease"* Boston, MA, July 30-August 3, 2005.

Verma S., Wendt M.M., Gursky O., Röhm K.H. Mutational Analysis of the Dimer Dimer Interface of *E. coli* Asparaginase II, an Enzyme Used in Leukemia Treatment. Eighteenth Symposium of the Protein Society *"Protein Structure, Function and Disease"* San Diego, CA, August 14-18, 2004.

Verma, S., Wendt, M. and Röhm K. H. Systematic site-directed mutagenesis to characterize subunit interactions in *E. coli* asparaginase II, an enzyme used in leukemia treatment. ELSO Meeting, Dresden, Germany, 20 - 24 September, 2003.

Verma S and Röhm K-H. Folding and stability of homotetrameric asparaginase II from E. Coli. Graduiertenkolleg Colloquium, Marburg, Germany, 11th December 2001.

Marburg, den 05. September 2005

Shikha Verma

Verma Shikha

Verzeichnis der akademischen Lehrer Meine akademische Lehrer in Marburg waren die Damen und Herren Eilers,Hasilik, Löffler, Müller, Röhm, Tampe.

In Meerut, Indien die Damen und Herren Sharma, Lal, Ramesh, Gupta, Singh, Kumar

Shikha Verma

Marburg, den 15. September 2005